

AD-A155 865

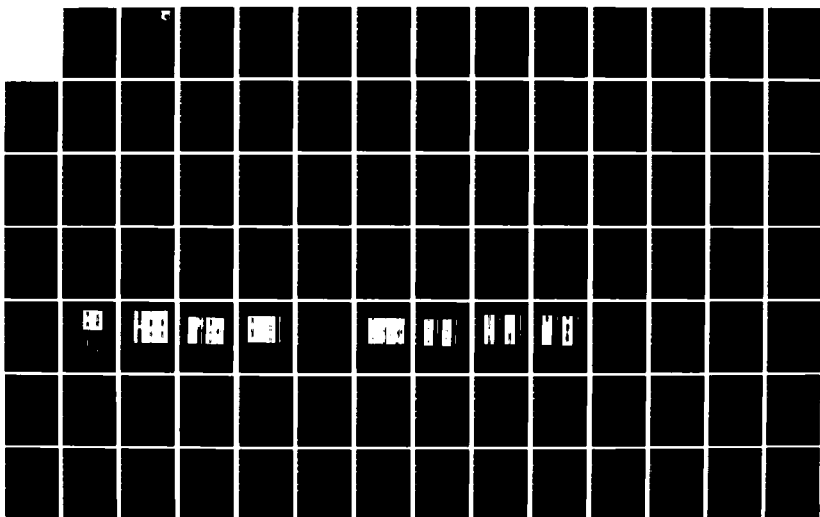
IMPROVED MATERIALS FOR COMPOSITE AND ADHESIVE JOINTS
(U) DAYTON UNIV OH RESEARCH INST R KIM ET AL JUL 84
UDR-TR-83-117 AFWAL-TR-84-4074 F33615-81-C-5056

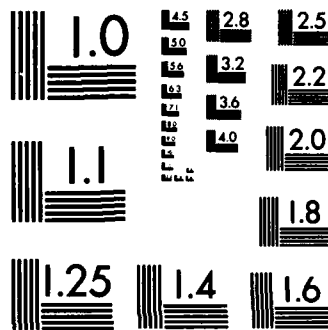
1/2

UNCLASSIFIED

F/G 11/4

NL





MICROCOPY RESOLUTION TEST CHART
NATIONAL BUREAU OF STANDARDS-1963-A

AD-A155 065

AFWAL-TR-84-4074



IMPROVED MATERIALS FOR COMPOSITE AND ADHESIVE JOINTS

R. Kim
W. Click
J. Hartness
M. Koenig
M. Rich
S. Soni

University of Dayton Research Institute
300 College Park Avenue
Dayton, OH 45469

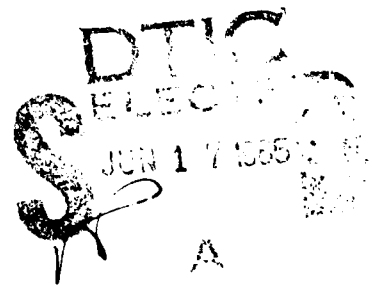
July 1984

Annual Report for Period 1 September 1982 to 31 August 1983

Approved for public release; distribution unlimited.

DTIC FILE COPY

MATERIALS LABORATORY
AIR FORCE WRIGHT AERONAUTICAL LABORATORIES
AIR FORCE SYSTEMS COMMAND
WRIGHT-PATTERSON AFB, OHIO 45433



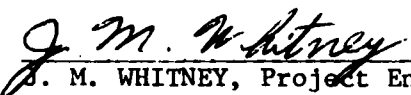
35 5 33 137

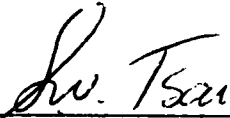
NOTICE

When Government drawings, specifications, or other data are used for any purpose other than in connection with a definitely related Government procurement operation, the United States Government thereby incurs no responsibility nor any obligation whatsoever; and the fact that the government may have formulated, furnished, or in any way supplied the said drawings, specifications, or other data, is not to be regarded by implication or otherwise as in any manner licensing the holder or any other person or corporation, or conveying any rights or permission to manufacture use, or sell any patented invention that may in any way be related thereto.

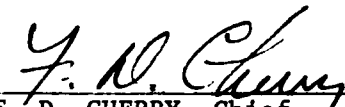
This report has been reviewed by the Office of Public Affairs (ASD/PA) and is releasable to the National Technical Information Service (NTIS). At NTIS, it will be available to the general public, including foreign nations.

This technical report has been reviewed and is approved for publication.


J. M. WHITNEY, Project Engineer
Mechanics & Surface Interactions Branch
Nonmetallic Materials Division


S. W. TSAI, Chief
Mechanics & Surface Interactions Branch
Nonmetallic Materials Division

FOR THE COMMANDER:


F. D. CHERRY, Chief
Nonmetallic Materials Division

"If your address has changed, or if you wish to be removed from our mailing list, or if the addressee is no longer employed by your organization, please notify AFWAL/MLBM, WPAFB, OH 45433 to help us maintain a current mailing list."

Copies of this report should not be returned unless return is required by security considerations, contractual obligations, or notice on a specific document.

4. PERFORMING ORGANIZATION REPORT NUMBER(S) UDR-TR-83-117			5. MONITORING ORGANIZATION REPORT NUMBER(S) AFWAL-TR-84-4074		
6a. NAME OF PERFORMING ORGANIZATION U of Dayton Research Institute		6b. OFFICE SYMBOL (If applicable)	7a. NAME OF MONITORING ORGANIZATION Mechanics & Surface Interactions Branch Materials Laboratory		
6c. ADDRESS (City, State and ZIP Code) University of Dayton Research Institute Dayton, OH 45469			7b. ADDRESS (City, State and ZIP Code) AFWAL/MLBM WPAFB, OH 45433		
8a. NAME OF FUNDING/SPONSORING ORGANIZATION Materials Laboratory		8b. OFFICE SYMBOL (If applicable) AFWAL/MLBM	9. PROCUREMENT INSTRUMENT IDENTIFICATION NUMBER F33615-81-C-5056		
8c. ADDRESS (City, State and ZIP Code) Same as 7b.			10. SOURCE OF FUNDING NOS.		
			PROGRAM ELEMENT NO. 62102F	PROJECT NO. 2419	TASK NO. 03
					WORK UNIT NO. 23
11. TITLE (Include Security Classification) Improved Materials for Composite and Adhesive Joints					
12. PERSONAL AUTHOR(S) R. Kim, W. Click, J. Hartness, M. Koenig, M. Rich and S. Soni					
13a. TYPE OF REPORT Interim		13b. TIME COVERED FROM 1Sep82 to 31Aug83		14. DATE OF REPORT (Yr., Mo., Day) July 1984	
				15. PAGE COUNT 182	
16. SUPPLEMENTARY NOTATION					
17. COSATI CODES			18. SUBJECT TERMS (Continue on reverse if necessary and identify by block number)		
FIELD	GROUP	SUB. GR.			
11	04		polyetheretherketone; composites; mechanical properties; unidirectional carbon tape; aluminum oxide; interface; epoxy; interphase; hygrothermal; carbon; fiber; fracture		
19. ABSTRACT (Continue on reverse if necessary and identify by block number) This report presents a summary of the work performed by the University of Dayton Research Institute under Contract No. F33615-81-C-5056 during the period 1 Sept 82 through 31 Aug 83. Research was conducted in the following areas: Processing and Evaluation of Composites, Adhesive Bonded Joints, Interface/Interphase Characterization, and Mechanics of Composites and Adhesive Bonded Joints. The work was performed at the Wright-Patterson Air Force Base, Ohio, with Dr. J. M. Whitney as project engineer. Literature figures: mechanical properties; aluminum oxide; composite materials; epoxy resins; carbon fibers.					
20. DISTRIBUTION/AVAILABILITY OF ABSTRACT UNCLASSIFIED/UNLIMITED <input checked="" type="checkbox"/> SAME AS RPT. <input type="checkbox"/> DTIC USERS <input type="checkbox"/>			21. ABSTRACT SECURITY CLASSIFICATION Unclassified		
22a. NAME OF RESPONSIBLE INDIVIDUAL J. M. Whitney			22b. TELEPHONE NUMBER (Include Area Code) (513) 255-6685		22c. OFFICE SYMBOL AFWAL/MLBM

Unclassified

SECURITY CLASSIFICATION OF THIS PAGE

18. (Continued)

stoichiometry; XPS; surface chemistry; modulus; strain; failure; curing stresses;
constant-life; damage; delamination; interlaminar stresses; fracture toughness

Unclassified

SECURITY CLASSIFICATION OF THIS PAGE

FOREWORD

This report was prepared by the University of Dayton Research Institute under Air Force Contract No. F33615-81-C-5056, Project No. 2419, Task No. 241903. The work was administered under the direction of the Nonmetallic Materials Division Air Force Wright Aeronautical Laboratories, Materials Laboratory, Air Force Systems Command, with Dr. J. M. Whitney (AFWAL/MLBM) as Contract Monitor.

This report was submitted in October 1983 and covers work conducted from 1 Sept. 82 through 31 Aug. 1983.

Personnel who contributed to this research are: W. E. Click, J. T. Hartness, R. Y. Kim, M. Koenig, M. J. Rich, and S. R. Soni.

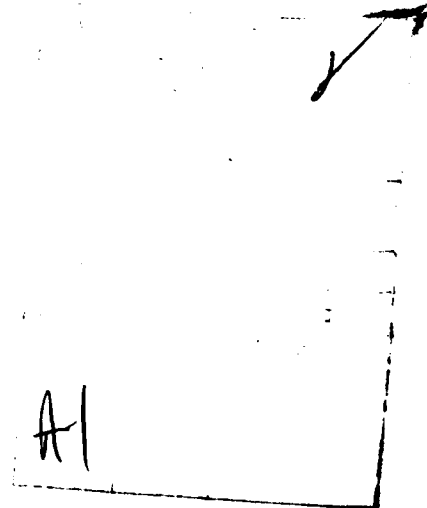


TABLE OF CONTENTS

Section		Page
I	PROCESSING AND EVALUATION OF COMPOSITES	1
	1. FAILURE RESISTANT COMPOSITE CONCEPTS	1
	a. Mechanical Testing	1
	b. Composites Fabricated	2
	2. RELATIONSHIP BETWEEN NEAT RESIN AND IN SITU COMPOSITE PROPERTIES	5
	3. MATERIAL DEVELOPMENT	6
	a. Polyetheretherketone (PEEK) Composites	6
	1) PEEK film/Graphite Cloth	6
	2) PEEK film/Glass Cloth	7
	3) PEEK Prepreg	8
	b. Liquid Crystal Polymers (LCP)	16
II	ADHESIVE BONDED JOINTS	22
	1. EXPERIMENTAL MATRICES	22
	a. Epon 828/MPDA	22
	b. 5208 Epoxy	27
	c. Liquid Chromatography Studies of High "n" Epoxy Monomers	27
III	INTERFACE/INTERPHASE CHARACTERIZATION	29
	1. ALUMINUM OXIDE/EPOXY INTERPHASE	29
	a. Experimental	29
	b. Materials	29
	2. CARBON FIBER/EPOXY INTERPHASE	30
	a. XPS of Carbon Fibers	30
	b. Moisture Effects on Interfacial Properties	39
	1) Materials	39
	2) Results and Discussion	40
	a) 20°C	40
	b) 70°C	40
	c) 125°C	46

TABLE OF CONTENTS (CONCLUDED)

Section	Page
III	INTERFACE/INTERPHASE CHARACTERIZATION (CONTINUED)
	c. Effects of Fiber Plasma Treatment 52
	d. Flow Microcalorimetry 53
IV	MECHANICS OF COMPOSITES AND ADHESIVE BONDED JOINTS 56
	1. FAILURE STUDY 56
	a. Maximum Stress 57
	b. Maximum Strain 59
	c. Quadratic Polynomial 59
	d. Results and Discussion 60
	2. EFFECTS OF CURING STRESSES ON LAMINATES 72
	3. FATIGUE STUDY 81
	a. Fatigue Behavior of Graphite/Epoxy 81
	b. Fatigue Behavior of Graphite/Thermo- plastic Composites 103
	4. FRACTURE TEST 124
	5. DELAMINATION STUDY 126
V	PUBLICATIONS AND PRESENTATIONS 133
	REFERENCES 137
	APPENDIX A 139

LIST OF ILLUSTRATIONS

Figure		Page
1	Tensile Stress vs. Strain (+30/-30 ₂ /+30/90 ₂) _s .	15
2	XPS Spectra of the Carbon 1s, Oxygen 1s, and Nitrogen 1s Regions for Three Hygrothermal Conditions.	32
3	Carbon 1s Peak from a DER330-Coated AS4 Fiber (#F070).	34
4	Spectra of the Ta _{4f} Photoelectron Peaks from Ta ₂ O ₅ Using (A) Aluminum X-rays, (B) Magnesium X-rays, and (C) Monochromatized Aluminum X-rays.	36
5	S 2p XPS Spectra from MoS ₂ Obtained Using a Mg K α X-ray Source with Analyzer Resolutions of (a) 1.3, (b) 0.78, (c) 0.46, and (d) 0.26 eV.	37
6	Carbon 1s Photoelectron Spectra Obtained from a Carbon Fiber Specimen.	38
7	Photomicrographs of AS1 and AS1-C Fibers Under Strain; No Conditioning.	42
8	Photomicrographs of AS Fiber Post 20°C Conditioning.	43
9	Photomicrographs of AS1 Fiber Post 20°C Conditioning.	44
10	Photomicrographs of AS1-C Fiber Post 20°C Conditioning.	45
11	Photomicrographs of AS1 Fiber Post 70°C Conditioning.	47
12	Photomicrographs of AS1-C Fiber Post 70°C Conditioning.	48
13	Photomicrographs of AS1 Fiber Post 125°C Conditioning.	49
14	Photomicrographs of AS1-C Fiber Post 125°C Conditioning.	50
15	Microcalorimeter Recorder Traces.	55
16	AIAA Failure Criteria Survey Response.	58

LIST OF ILLUSTRATIONS (CONTINUED)

Figure		Page
17	Failure Envelopes for $[0/90/+45]_s$ - Laminate on the Basis of Tsai, Wu Failure Criteria.	62
18	Failure Envelopes for $[0/90/+45]_s$ - Laminate on the Basis of Chamis Failure Criteria.	63
19	Failure Envelopes for $[0/90/+45]_s$ - Laminate on the Basis of Hoffman Failure Criteria.	64
20	Failure Envelopes for $[0/90/+45]_s$ - Laminate on the Basis of Hill Failure Criteria.	65
21	Failure Envelopes for $[0/90/+45]_s$ - Laminate on the Basis of Maximum Stress Failure Criteria.	66
22	Failure Envelopes for $[0/90/+45]_s$ - Laminate on the Basis of Maximum Strain Failure Criteria.	67
23	Failure Envelopes for $[0/90/+45]$ - Laminate on the Basis of Maximum Strain Failure Criteria, $S = 99$ mPa.	68
24	Failure Envelopes for $[0/90/+45]$ - Laminates on the Basis of Tsai, Wu Criteria for Idealized Material.	69
25	Failure Envelopes for $[0/90/+45]$ - Laminate on the Basis of Maximum Strain Failure Criteria for Idealized Material.	70
26	Comparison of Predicted and Experimental Strengths for $[\phi/90/-\phi]_s$ - Laminates.	73
27	Comparison of Predicted and Experimental Strengths for $[\phi/0/-\phi]_s$ - Laminates.	74
28	Stress Component σ_x Near the Free Edge of $[0_2/90]_s$ Laminate Along the Width at the 0/90 Interface, Due to Residual Strains.	77
29	Stress Components σ_x Near the Free Edge of the $[0_2/90_2]_s$ Laminate Along the Width at the 0/90 Interface, Due to Residual Strains.	78
30	Stress Component σ_x Near the Free Edge of the $[0_2/90_4]_s$ Laminate Along the Width at the 0/90 Interface, Due to Residual Strains.	79

LIST OF ILLUSTRATIONS (CONTINUED)

Figure		Page
31	Stress Component σ_x Near the Free Edge of the $[0_2/90_8]_s$ Laminate Along the Width at the 0/90 Interface, Due to Residual Strains.	80
32	Crack Density vs. Applied Uniaxial Tensile Stress for Gr/Ep T300/1034C with $[0/45/90/-45]_{2s}$.	84
33	Microphotograph Showing Cracks of $[0/45/90/-45]_{2s}$ Laminate at 80 ksi of Static Tension.	86
34	S_r -N Curves for Positive Mean Stress, S_m ($S_r = S_{max} - S_m$).	89
35	S-N Curves for Negative Mean Stress, S_m ($S_r = S_{max} - S_m$).	90
36	Constant Life Curve for Gr/Ep T300/1034C with $[0/45/90/-45]_{2s}$ Orientation.	91
37	Crack Density vs. Number of Cycle for Gr/Ep T300/1034C with $[0/45/90/-45]_{2s}$.	92
38	Crack Density vs. Number of Cycle for Gr/Ep T300/1034C with $[0/45/90/-45]_{2s}$.	93
39	Crack Density vs. Number of Cycle for Gr/Ep T300/1034C with $[0/45/90/-45]_{2s}$.	94
40	Crack Density vs. Number of Cycle for Gr/Ep T300/1034C with $[0/45/90/-45]_{2s}$.	95
41	Crack Density vs. Number of Cycle for Gr/Ep T300/1034C with $[0/45/90/-45]_{2s}$.	96
42	Crack Density vs. Number of Cycle for Gr/Ep T300/1034C with $[0/45/90/-45]_{2s}$.	97
43	Crack Density vs. Number of Cycle for Gr/Ep T300/1034C with $[0/45/90/-45]_{2s}$.	98
44	Crack Density vs. Number of Cycle for Gr/Ep T300/1034C with $[0/45/90/-45]_{2s}$.	99
45	Crack Density for Each Angle Ply for Gr/Ep T300/1034C with $[0/45/90/-45]_{2s}$.	101

LIST OF ILLUSTRATIONS (CONTINUED)

Figure		Page
46	Microphotograph Showing the Damage Developed at the Region Between the End Tab and the Side Support Device Under Compression Fatigue.	102
47	Change of Longitudinal Modulus as Function of Number of Cycle for Gr/Ep T300/1034C with [0/45/90/-45] _{2s} .	104
48	Change of Longitudinal Modulus as Function of Number of Cycle for Gr/Ep T300/1034C with [0/45/90/-45] _{2s} .	105
49	Change of Longitudinal Modulus as Function of Number of Cycle for Gr/Ep T300/1034C with [0/45/90/-45] _{2s} .	106
50	Change of Longitudinal Modulus as Function of Number of Cycle for Gr/Ep T300/1034C with [0/45/90/-45] _{2s} .	107
51	Change of Longitudinal Modulus as Function of Number of Cycle for Gr/Ep T300/1034C with [0/45/90/-45] _{2s} .	108
52	Change of Longitudinal Modulus as Function of Number of Cycle for Gr/Ep T300/1034C with [0/45/90/-45] _{2s} .	109
53	Change of Longitudinal Modulus as Function of Number of Cycle for Gr/Ep T300/1034C with [0/45/90/-45] _{2s} .	110
54	Change of Longitudinal Modulus as Function of Number of Cycle for Gr/Ep T300/1034C with [0/45/90/-45] _{2s} .	111
55	Microphotograph Showing the Damage Through the Thickness for Gr/Ep T300/1034C with [0/45/90/-45] _{2s} .	112
56	Microphotograph Showing the Damage Through the Thickness for Gr/Ep T300/1034C with [0/45/90/-45] _{2s} .	113
57	X-ray Picture Showing Delamination Growth as Function of Fatigue Cycle, n for T300/1034C Gr/Ep.	114
58	X-ray Picture Showing Delamination Growth as a Function of Fatigue Cycle, n for T300/1034C Gr/Ep.	115

LIST OF ILLUSTRATIONS (CONCLUDED)

Figure		Page
59	X-ray Picture Showing Delamination Growth as Function of Fatigue Cycle, n for T300/1034C Gr/Ep.	116
60	X-ray Picture Showing Delamination Growth as Function of Fatigue Cycle, n for T300/1034C Gr/Ep.	117
61	X-ray Picture Showing Delamination Growth as Function of Fatigue Cycle, n for T300/1034C Gr/Ep.	118
62	X-ray Picture Showing Delamination Growth as Function of Fatigue Cycle, n for T300/1034C Gr/Ep.	119
63	X-ray Picture Showing Delamination Growth as Function of Fatigue Cycle, n for T300/1034C Gr/Ep.	120
64	X-ray Picture Showing Delamination Growth as Function of Fatigue Cycle, n for T300/1034C Gr/Ep.	121
65	Microphotograph Showing Fiber Breaks in the 0 Deg. Ply for Gr/Ep T300/1034C with $[0/45/-45/90]_{2s}$.	123
66	Interlaminar Stress Distribution Along Specimen Width for $[0/+45/90]_s$.	128
67	Interlaminar Stress Distribution Along Specimen Width for $[0/90/+45]_s$.	129
68	T300/1034C $[0_3/45_3/-45_3/90_3]$ C-C Fatigue $S_{max} = 45$ ksi #3-10-2.	131
69	T300/5208 $[0/90/+45]$ T-T Fatigue, $S_{max} = 50$ ksi #54-5.	132

of course a most important one as well as being studied by the Morphology Group in the Polymer Branch. Crystallinity determinations have been made on various PEEK systems as a function of processing (see Table 3). Determinations were made using DSC. For 100% crystallinity 31 cal/gm was used. This number was supplied from ICI.

ICI's recommended processing is shown in Table 4. The process calls for the use of an aluminum picture frame slightly thinner (10 mils) than the final composite thickness. On both sides, to aid in handling, a 5 mil. thick heat tempered aluminum foil was used. In our attempts to duplicate this process it was determined that less than desirable parallelism existed in the press to fabricate high quality panels. The press apparently is beyond adjustment without a major overhaul. Based on this situation it was determined that all panels would be obtained from ICI free of charge and the evaluation of the PEEK material would be shared with them. A test matrix was determined and is shown in Appendix A. This is not considered an engineering data base but a preliminary data generation program.

Some additional effects of slow cool on the APC-1 prepreg were demonstrated when an "edge delamination specimen" was fabricated. The layup builds considerable out of plane stress into the midplies. The layup sequence is as follows: $[+30/-30/-30/+30/90/90]_S$. This composite slow cooled using matched die molding and possessed considerable cracks in the 90's as well as some cracks in the 30's prior to testing. The same panel supplied to us from ICI resulted in no cracks. The stress strain curve of this laminate is shown in Figure 1 with graphite/epoxy data. Little or no delamination occurs prior to outerply failure. This phenomenon is not observed with the graphite/epoxy system in which there is always delamination between the -30's and 90's prior to complete failure.

Another laminate of interest called "first ply failure", consists of a stack sequence of $[+45, 90, -45, 90, +45, 90, -45, \overline{90}]_S$ and $[+45, -45, +45, -45, 90, 90, 90, \overline{90}]_S$. Both

TABLE 2
MECHANICAL PROPERTIES

PEEK/X-AS
Unidirectional
Slow Cool

Test	Strength 10^3 psi	Mod. 10^6 psi	Strain-to-failure %
0° Tensile RT	285	18.47	1.43
90° Tensile RT	7.64	1.44	0.53
0° Flexural RT	287.4	19.55	-
0° Flexural 250°F	228.9	19.02	-
0° Flexural 350°F	129.4	16.82	-
90° Flexural RT	12.80	1.50	0.82
Density 1.60 gm/cc			
F.V. 55-56%			
Note: Fiber X-AS Courtaulds	525	32.36	1.5

Tape prepreg is available in approximate 3 ft. lengths 6 in. wide x 0.005" thick with a fiber volume of 56%. The fiber is Courlaulds X-AS from Great Britian. The as received prepreg possessed good visual quality but photographic inspection revealed large variations in thickness across the width of the tape. This problem is serious in that the resin has a very high melt viscosity and thus unforgiving in correcting variations during composite processing. There is little or no resin loss during processing.

The PEEK resin in the APC-1 prepreg is not the same PEEK resin in the film form. The APC-1 resin is said to have a broader molecular weight distribution. This difference was engineered into the resin to bring about very rapid crystallization. Rapid crystallization brings about smaller crystallite size as well as improved toughness. The APC-1 system is designed for rapid cooldown during processing as will be described. There are advantages and disadvantages to rapid cooldown. The advantages are such as rapid processing, thermoforming, and improved toughness. The disadvantages are such as thermal shock resulting in residual stress, nonuniform crystallization, especially in thick parts and possible fabrication problems in handling a large part that has to be rapidly cooled. These disadvantages bring about the need for a material that is amenable to both fast and slow cool down. In terms of improving prepreg quality and developing a product that would have more versatility ICI, Great Britian is aware of these problems and is working on solving them.

The initial composites fabricated from APC-1 prepreg were slow cooled using matched die molds. The properties were good but no measurements were made on toughness such as the Mode I test. Later tests on the Mode I using slow cooling resulted in lower G_{1C} values such as 4 in. lbs./in.² versus 8-10 in. lbs./in.² for the fast cool material. The slow cool properties are shown in Table 2.

The entire question of processing, morphology and properties as well as understanding resin and fiber interphase is

TABLE 1
MECHANICAL PROPERTIES S-7781 GLASS CLOTH/PEEK FILM

Material	Density gm/cc	Fiber Vol. %	Flex. Strength $\times 10^3$ psi	Norm. Flex Strength $\times 10^3$ psi	Flex. Mod. $\times 10^6$ psi	SBS $\times 10^3$ psi	Norm. SBS $\times 10^3$ psi	Comments
Glass 7781 Epoxy	1.79	50.97	86.10	-	4.30	7.23	-	No voids
Heat Cured Glass PEEK	1.81	47.50	52.90	63.40	3.06	3.93	5.71	No voids
S-1 Glass PEEK	1.87	65.8%	74.60	95.97	2.36	4.78	5.97	Slight void slight crack
S-11 Glass PEEK	1.81	66.61	80.24	107.76	2.27	5.07	6.50	2.26% voids
S-111 PEEK	1.87	63.59	97.00	121.21	2.44	5.36	6.70	No voids
S-1V PEEK	1.87	66.03	87.17	107.89	2.30	6.57	8.14	0.6% void

It is also theorized that the silane reacts chemically with the glass and also offers itself as an interpenetrating polymer network (IPN) with the unreactive thermoplastic of choice. This interface work then brings about an improved bond between the glass and thermoplastic. One of the obvious requirements was for a high temperature finish in that the PEEK matrix must see 720°F for some period of time in order to melt and result in good composite consolidation. It is understood that the PEEK composite upper temperature use will be much lower, probably being 350°F maximum.

All supplied finishes were put into a slightly acidic water solution pH 4-5 to coat the fabric. The glass was dried approximately seven minutes at 240°F prior to use. Composites were fabricated at 750°F for two hours at 400 psi. Panels were tested in flexure and short beam shear. The results are given in Table 1. A choice was made to use Silane III as Ed Plueddemann from Dow Chemical indicates that Silane IV is not that commercially feasible. Properties were evaluated with good impact in mind. A search of the literature indicates that after good adhesion is obtained across the interface, a slight increase in shear strength may not do much for impact strength. A curve from Broutman's data seems to level off for good shear strength vs. impact strength.

Silane III has been sampled to major glass weavers from Dow for testing in polyimide laminates and other high-temperature resins. According to Plueddemann initial results look good. Based on these results six 4" x 6" PEEK/Silane III glass cloth panels will be fabricated and bonded on to supplied honey-cone with a preferred adhesive supplied from Ciba-Geigy Corp.

3) PEEK Prepreg

The evaluation of PEEK carbon composites entered into a new stage of development with the availability of uni-directional carbon prepreg. The prepreg is available from ICI, Great Britian and is designated APC-1 (aromatic polymer composite).

including mechanical properties, chemical and environmental resistance have been performed and documented. The utilization of film and bidirectional cloth to fabricate high quality composites is described. Composite characterization included physical and mechanical properties such as flexural, shear modulus, and Mode I Peel. All test procedures and results are documented in the paper. "Keywords": Composites, Thermoplastic, Semi-crystalline, Graphite, Cloth. "A Comparative Study on Fatigue Behavior of Polyetheretherketone and Epoxy with Reinforced Graphite Cloth"

Abstract: This paper describes the results of a series of fatigue tests conducted on graphite cloth reinforced polyetheretherketone and epoxy matrix composite to evaluate their fatigue performance. The influence of matrix and fiber dominated properties on the fatigue behavior of the laminates was investigated. Different fatigue failure modes were investigated using three types of laminates, $[\pm 45]_{2s}$, $[0/90/\pm 45]_s$, and $[0,90]_{2s}$. Tensile coupons of each laminate were fatigued until final failure or to the prescribed cycle under several fatigue stress levels at laboratory environment. The major parameters studied in this paper were S-N relationship and stiffness change. The damage incurred during fatigue tests was also examined at several intervals of fatigue life by interrupting the fatigue test. The fatigue data indicated that the polyetheretherketone system shows excellent fatigue properties and appears to be superior to the epoxy system in overall fatigue performance.

2) PEEK film/Glass Cloth

An evaluation was initiated to investigate a compatible finish for glass cloth and PEEK resin. The finishes supplied from Dow Chemical were evaluated and are as follows:

- Silane I - B-2014-107D (silane-modified melamine) from hexamethoxymethylmelamine
- Silane II - Z-6020, (N, Beta-aminoethyl-gamma-aminopropyl-trimethoxysilane), $H_2N(CH_2)_2NH(CH_2)_3Si(OCH_3)_3$
- Silane III - 5586-120-10, (monophenylamino functional silane)
- Silane IV - XZ-8-5042, (methoxytolyltrimethoxysilane)
 $(MeO)_3 Si - CH_2OCH_3$

Autoclave processing has begun on this system using an internal pressurized bag to reduce void formation. Void formation seems to result from the volatile nature of the mPDA. As soon as quality composites have been fabricated using this technique or another satisfactory technique a special batch of AS-4 fiber will then be used to fabricate the panels for the program.

3. MATERIAL DEVELOPMENT

a. Polyetheretherketone (PEEK) Composites

The work effort on this material involved three areas of effort. The first was the evaluation of PEEK film and bidirectional graphite cloth. This effort was completed and resulted in two SAMPE papers. The first on the evaluation of mainly static properties and the second on fatigue properties.

A second and small effort looked at combining PEEK film and glass cloth which also involved evaluating some finishes that would improve the bonding between PEEK film and glass cloth.

The last effort and by far the major effort which is ongoing is the evaluation of PEEK prepreg developed by ICI, Great Britain.

1) PEEK film/Graphite Cloth

An abstract of the paper entitled "Polyetheretherketone Matrix Composites" which was presented October 1982 "14th National SAMPE Technical Conference" describes this work. The paper appears in Appendix I. The fatigue work resulted in a paper entitled "A Comparative Study on Fatigue Behavior of Polyetheretherketone and Epoxy with Reinforced Graphite Cloth" which was presented April 1983 "28th National SAMPE Symposium and Exhibition". An abstract describes this work and the entire paper appears in Appendix I. "Polyetheretherketone Matrix Composites", Abstract: Polyetheretherketone resin has been characterized and developed as a matrix for graphite reinforced composites. This resin offers exceptional toughness as well as chemical resistance. Successful processing conditions have been developed using film with bidirectional cloth. Characterization of neat resin properties

<u>Material</u>	<u>Lay-up Orientation</u>	<u>No. of Plies</u>	<u>Size</u>
T300/1034-C	[90/+45/0/-45/90] _s		10" x 10"
"	[90/90/+45/+45/0/0/-45/-45] _s		"
AS4-3502	[0 ₆ /+60/+60/0 ₂] _s		6" x 6"
AS 3501-6	[0] ₁₂	12	6" x 6"
MY720 DDS	0°	12	"
828-mPDA	0°	12	11" x 11"
"	"	"	5 x 5
"	"	"	"
"	"	"	"
"	"	"	"
"	"	"	"
"	"	8	10" x 5"
X-124-76C	0°	12	8 x 12
AS4-3502	0,+45,-45,90,0,+45,-45, 90,90,-45,+45,0/90,-45, +45,0	48	12 x 12
T300/1034-C	[0/+45/90/-45/0/+45/90/ -45] _s	16	24" x 24"
"	[0 ₄ /90 ₄] _T	8	
"	[+15 ₄ /-15 ₄] _T	8	
"	[+30 ₄ /-30 ₄] _T	8	
"	[0 ₄ /90 ₄] _s	16	

2. RELATIONSHIP BETWEEN NEAT RESIN AND IN SITU COMPOSITE PROPERTIES

This is a Task 44 program in which prepreg will be supplied in-house using Hercules graphite fibers and a special lot of Epon 828 epoxy with an mPDA hardener system. The fibers are also a special lot of AS-4 (untreated, oxidized, and epoxy coated). This system will then be used to fabricate composites and generate mechanical properties to understand the relationship between a characterized matrix, a characterized fiber and a yet to be characterized interphase between the two in the composite.

Prepreg tape has been successfully wound with a 40% by weight resin content, the desired amount, using AS-4 fiber with MY720/DDS epoxy resin.

<u>Material</u>	<u>Lay-up Orientation</u>	<u>No. of Plies</u>	<u>Size</u>
AS4-3502	$[90^\circ]_{4T}$	4	12" x 12"
"	$[90^\circ]_{8T}$	8	"
"	$[90^\circ]_{12T}$	12	"
"	$[90^\circ]_{16T}$	16	"
"	$[\pm 45/0/90]_S$	8	24" x 24"
"	$[\pm 45/90_2]_S$	8	"
1034-C	*see below	24	24" x 24"
*Following four panels were made from 1034-C			
	$[0/+45/-45/90/0/+45/-45/90/0/+45/-45/90]_S$		(2 ea.)
	$[0/90/0/90/0/90/0/90/0/90/0/90]_S$		(2 ea.)
	$[0/0/+30/-30/+60/-60/0/0/+30/-30/+60/-60]_S$		(2 ea.)
	$[+45/-45/+45/-45/+45/-45/+45/-45/+45/-45/+45/-45]_S$		(2 ea.)
976	0°	12	6" x 6"
HMF-133-76	$[0_2]_S$		"
"	$[0/30]_S$		"
"	$[\pm 30]_S$		"
"	$[\pm 15]_S$		"
ATS	0°	12	6" x 6"
"	$\pm 45^\circ$	12	"
976/1076	0°	"	"
"	"	"	"
"	"	"	"
"	"	"	"
1034C	$[0/\pm 45/90]_S$	8	24" x 24"
ATS	0° no bag cure	12	6" x 6"
1076-E	" "	"	"
1034-C	0°	"	24" x 24"
ATS	0° no bag cure	"	6" x 6"
1076-E	0°	"	"
T300/1034-C	$[0/+45/-45/90]_S$	8	10" x 10"
"	$[0/90/+45/-45]_S$	8	"
"	$[+30/-30/+30/-30/90/90]_S$		
" alum. @ midpt.	A1 A1		"
	$+30/-30/-30/+30/90/90/90/90/+30/-30/-30/+30$		

<u>Material</u>	<u>Lay-up Orientation</u>	<u>No. of Plies</u>	<u>Size</u>
AS4-3502	$[0_4/90_4]_s$	16	10" x 10"
"	$[0/90/0/90/0/90/0/90]$	"	"
"	$[+45/-45/+45/-45/90_3/\overline{90}]_s$	15	"
"	$[45/90/45/90/45/90/45/90]_s$	15	"
"	$[60/60/60/60/90_3/\overline{90}]_s$	"	"
"	$[60/90/60/90/60/90/60/90]_s$	"	"
"	0°		6" x 10"
"	"		"
"	"		"
"	"		"
MY720DDS	"	12	6" x 6"
			"
1034-C	$[0/\underline{+45}/90]_s$ alum. insert at midplane		10" x 10"
1034-C	$[0/90/\underline{+45}]_s$ alum. insert at midplane		"
"	$[\underline{+30}_2/90_2]_s$ "		"
"	$[0/\underline{+45}/90]_s$ "		"
"	$[0/90/\underline{+45}]_s$ Reruns of prev. panels incorrect template		"
"	$[0/90/\underline{+45}]_s$ used first time		"
"	$[\underline{+30}_2/90_2]_s$		"
HMF-133-34	$[0/90]_{2s}$		"
"	$[0/90/\underline{+60}/\underline{-60}]_s$		"
"	$[0/90/\underline{+75}/\underline{-75}]_s$		"
"	$[\underline{+15}/\underline{-15}/\underline{-15}/\underline{+15}]_{2s}$		"
1034-C	$[0/\underline{+45}/90/\underline{-45}]_{2s}$	16	24" x 24"
"	$[0^\circ]_{20T}$		12" x 12"
"	$[\underline{+45}_2]_s$		6" x 10"
"	0°	12	12" x 12"
"	0°	"	"
AS4-3502	$[30/\underline{-30}/\underline{-30}/30/90/90]_s$ alum. template @ mdplne.	"	9" x 24"

b. Composites Fabricated

<u>Material</u>	<u>Lay-up Orientation</u>	<u>No. of Plies</u>	<u>Size</u>
T300/1034C	$[0/+45/90/-45]_{2s}$	16	24" x 24"
"	$[0_8]_T$	8	12 x 12
"	$[90_8]_T$	8	"
"	$[+45_8]_T$	8	"
"	$[0_{12}]_T$	12	6 x 6 1/2" teflon at mdpt.
"	$[0_{12}]_T$	12	6 x 6 1" teflon at mdpt.
"	$[0_{12}]_T$	12	6 x 6 teflon spray at mdpt.
"	"		6 x 6
"	$[0_2/90_4/0_2]_s$	16	6 x 6 1" alum strip at mdpt.
AS1-3502	$[+45]_{2s}$	8	12" x 12"
AS4-828/DDS	90°	8	6" x 10"
AS4-80/20		8	
ATB/95/5	0°	8	1" x 4"
AS1-E707	0°	16	9 x 10
"	$[+45, \overline{90}]_{2s}$	15	
ATB #4	0° 22 hr cure		1 x 4
AS4-828 DDS	0°	11	3 x 6
AS4-DDS-828	0°	11	6 x 3
AS4-3502	$[+45/90/-45/90/+45/90/-45/\overline{90}]_s$	15	6 x 10
AS1-E707	"	15	6 x 10
AS4-3502	$0_4/90_4$		2 x 2
"	"		6 x 6
"	$[90^\circ_{1s}]_T$		6 x 10
1076-E	$[0^\circ_{12}]_T$		6 x 6
Kevlar MY-720	0°		6 x 6
AS4-3502	90°	4	12 x 12
"	"	8	"
"	"	12	"
"	"	16	"

SECTION I
PROCESSING AND EVALUATION OF COMPOSITES

1. FAILURE RESISTANT COMPOSITE CONCEPTS

a. Mechanical Testing

Routine mechanical testing was accomplished on supplied composite and neat resin samples that were under development and evaluation. The tests performed on these materials included tensile, four-point strain gaged flexure, four-point shear, mode-one peel, three-point flexure, as well as micro-tensile tests. Specimens were instrumented and tested at ambient and elevated temperatures.

A strain measurement system was developed to determine compression and tension modulus values simultaneously of various composites in four-point flexure.

A titanium scissors extensometer was designed and fabricated in order to test composite tensile specimens from -67°F to 600°F using either Instron or Satec environmental chambers.

Development work was initiated on a prototype isodynamic extensometer and calibration fixture for the testing of compact tensile specimens at elevated temperatures above 400°F. This work involved several design changes as the project proceeded. Calibration work was initiated on the final phase of the project using tungsten tensile specimens of the same design as the brittle resin castings. This test phase will include elevated temperature tests to 600°F. In preparation for this work 50 tungsten specimens were prepared.

Computer integration for the Instron test machines was initiated in order to have automatic data acquisition and reduction of all test specimens. Full details of this system will be documented when the work has been completed.

LIST OF TABLES (CONCLUDED)

Table		Page
19	Interfacial Shear Strength Data as a Function of Conditioning Temperature	41
20	Effects of Hygrothermal Conditioning on Neat Epoxy Material Properties	46
21	Surface Atomic Percent Concentration of Conditioned "AS" Fibers as Determined by XPS	52
22	Tensile Strength and Interfacial Shear Strength of Plasma Treated AS1 Fibers	53
23	Quadratic Polynomial Failure Criteria	59
24	Table of Failure Envelopes for $[0/90/+45]_s$ Laminates	71
25	Comparison of First Ply Failure Predictions in Strain Space	71
26	Average Stress Components $\bar{\sigma}_x$ and $\bar{\sigma}_z$, Nonmechanical (Sup.N) and Mechanical (Sup.M), over a Distance h_o (a Ply Thickness) from the Edge	76
27	Result of Static Strength	83
28	Fatigue Data	87
29	Onset of Delamination Under Fatigue (Delamination Occurred Prior to the Indicated Cycle)	122
30	Test Matrix of Mixed Mode Fracture for T300/1034C Graphite/Epoxy	125

LIST OF TABLES

Table		Page
1	Mechanical Properties S-7781 Glass Cloth/Peek Film	9
2	Mechanical Properties PEEK/X-AS	11
3	PEEK Crystallinity	13
4	PEEK Prepreg Processing	14
5	Static Mechanical Properties	17
6	Mechanical Properties Molded	21
7	Room Temperature Fracture Data for 828/mPDA .5"x.5" Compact Tension @ .002"/min Displacement Rate	22
8	Fracture Data for 828/mPDA 14.5 phr 1"x1"x.2" CT @ Room Temperature	23
9	Fracture Data for 828/mPDA 14.5 phr 2"x2"x.5" CT @ Room Temperature	23
10	Compact Tension Data for 828/mPDA 14.5 phr	24
11	828/mPDA Dogbones Tensile Test at R.T. CHS. = .02"/Min.	25
12	828/mPDA Dogbones Tensile Test at R.T. CHS. = .2"/Min.	25
13	G' Data for 828/mPDA	26
14	Density of Standard Cured and 175°C Postcured Stoichiometric Variants of Epon 828/mPDA	26
15	Compact Tension (K_Q) for 5208 Epoxy	27
16	Percent Concentration of Epoxy "n" Values from Liquid Chromatography	28
17	Mean Oxide Interfracture Distance Pre- and Post-Hygrothermal Exposure at 70°C for Five Months	30
18	Mean Oxide Interfracture Distance Pre- and Post-Hygrothermal Exposure at 125°C for ~ 120 Hours	30

TABLE 3
PEEK CRYSTALLINITY

Material	Conditions	% Cry	Notes
APC-1 Prepreg	As-received 36% wt resin	25.1	
APC-1 Prepreg	Quenched from melt	28.4	
APC-1 Composite #5	As-Received after testing	24.1	Tensile Test ± 45
APC-1 Composite #15	As-Received After testing	26.7	Tensile Test ± 45
PEEK Amorphous Film	As-Received	21.3	Amorphous
APC-1 Resin	From prepreg	25.2	Cut from prepreg
APC-1 Composite #15	Before test	27.9	-
APC-1 Composite #10	?	27.2	
APC-1 Composite	Thermal Aged 1000 hr 300°F	28.1	-
APC-2 Prepreg 24% Wt Resin	As-Received	25.78	-
APC-2 Composite 24% wt resin	Slow cooled from melt in press	18.8	-
APC-2 Prepreg	Slow cooled 2°C/min-N ₂	23.9	-
PEEK film/cloth 38% wt resin	Slow cooled from melt in press	31.3	-

TABLE 4
PEEK PREPREG PROCESSING

1. Preheat plattens to 720°F
2. Insert stack in press
3. Allow heating @ 1 min/ply
4. Apply 140-170 psi
5. Heat for 5 min @ 720°F
6. Remove
7. Insert in RT press under pressure
8. Cool rapidly to 50-60°C (120-140°F)
9. Remove

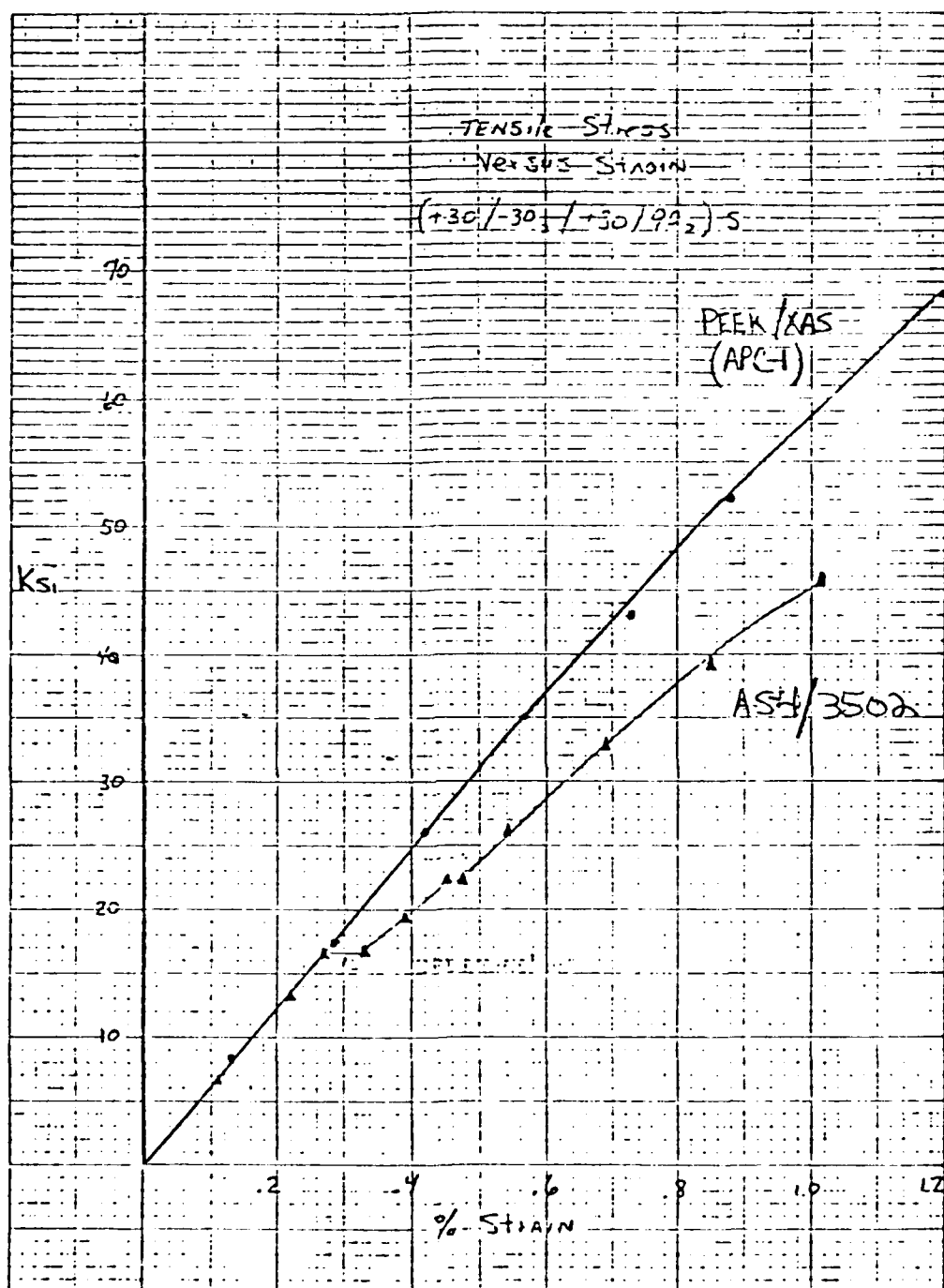


Figure 1. Tensile Stress vs. Strain $(+30/-30_2/+30/90_2)_S$.

of these laminates were fabricated using the picture frame and fast cool down technique. Both laminates possessed considerable voids but were tested just the same. A panel of each of these layups has been requested from ICI to better determine the effect of a high quality low void content specimen for this test. Despite the high void content of the previously described laminates, exceptional properties were obtained again due to the matrix influence. The next test being used to evaluate the toughness of this matrix is the Double Cantilever Beam (DCB) test. This test is used to measure the interlaminar fracture resistance as related to normal stress induced delamination. The critical strain energy release rate is calculated from the test, G_{IC} (in. lbs./in.²). DCB specimens were prepared from fabricated unidirectional 34 ply panels. Although some voids were observed in the panel, G_{IC} values were an order of magnitude higher for the PEEK/graphite over the epoxy, (8-10 in. lbs./in.² vs. 0.8-1 in. lbs./in.²). Despite this fact a panel has been ordered from ICI for retesting.

The following data in Table 5 is on the APC-1 PEEK/X-AS system following the test matrix as was described. Fatigue properties as described in the test matrix have been expanded and are being provided by the Mechanics Group and are discussed in Section IV.

b. Liquid Crystal Polymers (LCP)

Work was initiated to investigate a new thermoplastic from Celanese. These polymers are called liquid crystal because they are crystalline in the melt as well as in the solid state. They are self-reinforcing and are thus anisotropic. Two polymer types were received from Celanese, LCP 2000 and LCP 4060. The LCP 4060 is being developed for a composite matrix resin and this system was received as a unidirectional composite with Celion 6000 carbon fiber. The neat resins were received as injected molded plaques with flow lines of a nature to allow one to cut a tensile bar from each extreme of the plaque. The LCP 4060 was tested in 0° and 90° tension. The composite of LCP 4060 with 48%

TABLE 5
STATIC MECHANICAL PROPERTIES
TEST MATRIX

PEEK/XAS
APC-1

	-67°F	72°F	250°F	350°F
0° - Tensile Strength (ksi)		263.57	216.92	205.9
0° - Tensile Modulus (msi)		17.56	16.00	16.12
0° - % Strain-to-failure		1.39	1.22	1.14
0° - Poisson's Ratio			.375	.340
90° - Tensile Strength (ksi)		12.47	6.88	4.93
90° - Tensile Modulus (msi)		1.47	0.774	0.242
90° - % Strain-to-failure		0.88	2.23	5.09
+45° - Tensile Strength (ksi)		42.84		
+45° - Tensile Modulus (msi)		1.77		
+45° - % Strain-to-failure		18.95		
Quasi-isotropic Tension Strength (ksi)		98.81	87.10	74.39
Quasi-isotropic Tensile Modulus (msi)		6.54	6.14	5.69
Quasi-isotropic % Strain-to-failure		1.64	1.40	1.32
Quasi-isotropic - Poisson's Ratio		.286		
"Edge Delamination"				
[+30/90] - Tensile Strength (ksi)		61.92		
Tensile Modulus (msi)				
% Strain-to-failure		1.12		
"First Ply Failure"				
[+45/90] - Tensile Strength (ksi)				
Tensile Modulus (msi)				
% Strain-to-failure				

TABLE 5 (CONTINUED)
STATIC MECHANICAL PROPERTIES
TEST MATRIX

PEEK/XAS
APC-1

	-67°F	72°F	250°F	300°F	350°F
0° - Compression Strength (ksi)					
0° - Compression Modulus (msi)					
0° - Compression Strain-to-failure %					
Quasi-isotropic Compression Strength Modulus					
" " Strain-to-failure					
0° - 4 pt flexure					
Dry - Strength (ksi)		234.4	186.2	131.9	95.4
Dry - Modulus (msi)		16.73	17.60	14.43	12.05
Wet - Strength (ksi)		244.0	162.2	120.3	93.0
Wet - Modulus (msi)		17.80	16.17	14.07	12.75
TA - Strength		242.0	178.2	159.0	105.5
TA - Modulus (msi)		17.82	17.38	17.18	14.01
FV = 56%					
Wet = 0.2% equilibrium moisture gain: 160°F underwater					
TA = 1000 hrs @ 300°F circulating air oven					
4 pt.					
0° - Flexure Strength (ksi)		234.4	186.2	131.9	95.4
0° - Flexure Modulus (msi)		16.73	17.60	14.43	12.05

TABLE 5 (CONCLUDED)
STATIC MECHANICAL PROPERTIES
TEST MATRIX

PEEK/XAS
APC-1

	-67°F	72°F	250°F	300°F	350°F
4 pt 90° - Flexure Strength (ksi) 90° - Flexure Modulus (msi) 90° - Flexure Strain-to-failure %	18.70 1.59 1.05	20.25 1.46 1.52	19.04 1.66 S. G. failed	13.07 1.14 S. G. failed	10.03 0.67 S. G. failed
0° - 4 pt - interlaminar shear (ksi)		12.61	9.65	9.13	8.21
In-plane shear (+45)			Note: Tensile failure @ RT Comp & deformation @ 250°F +		
Rail Shear					
MODE-I DCB G_{IC} in. lbs./in ²		8-10			

FV of carbon was tested in flexure at RT and 235°F. The data is shown in Table 6. As noted in the table the mode of failure is compression at 235°F. The reason may be due to its low Tg or its low fiber volume. The Tg of the neat resin 4060 is approximately 100°C. In previous analysis of semi-crystalline thermoplastic materials useful properties were found above its Tg. This material may not follow the previous experience due to the nature of the material. The evaluation of the neat resin for chemical resistance was completed. Tensile dogbones were machined in the ordered direction (0°) and static loaded to 1000 psi while the gauge section was saturated with the agents of interest. The agents used are as follows: dichloromethane, skydrol (hydraulic fluids), and A. F. paint stripper. No effect was noticed after one week and the testing was terminated.

Moisture aging was completed on the 48% F.V. LCP-4060/C-6000 composite. The specimens were aged under water at 160°F for 72 days until an equilibrium moisture gain of 0.21% occurred. Flexure specimens were tested at 235°F against the 235°F dry condition. A dropoff of flexure strength was noticed as it achieved 71% of the hot dry condition.

Additional composites were evaluated as supplied from Celanese Research Company. Specimens with a higher fiber volume showed no improvement over the lower fiber volume composites. A Mode I specimen was tested with poor results. It is thought that the fiber may be interfering with the morphology of the LCP in the composite, thus preventing the translation of good fiber and neat resin properties. This information was transferred to the people concerned at Celanese Research Co. and no additional work is planned on this system.

TABLE 6
MECHANICAL PROPERTIES MOLDED
Neat Resin
LCP-4060

RT - Tensile	Strength 10^3 psi	Mod 10^6 psi	[%] Strain to failure
0° orientation	23.23	1.67	2.09
RT - Tensile			
90° orientation	7.23	0.484	2.16

Composite
LCP-4060/C-6000 48% FV

<u>3-pt Flexure</u>			
0° RT 32-1	220.9	14.95	-
0° 235°F* 32-1	119.2	13.40	-
90° Tensile RT	4.27	.856	0.495

* Mode of failure was compression which may be due to a low fiber volume or low Tg.

SECTION II
ADHESIVE BONDED JOINTS

1. EXPERIMENTAL MATRICES

a. Epon 828/MPDA

A program was initiated this past year to characterize Epon 828 epoxy resin with meta-phenylene diamine (MPDA) curing agents including 7.5, 10, 14.5 (stoichiometric), 20, and 25 parts per hundred resin (phr).

The 828 epoxy was selected to be used as a model compound for development of evaluation techniques that will be employed to characterize other polymers to be used in fiber reinforced composites.

Three methods that have been used for evaluation are: (1) compact tension (CT) for fracture energy determination; (2) tensile testing in neat dogbone configuration; and (3) rheology to determine physical properties.

Initial testing of CT specimens was done on .5"x.502" specimens with a nominal thickness of .125". Data on the effects of curing agent variants of 828/MPDA on the fracture characteristics are shown in Table 7. K_Q has a maxima at stoichiometry.

TABLE 7
ROOM TEMPERATURE FRACTURE DATA FOR 828/MPDA
.5"x.5" COMPACT TENSION @ .002"/MIN DISPLACEMENT RATE

<u>MPDA (phr)</u>	<u>No. of Spec's</u>	<u>Avg. K_Q</u>
7.5	2	.486
10	12	.499
14.5	4	.845
20	4	.807
25	1	.730

For the stoichiometric system, CT specimens 1"x1"x.2" and 2"x2"x.5" were tested to determine the specimen size effect on the K_Q values (see Tables 8 and 9). K_Q appears to be independent of specimen size providing that critical geometric ratios are maintained.

Strain rate effects on 828/MPDA 14.5 phr are shown in Table 8. Those specimens were nominal 1"x1"x.2" CT specimens.

TABLE 8
FRACTURE DATA FOR 828/MPDA 14.5 phr
1"x1"x.2" CT @ ROOM TEMPERATURE

Sample No.	Test Rate (in./min.)	Avg. K_Q
MA01F-5	.004	.726
MA01F-6	.004	.711
MA01F-7	.004	.767
MA01F-8	.04	(First Crack .745)
9	.04	(Second Crack .868)
MA01F-3	.001	.832
MA01F-4	.001	.803

TABLE 9
FRACTURE DATA FOR 828/MPDA 14.5 PHR
2"x2"x.5" CT @ ROOM TEMPERATURE

Spec. No.	Strain Rate (in./min.)	Avg. K_Q
MA01F-2F1	.004	.732
MA01F-2F2	.004	.714
MA01F-2F3	.008	.708
MA01F-2F4	.008	.707

Temperature effects on the K_Q value of 828/MPDA 14.5 phr are shown in Table 10. Those specimens were CT tested at room temperature (RT), 60°C, 90°C, 120°C, 130°C, and 150°C.

Tensile dogbone testing on .040" thick specimens with MPDA variants and two decade strain rates were tested for curing agent and strain rate effects. Data are shown in Tables 11 and 12. Similar trends are observed in the data for both the 0.02 and 0.2 in./min. strain rate.

Rectangular torsion (beam configuration) tests were performed on the RMS test machine on 828/MPDA with curing agent concentrations of 7.5, 10, 14.5, 20, and 25 phr.

TABLE 10
COMPACT TENSION DATA FOR 828/MPDA 14.5 phr

Spec. No.	Spec. Thickness (in.)	Temp. of Test	K_Q (MPa·m ^{1/2})
MA01D-F1	.125	R.T.	.761
" F2	.125	"	.772
MA01B-F4	.100	"	.748
" F5	.100	"	.743
MA01D-F3	.125	60°C	.752
" F4	.125	"	.936
MA01B-F6	.100	"	1.445
" F7	.100	"	1.040
" F7B	.100	"	1.370
MA01D-F5	.125	90°C	1.567
" F6	.125	"	1.127
MA01B-F8	.100	"	1.994
" F8A	.100	"	1.739
" F9A	.100	"	1.929
MA01D-F7	.125	120°C	2.203
" F8	.125	"	1.961
MA01B-F11	.100	"	1.907
" F12	.100	"	1.939
MA01B-F15	.100	130°C	1.790
MA01D-F9	.125	150°C	1.484
" F10	.125		1.419
MA01B-F14	.100		0.907

TABLE 11
828/mPDA DOGBONES TENSILE TEST AT R.T.
CHS. = .02"/MIN.

mPDA Conc.	Stress (psi)	% Strain	Modulus
7.5 phr	9557	1.63	714,000
10	13,714	3.43	609,000
14.5	13,378	4.68	503,800
20	12,928	5.08	528,700
25	13,929	4.72	579,000

TABLE 12
828/mPDA DOGBONES TENSILE TEST AT R.T.
CHS. = .2"/MIN.

mPDA Conc.	Stress (psi)	% Strain	Modulus
7.5 phr	8178	1.34	727,000
10	13,935	2.54	719,300
14.5	13,649	3.9	563,300
20	14,072	5.0	534,300
25	15,054	4.5	612,700

G' data were extracted from the rheometric data for the five concentrations of 828/MPDA and are presented in Table 13.

TABLE 13
G' DATA FOR 828/MPDA

<u>MPDA (phr)</u>	<u>RT Modulus</u>	<u>RT Tan δ</u>	<u>Rubber Modulus</u>	<u>Tg</u>
7.5	1.5×10^{10}	$\sim 1.5 \times 10^{-2}$	9×10^6	58°C
10	1.2×10^{10}	$\sim 1.5 \times 10^{-2}$	4×10^7	101°C
14.5	1.1×10^{10}	2.5×10^{-2}	1.5×10^8	167°C
20	1.1×10^{10}	2×10^{-2}	7×10^7	133°C
25	1.3×10^{10}	1.7×10^{-2}	2×10^7	112°C

Density measurements were made on a series of stoichiometric variants of Epon 828/MPDA, namely 7.5, 10, 14.5, 20, and 25 phr MPDA. One set of samples was cured per usual at 75°C for two hours followed by 125°C for two hours. The other set received a postcure at 175°C for six hours in argon in addition to the standard cure schedule. Densities were measured in a density gradient column of sodium fluoride and water maintained at 18°C. The reported values in Table 14 have a theoretical accuracy of ± 0.0001 gm/cc. Postcuring at 175°C results in a density reduction for these materials.

TABLE 14
DENSITY OF STANDARD CURED AND 175°C POSTCURED
STOICHIOMETRIC VARIANTS OF EPON 828/MPDA

<u>MPDA Concentration (phr)</u>	<u>Density (gr/cc)</u>	
	<u>Standard Cured</u>	<u>Postcured</u>
7.5	1.2134	1.2131
10	1.2144	1.2106
14.5	1.2134	1.2106
20	1.2147	1.2142
25	1.2173	1.2166

epoxy-compatible coating applied by the manufacturer and designated in this report as AS1-C. In addition, a fiber similar to AS1 and designated as AS was evaluated at 20°C only. All fibers were manufactured by Hercules, Inc..

Specimens were fabricated using Epon 828 resin cured with 14.5 phr mPDA. A curing schedule of two hours at 75°C followed by two hours at 125°C was rigidly maintained.

Details of specimen fabrication have been reported previously.⁽⁶⁾

2) Results and Discussion

(a) 20°C

When tested in the saturated condition (WET), the three fiber systems studied all exhibit a depression in interfacial shear strength (see Table 19). The AS system exhibits the greatest magnitude in change with over a 50 percent reduction of τ (10.7 ksi "as received" vs. 4.9 ksi WET). Dehydration results in nearly full recovery to "as received" values for each respective fiber. Tested AS/WET samples when dehydrated and retested only partially recovered their original shear strength (6.2 ksi WET (σ)/DEHYD vs. 10.7 ksi "as received"). No recovery in τ was attained when the tested AS1/WET and AS1-C/WET specimens were dehydrated and retested. The photoelastic stress patterns for WET or DEHYD samples are unchanged in character with respect to the "as received" case except for the AS/WET which is much more diffuse (see Figures 7-10).

Paralleling the reversibility of interface properties are the neat resin material properties. Moisture loss was unavoidable when measuring T_g . Consequently, the T_g values are valid only as a qualitative indicator of the material response to water sorption. Both T_g and tensile modulus are depressed in samples conditioned at 20°C. Dehydration at 20°C results in almost full recovery of these properties (see Table 20).

(b) 70°C

Conditioning at 70°C results in greater reduction of τ than 20°C conditioning for AS1 and AS1-C systems

result in a lower signal-to-noise ratio after deconvolution compared to scan C. Note also that the MgK α satellite peak has been eliminated in scan B.

Selected carbon spectra are being analyzed more carefully using these two programs. Future fiber work will encompass the use of these programs to reduce data collection time and improve quantitative information.

b. Moisture Effects on Carbon fiber/Epoxy Interfacial Properties

To investigate the degradation mechanisms of carbon fiber-epoxy matrix composites, a series of single filament coupons was hygrothermally conditioned at either 20, 70, or 125°C until saturated. Interfacial shear strength (τ) was calculated according to the relationship

$$\tau = \frac{\sigma_f}{2\beta} \Gamma\left(1 - \frac{1}{\alpha}\right)$$

where σ_f is the fiber tensile strength at the critical length ℓ_c , α and β are the Weibull shape and scale parameters of the length to diameter aspect ratio distribution, and Γ is the gamma function.⁶ Specimens were tested in the hydrated state (WET) as well as the dehydrated state (DEHYD) which is the result of a single hydration/dehydration cycle. Dehydration was accomplished by heating the samples at the same conditioning temperature except for the 20°C series which was dried at 50°C for the sake of expediency. In addition to measurement of τ , the photoelastic stress pattern for each fiber/conditioning temperature was documented to qualitatively assess stress distribution at the interphase. Matrix response to conditioning was evaluated by measurement of tensile modulus on strain gaged specimens and by measurement of Tg by thermal mechanical analysis (TMA). X-ray photoelectron spectroscopy was used to evaluate fiber surface chemistry as a function of conditioning temperature.

1) Materials

Two fibers were used in this study: 1) a surface treated type II PAN based AS1 fiber; and 2) AS1 fibers with an

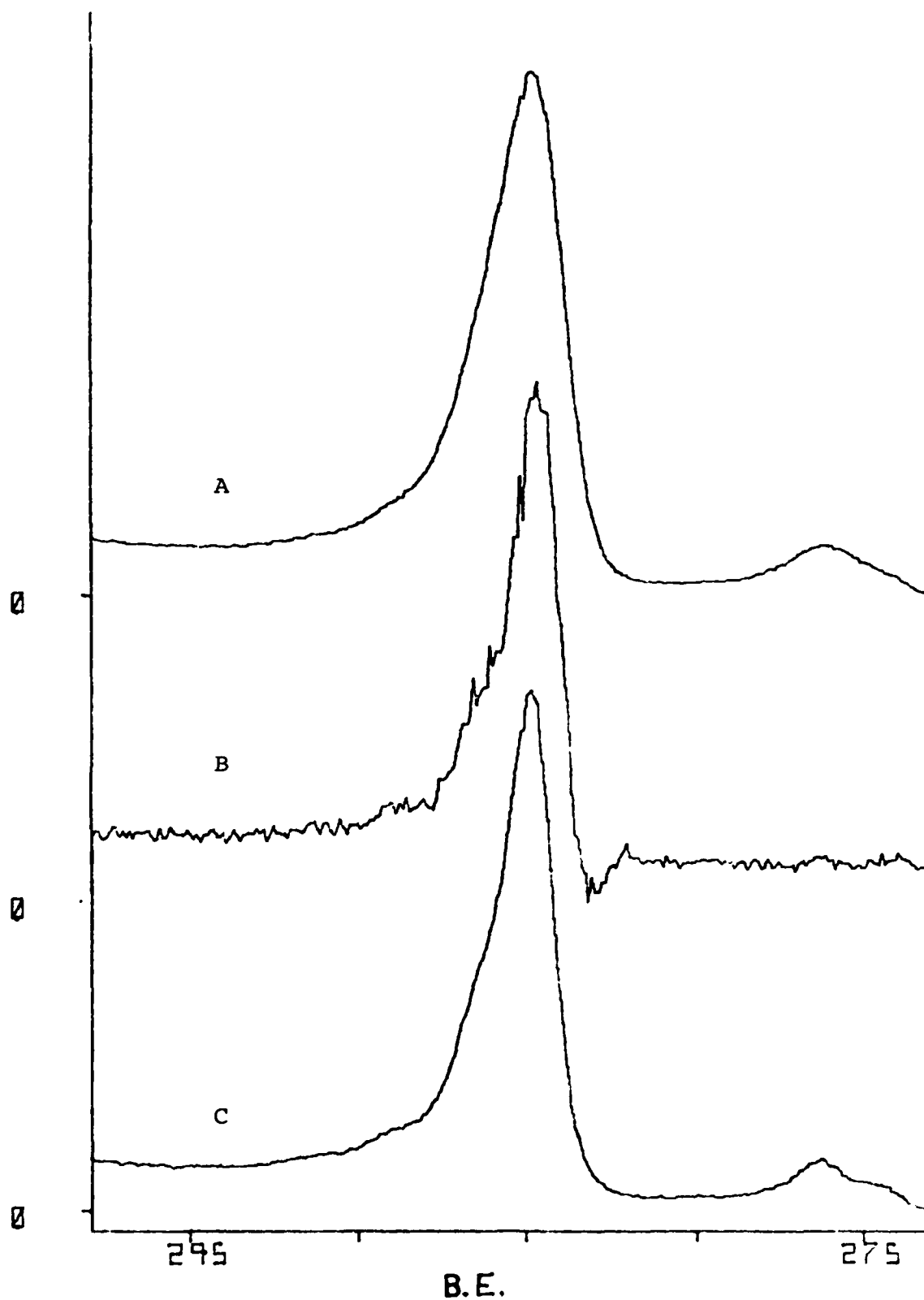


Figure 6. Carbon 1s Photoelectron Spectra Obtained from a Carbon Fiber Specimen. (A) Low Resolution Spectrum; (B) Low Resolution Spectrum After Deconvolution; (C) High Resolution Spectrum.

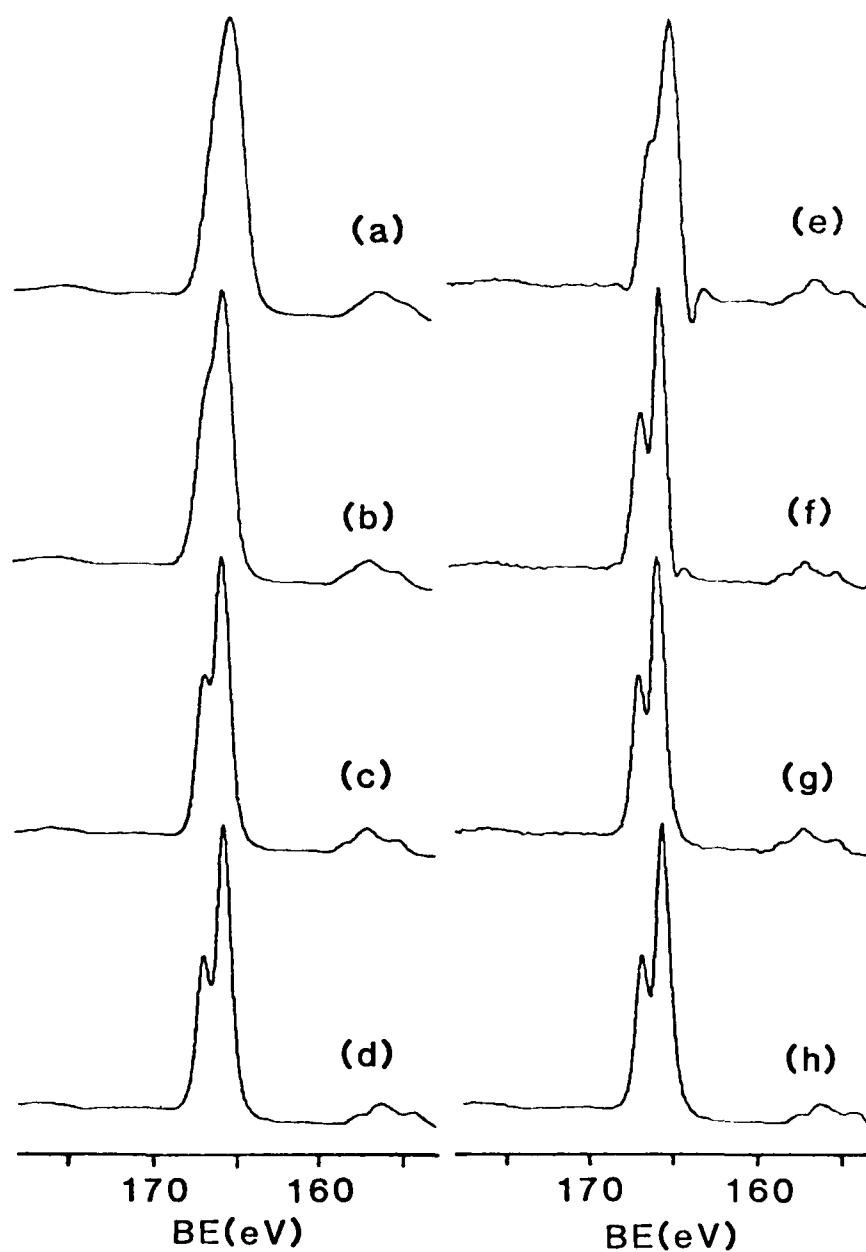


Figure 5. S 2p XPS Spectra from MoS_2 Obtained Using a Mg $K\alpha$ X-ray Source with Analyzer Resolutions of (a) 1.3, (b) 0.78, (c) 0.46, and (d) 0.26 eV. Dwell time was 2s, step width 0.1 eV, and 10 scans were taken. The results obtained after deconvoluting the data in (a), (b), (c), and (d) with Gaussians representing the four analyzer resolutions are shown in (e), (f), (g), and (h), respectively.

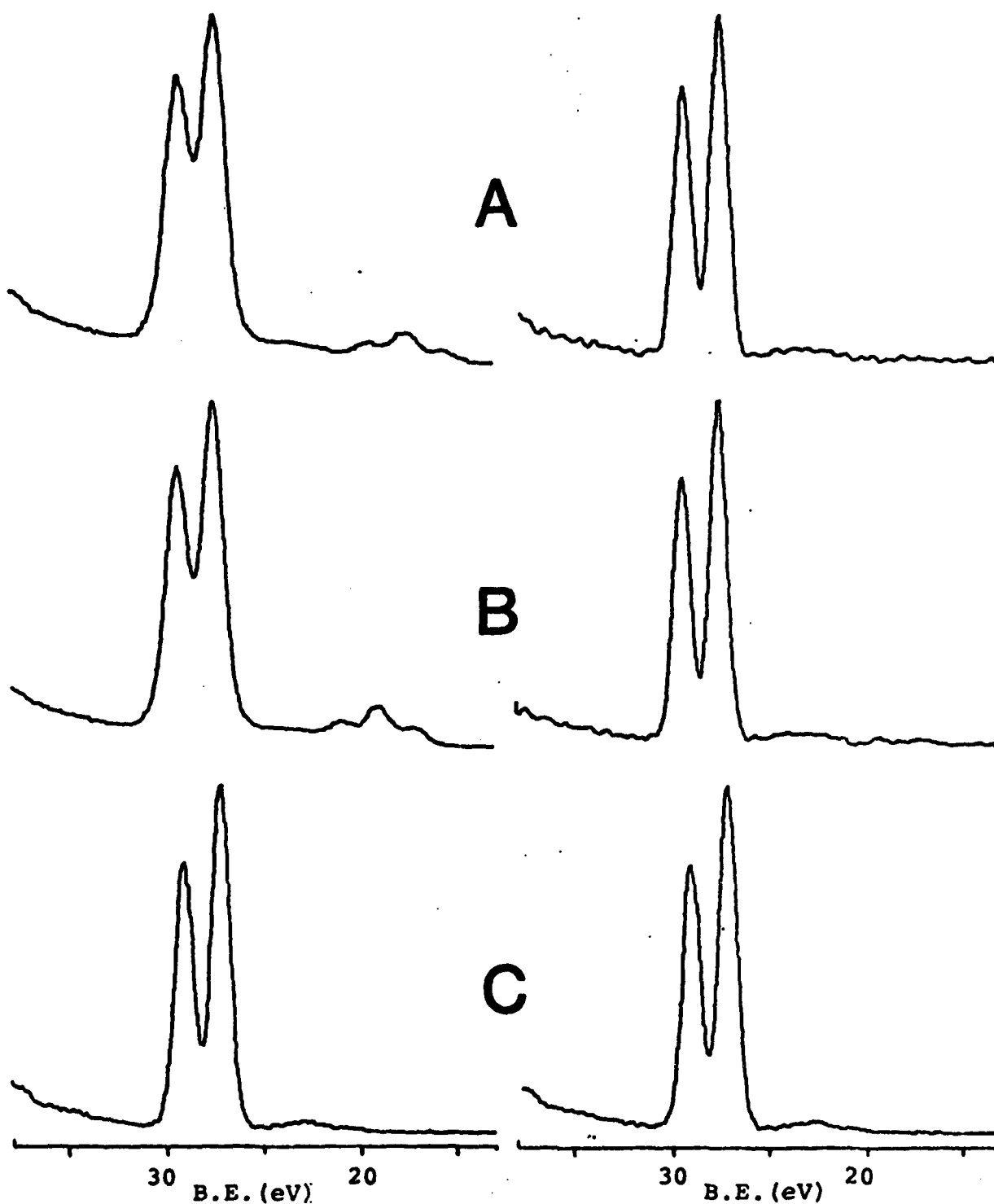


Figure 4. Spectra of the Ta_{4f} Photoelectron Peaks from Ta_2O_5 Using (A) Aluminum X-rays, (B) Magnesium X-rays, and (C) Monochromatized Aluminum X-rays. The raw data is on the left and the results after removing the x-ray broadening by deconvolution are shown on the right.

Figure 4 shows high resolution scans of the tantalum 4f peaks from an anodized piece of Ta_2O_5 . The spectra on the left side have all been taken at the same instrument settings for the three x-ray sources on this spectrometer, i.e., $MgK\alpha$, $AlK\alpha$, and monochromatic $AlK\alpha$. The spectra on the right have been deconvoluted to remove the respective x-ray lineshapes from the data. Notice that all the spectra exhibit improved separation of the two peaks, and all spectra are virtually identical to each other, which is to be expected if the x-ray lineshapes have been accurately removed from these spectra.

Figure 5 shows XPS spectra of the sulfur 2p doublet from a MoS_2 crystal. The spectra on the left have been recorded using $MgK\alpha$ x-rays with various instrument resolution settings. On the right are the results of deconvoluting to remove the instrument broadening function. As expected, the three lower spectra are identical after deconvolution; however, the top spectra, taken at the lowest resolution, looks quite different and a bit distorted. This points out that there is a limit on the amount of improvement which can be expected from deconvolution, namely 30 percent improvement in the full width at half-maximum (FWHM) of each peak. This limitation has also been noted by other workers.⁵

The main value in using deconvolution is a savings in data acquisition time to record spectra while still maintaining the ability to retrieve a high resolution scan from the data, if necessary. An example of the usefulness of deconvolution for carbon fiber data is shown in Figure 6. This figure shows three carbon 1s XPS spectra acquired from a bundle of AS4 fibers which had been coated with DER330 epoxy by the manufacturer and subsequently extracted with methyl ethyl ketone to remove this coating. Scan A is a low resolution scan which took 25 minutes to accumulate, scan B is the same data after deconvolution, and scan C is a high resolution scan of the same specimen which took four hours and 10 minutes to acquire. As is evident from this figure, the resolution of scans B and C is comparable, yet scan B required only 1/10 of the time to acquire. However, this shorter acquisition time did

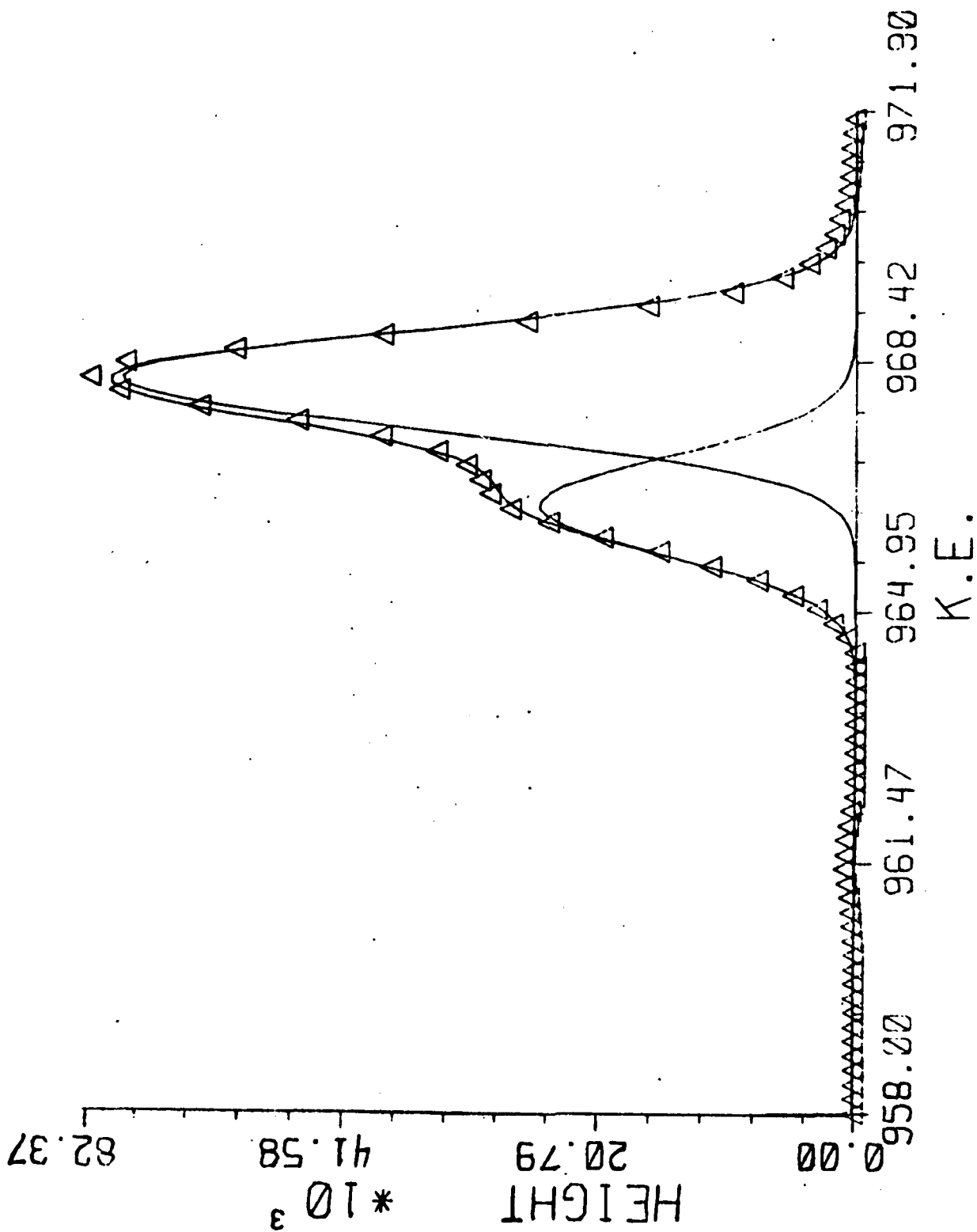


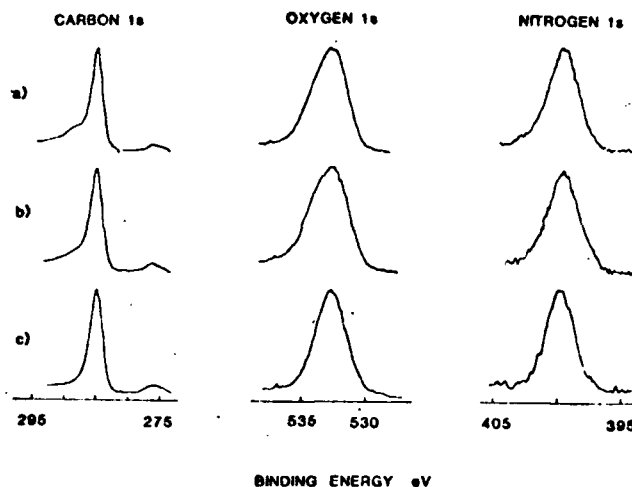
Figure 3. Carbon 1s Peak from a DER330-Coated AS4 Fiber (#F070). Triangles represent the data points, and solid lines show the two component peaks and their sum.

compatible for use as input to the PRIME computer has been successfully completed and tested. This has improved the data interpretation and quantification capabilities of the XPS system by permitting use of powerful computing techniques to be used. Two computing routines that are particularly useful for XPS data and now available on the PRIME computer are curve-fitting and deconvolution.

The curve fitting computer program uses nonlinear regression to fit Gaussian or Lorentzian peaks to a set of overlapping data peaks. The peak heights, widths, and positions can be specified and either held constant or allowed to vary. A fixed peak height ratio can also be specified when fitting pairs of doublet peaks. The variable parameters are then optimized by the program and the "best fit" values displayed. The program then graphically displays the data, the individual component peaks, and the "best fit" line through the data points.

An example of this procedure is shown in Figure 3 which is a graph of the carbon 1s spectrum from an AS4 fiber coated with approximately 1000Å of DER330 epoxy. This spectrum has been fitted with two component peaks of equal width (1.8 eV). The curve-fitting result shows a separation of 1.8 eV for these two peaks, which is within the range expected between carbon-singly-bonded-to-carbon peaks and carbon-singly-bonded-to-oxygen peaks.³ The ratio between the two peaks, 0.41, is in excellent agreement with the theoretical yield from this epoxy, 0.43, which was calculated from the molecular structure of the repeat unit in this epoxy. Analysis of the data from the pure compounds will permit a more direct method of determining the type of bonding existing on the fiber surface.

The deconvolution computer program uses the van Cittert iterative technique⁴ to mathematically remove x-ray and analyzer induced broadening of the XPS peaks, thereby improving the resolution of the data. These two broadening functions have been accurately determined for the KRATOS XPS system in our lab, which is equipped with three x-ray sources and four different analyzer slit widths. The effects of using deconvolution to remove x-ray and analyzer broadenings can be seen in Figures 4 and 5, respectively.



Surface Concentrations
(atom percent)

	<u>Carbon 1s</u>	<u>Oxygen 1s</u>	<u>Nitrogen 1s</u>
a)	82%	11%	4.5%
b)	86%	10%	2.5%
c)	89%	8.5%	1.0%

Figure 2. XPS Spectra of the Carbon 1s, Oxygen 1s, and Nitrogen 1s Regions for Three Hygrothermal Conditions: a) AS Fiber "As Received", b) AS Fiber After 70°C Treatment, and c) AS Fiber After 125°C Treatment, and a Table of the Surface Concentrations of these Elements.

temperature ($\sim 5 \times 10^{-5}$ Torr). Since the x-ray photoelectron spectrometer requires a pressure of 10^{-7} or lower to operate satisfactorily, cooling the sample down to liquid nitrogen temperatures was necessary to solve this problem. The resulting carbon and oxygen spectra were especially broad, indicating that some differential sample charging was occurring.

During the past year the necessary hardware and software have been received and installed to permit the transfer of data from our x-ray photoelectron spectrometer to the PRIME computer located in Building 652 of the Materials Laboratory. A computer program to convert the XPS data file structure to a structure

to analyze these compounds to generate reference spectra which can be used to interpret spectra from the carbon fibers. Analyzed were a graphite single crystal, polyethylene, polyethylene glycol, poly (n-vinyl carbazole), and two epoxy resins similar to Epon 828. Each of these compounds contains a different type of C-C or C-O bond which results in different characteristic carbon and oxygen XPS spectra. The line positions of the carbon and oxygen peaks as measured from these compounds can be used to interpret the types of carbon and oxygen bonding present on the carbon fiber surfaces.

To investigate the degradation mechanisms of composite properties in response to moisture sorption, a series of single filament coupons were conditioned in water vapor at either 20°C or 125°C until saturated. XPS was conducted on AS fibers before and after hygrothermal exposure for two weeks at either 70°C or 125°C. Samples were dried in argon prior to analysis. The atomic percent concentration of carbon, oxygen, and nitrogen were determined and are tabulated in Figure 2. The 125°C treatment altered the surface concentrations of these three species, indicating that some reduction of the oxidized fiber surface occurred with this treatment. The high resolution scans of the carbon 1s and oxygen 1s peaks confirm this finding. From Figure 2 it can be seen that the small carbon 1s peak at ~289 eV BE, which is clearly visible in the spectrum obtained from the AS fiber in the "as received" condition, is completely absent in the spectrum from the AS fiber after treatment at 125°C. This peak is due to -COOH and -COOR groups on the fiber surface. Also, the C 1s peak has broadened due to an increase in C=O and C-O bonding on the surface. Likewise, the oxygen 1s peak has lost intensity on the high binding-energy side which signifies a loss in -OH groups on the surface. These together indicate the reduction of -COOH and -COOR groups to aldehyde and ketone groups on the fiber surface.

The interaction of 1,3-phenylenediamine (mPDA) with the carbon fiber surface is now being investigated. Initial attempts at obtaining an XPS spectrum of the pure mPDA were unsuccessful because of the relatively high vapor pressure of mPDA at room

125°C, respectively. In each case ℓ_o decreases after conditioning. This reduction is most likely attributable to degradation of the anodic oxide fracture strength. Further experimentation in this area is ongoing.

TABLE 17
MEAN OXIDE INTERFRACTURE DISTANCE PRE- AND POST-HYGROTHERMAL
EXPOSURE AT 70°C FOR FIVE MONTHS

<u>Alloy</u>	Mean Interfracture Distance	
	<u>Pre-Exposure (inches)</u>	<u>Post-Exposure (inches)</u>
Al-99.99%	$1.6121 \cdot 10^{-3}$	$1.4262 \cdot 10^{-3}$
Al-99.99%	$1.5753 \cdot 10^{-3}$	$1.3250 \cdot 10^{-3}$
2024-T4	$4.87 \cdot 10^{-4}$	$4.15 \cdot 10^{-4}$
2024-T4	$4.92 \cdot 10^{-4}$	$4.02 \cdot 10^{-4}$
6061-T3	$4.63 \cdot 10^{-4}$	$3.56 \cdot 10^{-4}$

TABLE 18
MEAN OXIDE INTERFRACTURE DISTANCE PRE- AND POST-HYGROTHERMAL
EXPOSURE AT 125°C FOR ~120 HOURS

<u>Alloy</u>	Mean Interfracture Distance	
	<u>Pre-Exposure (inches)</u>	<u>Post-Exposure (inches)</u>
Al-99.99%	$1.6 \cdot 10^{-3}$	$1.2 \cdot 10^{-3}$
2024-T4	$4.62 \cdot 10^{-4}$	$4.52 \cdot 10^{-4}$
6061-T6	$4.64 \cdot 10^{-4}$	$3.56 \cdot 10^{-4}$

2. CARBON FIBER/EPOXY INTERPHASE

a. XPS of Carbon Fibers

A number of pure compounds were analyzed this year by means of x-ray photoelectron spectroscopy (XPS). It was necessary

SECTION III

INTERFACE/INTERPHASE CHARACTERIZATION

Performance of adhesively-bonded structures is intimately linked to the structure and properties of the interphase that exists between constituent members. The interphase is a complex region influenced by a number of variables such as bulk properties, surface morphology, and surface chemistry of each component. This section attempts to assess interphase parameters governing adhesion, and ultimately performance, in bonded materials. Two systems were studied, namely the aluminum oxide/epoxy interphase and the carbon fiber/epoxy interphase.

1. ALUMINUM OXIDE/EPOXY INTERPHASE

a. Experimental

Recent efforts have been directed at evaluating the effects of water on aluminum oxide/epoxy interphase properties. Test specimens consist of phosphoric acid anodized aluminum wires axially aligned in an epoxy matrix tensile coupon. Application of tensile load to the specimen induces multiple radial cracks within the oxide. The mean oxide interfracture distance (l_o) is sensitive to changes occurring at the interphase. In this study l_o was measured prior to and after hygrothermal conditioning. A detailed account of the testing technique can be found elsewhere.¹ Previous work on hygrothermal effects on aluminum oxide/epoxy interphase properties has been reported.²

b. Materials

Three aluminum wires of different composition are currently being studied: 99.99 percent pure Al, 2024-T3, and 6061-T6. The wires have diameters of 0.005 in. prior to phosphoric acid anodization at 60 volts for 20 minutes. The matrix used is Epon 828 cured with 14.5 phr mPDA. A cure schedule of two hours at 75°C followed by two hours at 125°C was rigidly maintained.

Tables 17 and 18 report the mean oxide interfracture distance before and after hydrothermal conditioning at 70°C and

dissolved in a solution of 60 percent tetrahydrofuran (THF) and 40 percent hexane by volume and separated using a Waters Associates Prep. LC/system 500 with a silica column. Peak separations of the various fractions were not well defined, requiring a second pass through. Following separation analysis was done using a Waters Associates model 244 liquid chromatograph using a silica column and a carrier of 55 percent THF and 45 percent hexane. Table 16 contains the results, including the original Epon 1001F, the N=2 fraction, and the N=4 fraction. Note that in the original 1001F sample, the N=2 component is only 21 percent of the total. The collected n=2 and n=4 fractions will be used to study crosslink density in the cured epoxy. Liquid chromatographic analysis of other long chain bisphenol A-epichlorohydrin epoxies is ongoing.

TABLE 16
PERCENT CONCENTRATION OF EPOXY "n" VALUES
FROM LIQUID CHROMATOGRAPHY

Repeat Unit "n" Value	Original Epon 1001F	Concentrated N2 Fraction	Concentrated N4 Fraction
0	25	6	1
1	3	10	1
2	21	73	13
3	6	9	15
4	14	1	55
5	6	< 1	12
6	9	< 1	< 1
7	4		
8	4		
9	3		
10	3		

b. 5208 Epoxy

CT testing was done on 5208 epoxy .5"x.5"x.1" chips to determine temperature effects on K_Q values. Data are shown in Table 15.

TABLE 15
COMPACT TENSION (K_Q) FOR 5208 EPOXY

Spec. No.	Test Temperature	K_Q (MPa·m ^{1/2})
CL-1	RT	.540
CL-2		.527
CLA-1		.510
CL-3	100°C	.432
CLA-2		.368
CLA-3		.381
CLA-4		.368
CL-4	150°C	.378
CL-5		.368
CL-6		.350
CLA-5		.327
CLA-6		.363
CLA-7		.310
CL-7	200°C	.528
CL-8		.542
CL-9		.511
CLA-8		.504
CLA-9		.473
CLA-10		.468
CL-10	250°C	.238
CL-12		.212
CLA-11		.157
CLA-12		.161
CLA-13		.162

c. Liquid Chromatography Studies of High "n" Epoxy Monomers

Fractionation of Epon 1001F, an epoxy derivative of bisphenol A and epichlorohydrin that is marketed as having N=2 chain length, was attempted to isolate the N=2 component. The epoxy was

TABLE 19
INTERFACIAL SHEAR STRENGTH DATA AS A FUNCTION OF
CONDITIONING TEMPERATURE

		Conditioning Temperature	α	β	σ_f $\times 10^3$ psi	τ $\times 10^3$ psi
AS	as received	None	3.3	41.7	680	10.6
AS	WET	20°C	3.3	85.1	630	4.8
AS	DEHYD	20°C	3.5	45.3	680	9.6
AS	WET(σ)/DEHYD	20°C	3.6	66.4	650	6.2
AS1	as received	None	3.5	38.8	650	10.7
AS1	WET	20°C	3.7	49.5	615	7.8
AS1	DEHYD	20°C	3.3	43.5	630	9.4
AS1-C	as received	20°C	3.1	26.8	675	16.0
AS1-C	WET	20°C	3.5	40.7	650	10.2
AS1-C	DEHYD	20°C	4.0	32.0	665	12.8
AS1	WET	70°C	3.2	61.2	580	6.2
AS1	DEHYD	70°C	3.6	46.12	625	8.6
AS1-C	WET	70°C	3.7	47.8	625	8.2
AS1-C	DEHYD	70°C	3.9	45.0	620	8.5
AS1	WET	125°C	2.5	211.0	570	2.0
AS1	DEHYD	125°C	3.5	83.1	630	4.8
AS1-C	WET	125°C	3.6	46.1	650	9.0
AS1-C	DEHYD	125°C	3.2	46.7	650	9.1

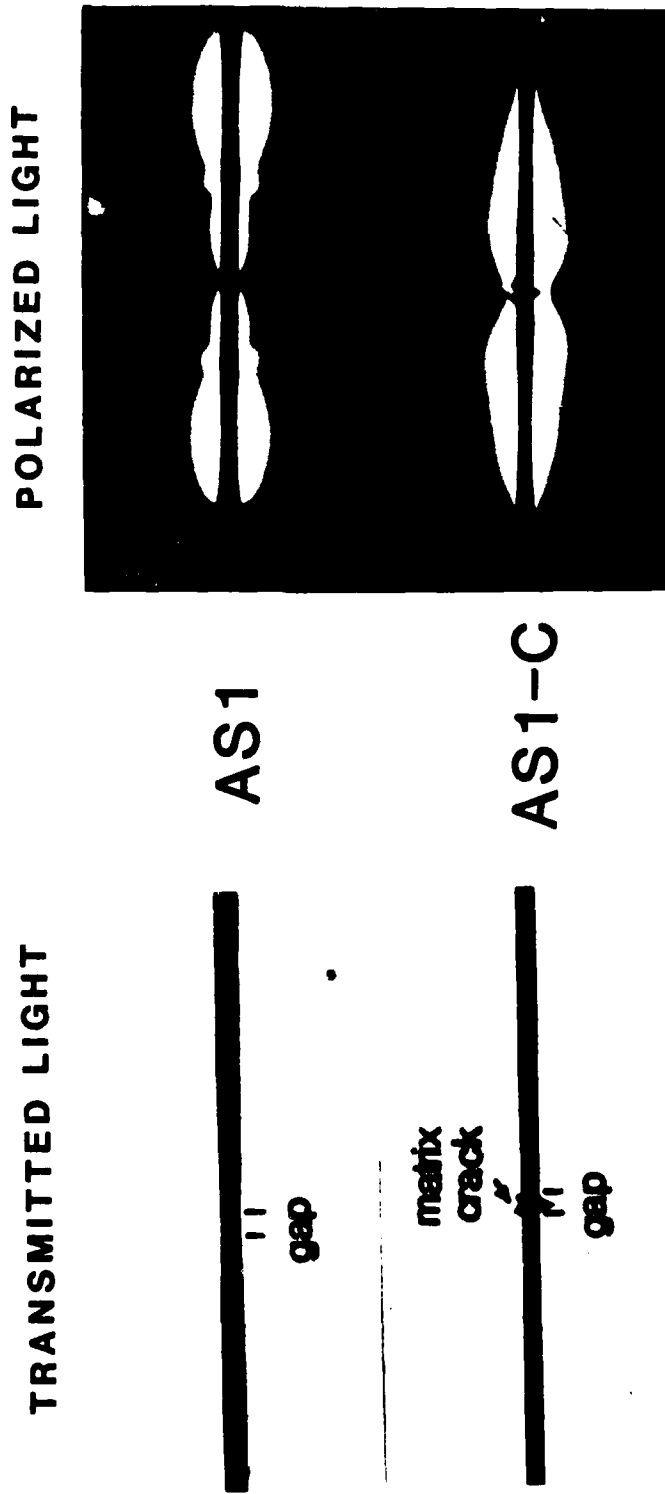


Figure 7. Photomicrographs of AS1 and AS1-C Fibers Under Strain; No Conditioning.

AS 20C

WET



DEHYD.



WET(σ)/DEHYD.

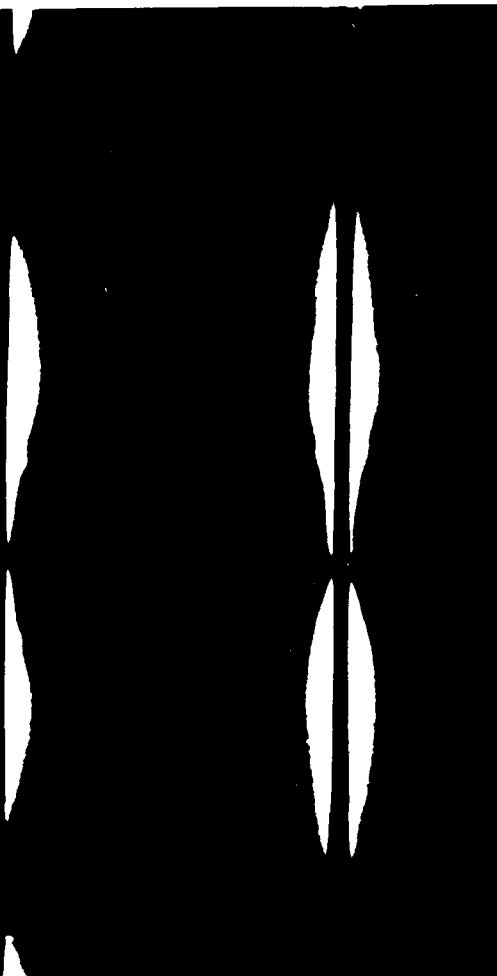


Figure 8. Photomicrographs of AS Fiber Post 20°C Conditioning.

AS1 20C

POL.

WET

TRANS.

POL.

DEHYD.

TRANS.

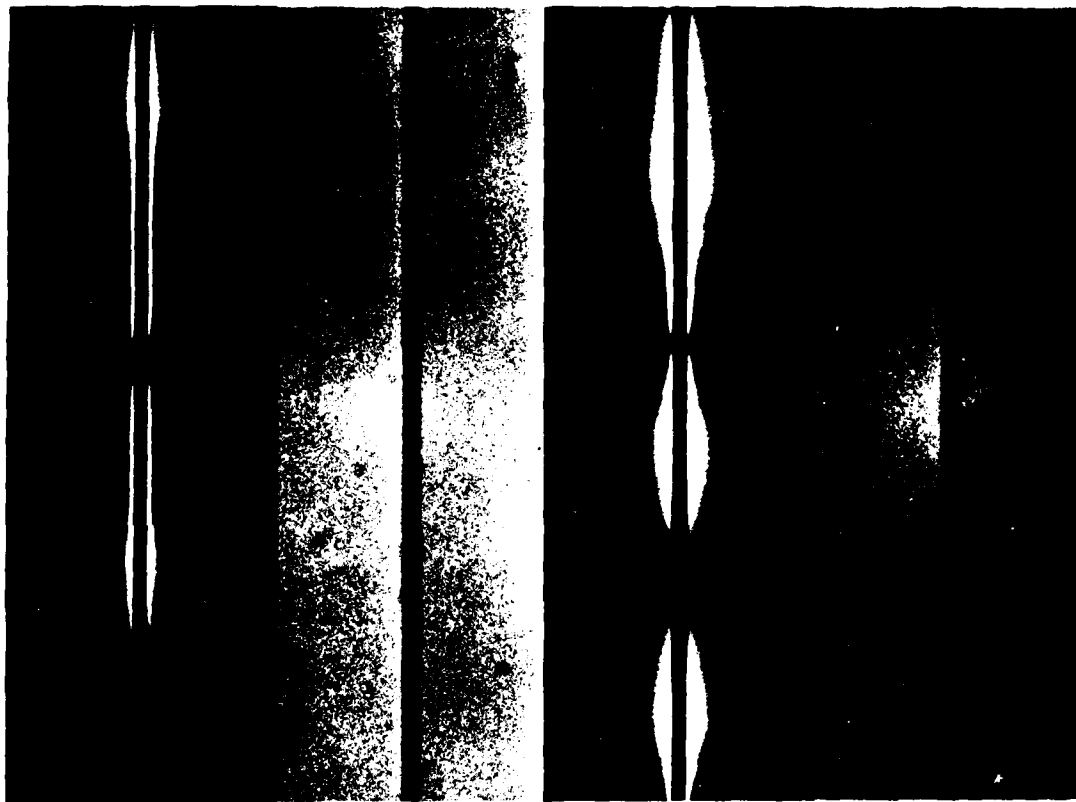


Figure 9. Photomicrographs of AS1 Fiber Post 20°C Conditioning.

AS1-C 20C

POL.

WET

TRANS.

POL.

DEHYD.

TRANS.

Figure 10. Photomicrographs of AS1-C Fiber Post 20°C Conditioning.

TABLE 20
EFFECTS OF HYGROTHERMAL CONDITIONING ON
NEAT EPOXY MATERIAL PROPERTIES

<u>% mPDA</u>	<u>Exposure Condition</u>	<u>Tg (°C)</u>	<u>Tensile Modulus (x10³ psi)</u>
14.5	"as cast"	166	525
14.5	20°C-WET	146	446
14.5	20°C-DEHYD	150	492
14.5	125°C-WET	129	426
14.5	125°C-DEHYD	162	452
7.5	"as cast"	62	695
7.5	125°C-WET	67	600
7.5	125°C-DEHYD	88	595

tested in the WET state (see Table 18). The photoelastic stress patterns of the AS1/WET and AS1/DEHYD are similar to the AS1 fiber not conditioned (see Figures 7 and 11). As a result of conditioning in the AS1-C system, failure has changed from matrix to interfacial failure (see Figures 7 and 12). Dehydration at 70°C results in moderate recovery of τ for the AS1 fiber only. The AS1-C system sustains irreversible loss in interfacial shear strength following conditioning at this temperature. However, τ for the AS1/DEHYD and AS1-C/DEHYD is the same.

(c) 125°C

AS1/WET specimens exhibited extensive interphase damage and multiple fiber breaks prior to loading. An acute decrease in τ to 2.0 ksi was measured for the AS1/WET system of which only a small recovery to 4.8 ksi is achieved upon dehydration (see Table 18). The photoelastic stress pattern for this fiber conditioned at 125°C is significantly different in both the WET and DEHYD state than the not conditioned case (see Figures 7, 13, and 14). Concurrent with the decrement of τ are reductions in both Tg and tensile modulus of conditioned neat samples. TMA indicates that the Tg of the wet specimens approaches that of the

AS1 70C

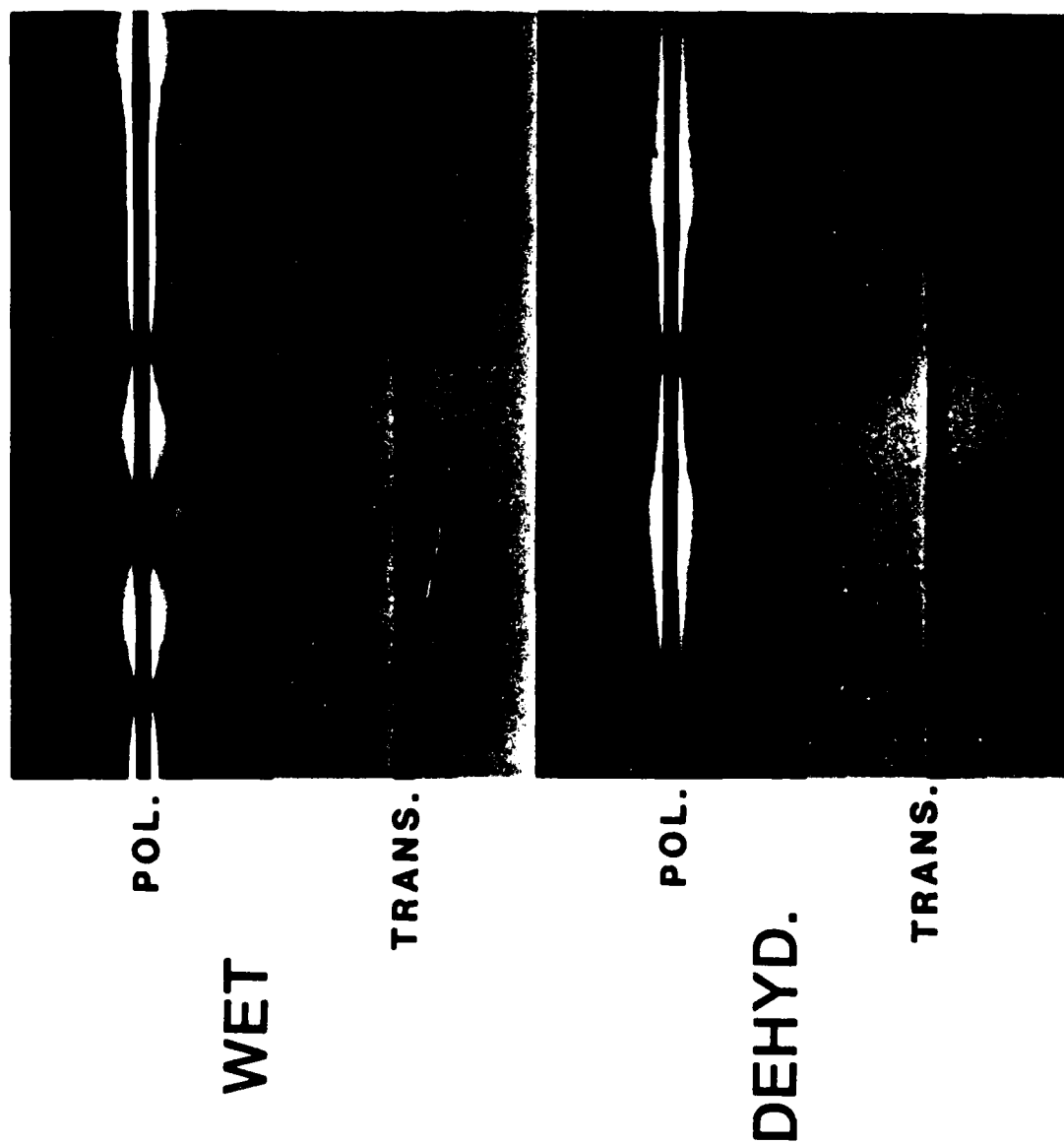
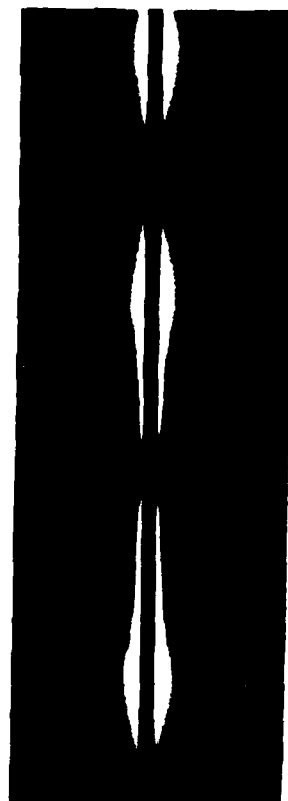


Figure 11. Photomicrographs of AS1 Fiber Post 70°C Conditioning.

AS1-C 70C



POL.

WET

TRANS.



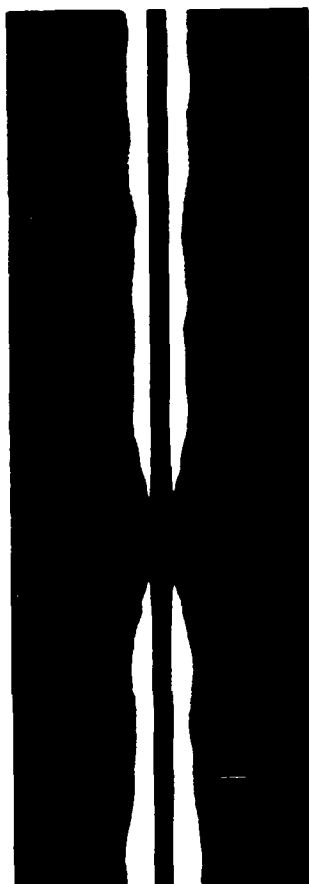
POL.

DEHYD.

TRANS.

Figure 12. Photomicrographs of AS1-C Fiber Post 70°C Conditioning.

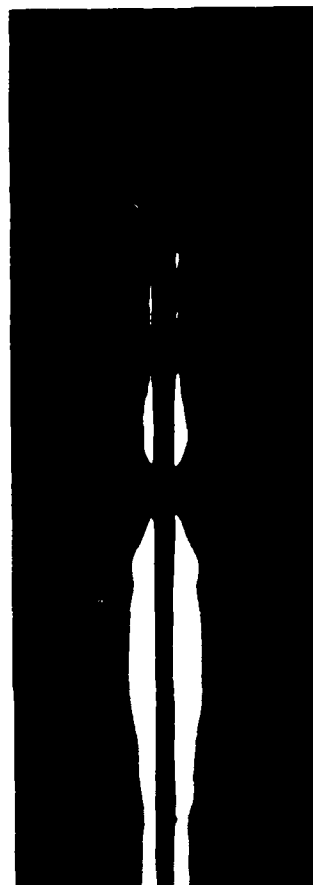
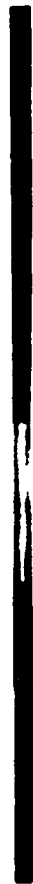
AS1 125C



POL.

WET

TRANS.



POL.

DEHYD.

TRANS.



Figure 13. Photomicrographs of AS1 Fiber Post 125°C Conditioning.

AS1-C 125C

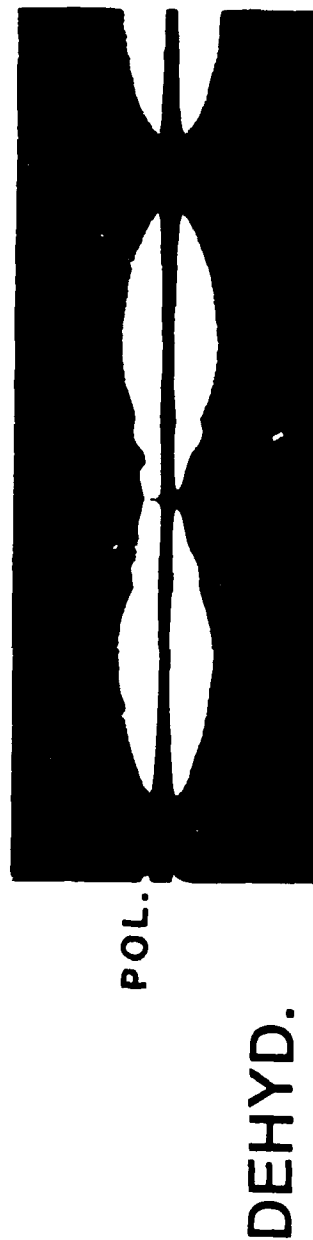
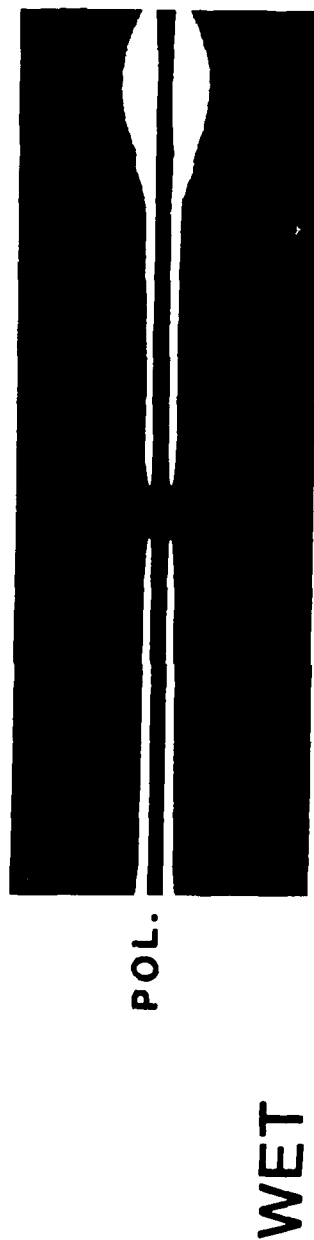


Figure 14. Photomicrographs of AS1-C Fiber Post 125°C Conditioning.

conditioning temperature of 125°C. Tensile modulus is depressed by ~20 percent with only a slight recovery after dehydration (see Table 19).

AS1-C specimens also suffer loss of interfacial shear strength after hygrothermal conditioning at 125°C. Multiple radial cracks at the interface were observed prior to loading. But unlike the AS1 system which sustained ~80 percent loss of interfacial shear strength, τ was limited to ~40 percent reduction from 16.0 ksi "as received" to 9.0 ksi WET. Dehydration of unstressed samples revealed that the radial cracks had dissipated and that no improvement in τ is attained. However, the AS1-C fibers retain a twofold increase in τ over the uncoated AS1 fibers that have undergone the same hydration/dehydration cycle.

Previous work has shown that the coating acts to form a brittle interphase that promotes shear transfer from matrix to fiber and correspondingly results in a higher value for τ (15.5 ksi for ASC vs. 10.7 ksi for AS).⁷ Because this interphase is deficient in curing agent, its material properties can be inferred by measuring mechanical properties of specimens having only half (7.5 phr) the stoichiometric amount of 14.5 phr mPDA. From Table 19 it can be seen that the tensile modulus for the 7.5 phr mPDA material is irreversibly lost following conditioning but is significantly greater than the stoichiometric samples. The conditioning temperature is well above the measured T_g which could allow the interphase to behave more like a rubbery material and result in interfacial stress abatement.

XPS was conducted on AS fibers before and after hygrothermal exposure for two weeks at either 70°C or 125°C. Samples were dried in argon prior to analysis. The atomic percent concentration of carbon, oxygen, and nitrogen was determined and tabulated in Table 21. The 125°C treatment has significantly altered the surface concentrations of these three species.

From this study it can be concluded that moisture effects on fiber-matrix interphase properties are dependent

TABLE 21
SURFACE ATOMIC PERCENT CONCENTRATION OF CONDITIONED
"AS" FIBERS AS DETERMINED BY XPS

<u>Exposure Conditions</u>	<u>Carbon 1s</u>	<u>Oxygen 1s</u>	<u>Nitrogen 1s</u>
"as spun"	82%	11%	4.5%
70°C	86%	10%	2.5%
125°C	89%	8.5%	1.0%

on the temperature of the hygrothermal exposure. At low temperature (20°C) loss of interfacial shear strength is associated with changes in matrix material properties. Moisture effects at this temperature appear to be largely reversible upon dehydration. At the higher temperatures used in this study, decreases in τ may be due to a combination of loss of matrix properties as well as changes in interfacial chemistry. Generally, dehydration does not result in full restoration of interfacial shear strength after elevated temperature conditioning.

c. Effects of Fiber Plasma Treatments

In other areas, AS1 fibers were subjected to reactive plasmas in an attempt to alter fiber surface chemistry and evaluate its effects on fiber-matrix interphase properties by use of the single filament coupon test. Cold plasmas (less than 300°C) were generated by an International Plasma Corporation 4000 unit using radio frequency radiation. A fiber tow was placed in the center of the reaction chamber and treated for different time periods. Power was held constant at 50 watts with a chamber vacuum of 150 μ m. Structural damage to the fiber by the plasma was assessed by measuring single filament tensile strength at 0.3 mm gage length after treatment. Table 22 reports results for two plasmas, oxygen and nitrogen. Tensile strength decreases with duration of treatment. When tested in Epon 828-mpDA epoxy, the AS1 fiber treated in an ammonia plasma for 10 minutes decreased in τ when compared to the "as received" case. No evaluation of

surface chemistry was conducted. Nonetheless, the benefits that plasma treatments may provide to interfacial adhesion may be offset by the fiber structural damage induced.

TABLE 22
TENSILE STRENGTH AND INTERFACIAL SHEAR STRENGTH OF
PLASMA TREATED ASI FIBERS

Plasma	Exposure Time (minutes)	σ_f ($\times 10^3$ psi)	Weibull Parameters		τ ($\times 10^3$ psi)
			α	β	
NH ₃	10	616 \pm 101	3.1	49.0	8.6
NH ₃	30	563 \pm 87	Not Measured		
NH ₃	60	390 \pm 104			
NH ₃	150	395 \pm 117			
O ₂	10	547 \pm 50	3.5	35.5	9.9

d. Flow Microcalorimetry

Flow microcalorimetry is a technique whereby heat effects caused by adsorption of components from a carrier fluid onto an adsorbent bed are detected and plotted on a potentiometric recorder. Analysis of the resultant exothermic and endothermic peaks permits the solid-liquid interactions to be partitioned as either physisorption or chemisorption. Consequently, a prudent selection of solutes differing in functionality, such as acidic or basic molecules, will provide information on the surface reactivity of the adsorbent.

In practice an inert carrying fluid, such as cyclohexane, and the solute to be adsorbed are fed to the sample chamber containing approximately 0.04 gm of chopped carbon fiber. The delivery of the two liquids is precisely governed by two micropumps each controlling the flow from a syringe. Experimentation can be conducted in two modes, either pulse or saturation adsorption. In pulse adsorption a small volume of solute (~ 25 μ l) is injected into the carrier liquid, whereas in saturation adsorption the solute is continuously pumped in the sample chamber along with the

carrier liquid. In each case the thermal events associated with the adsorption processes are detected by thermistors located in the walls of the sample chamber and are plotted on a potentiometric recorder.

The pulse injection of a physisorbed solute should result in a reproducible recorder trace of the thermal adsorption-desorption peaks. Unexpectedly this did not occur with short chain alcohols. Both peak height and shape changed with repetitive injections. Because an occasional air bubble exited the chamber during testing, a simulation was made from glass tubing packed to the same density with carbon fibers to accurately model the sample chamber. When filled with solvent, air bubbles were observed trapped both above and below the sample chamber and also within the fiber volume. The bubbles could not be dislodged by filling the chamber from the bottom or by flushing using the highest solvent flow rate possible. Therefore, the microcalorimeter chamber was evacuated using a cold trap to prevent sample contamination from backstreaming. The chamber was then filled with degassed solvent from a reservoir evacuated to the solvent vapor pressure. Subsequent testing with the alcohol solutes yielded reproducible peak areas 15 times smaller than before. The alcohol-air interaction may have been occurring with the entrapped bubbles and/or with gases adsorbed on the fiber surface prior to degassing.

Operation at maximum recorder sensitivity is often required. During operation at this extreme sensitivity, the recorder background noise has been a persistent problem. The cause was eventually traced to a stick/slip action of the teflon syringe plunger which supplies the carrier fluid. The resultant flow rate variations are recorded as abrupt temperature changes mimicking baseline noise. A controlled and pulseless delivery system is, therefore, being developed. As seen in Figure 15, the exothermic peak indicated by the arrow would have been impossible to discern if superimposed on the typical syringe background noise shown.

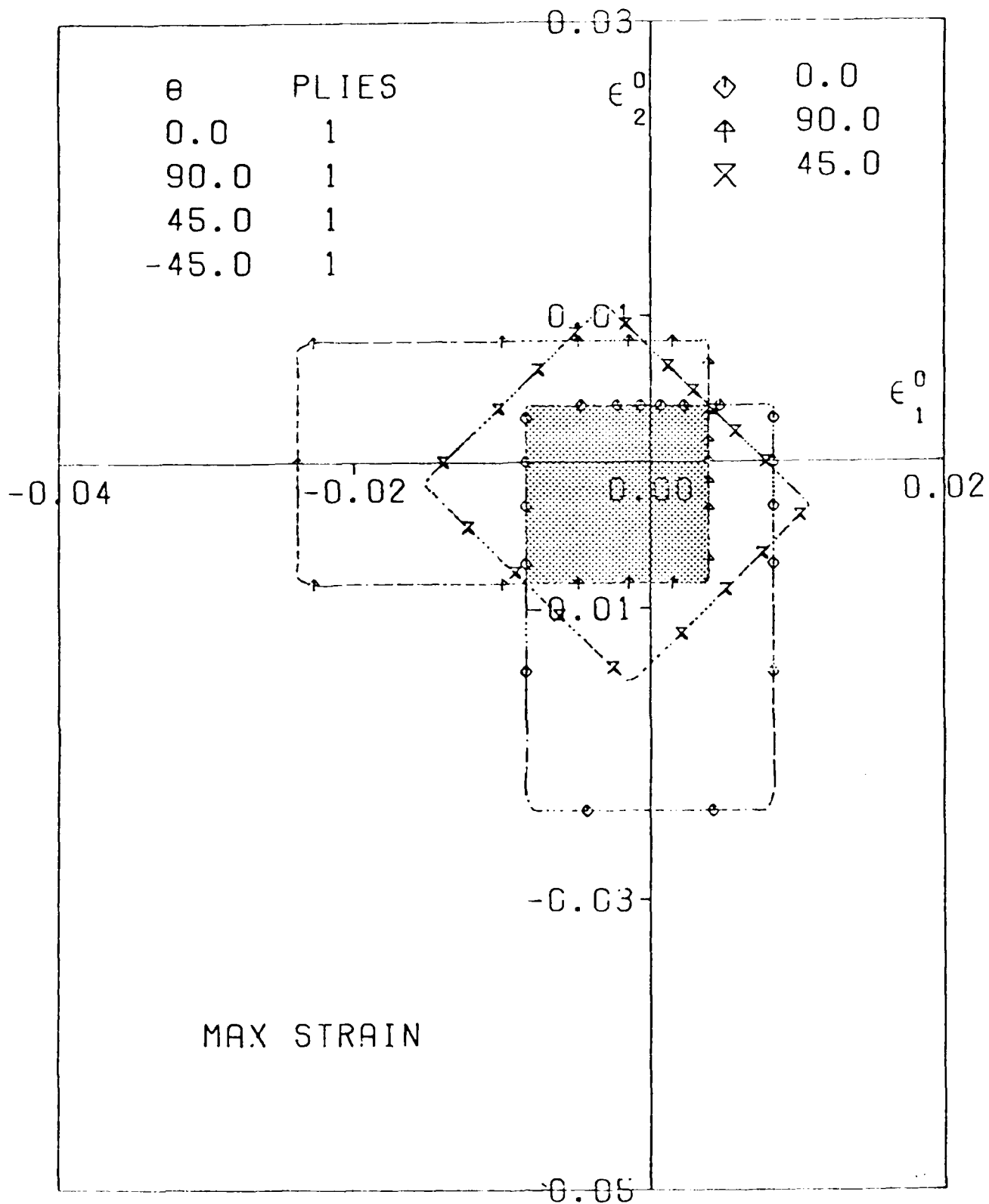


Figure 23. Failure Envelopes for [0/90/+45] - Laminate on the Basis of Maximum Strain Failure Criteria, $S = 99$ mPa.

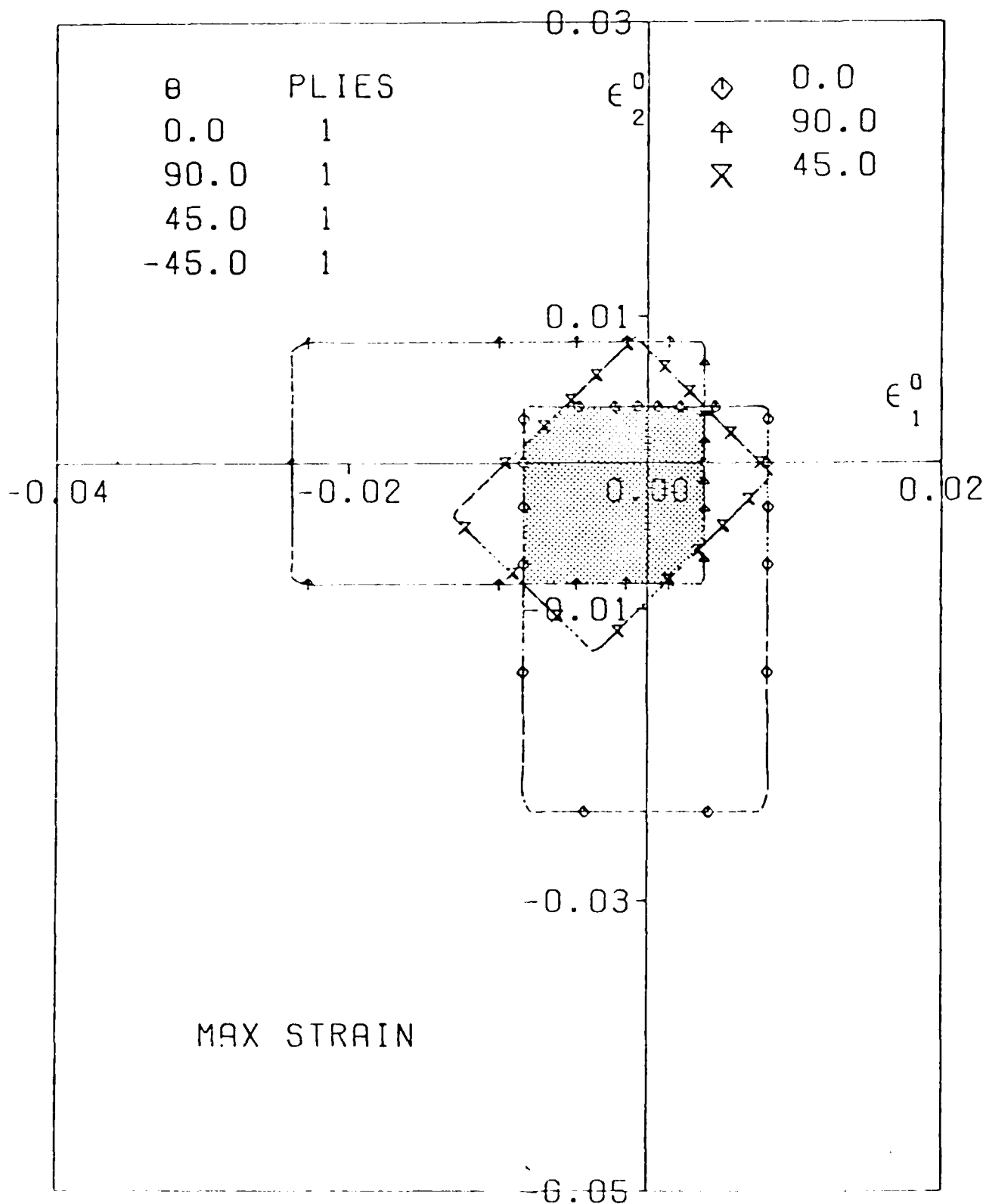
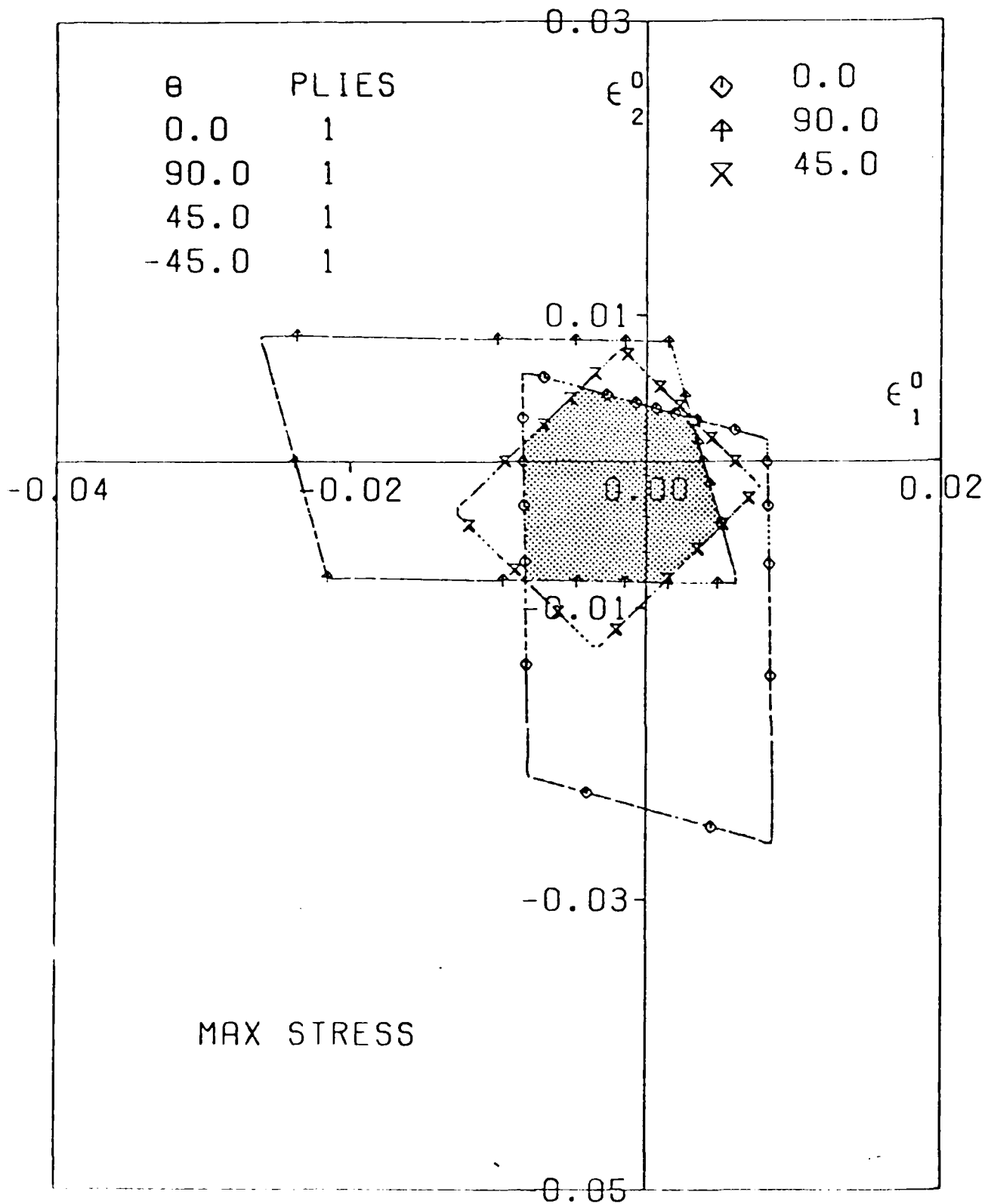


Figure 22. Failure Envelopes for $[0/90/+45]_S$ - Laminate on the Basis of Maximum Strain Failure Criteria.



Failure 21. Failure Envelopes for $[0/90/+45]_s$ - Laminate on the Basis of Maximum Stress Failure Criteria.

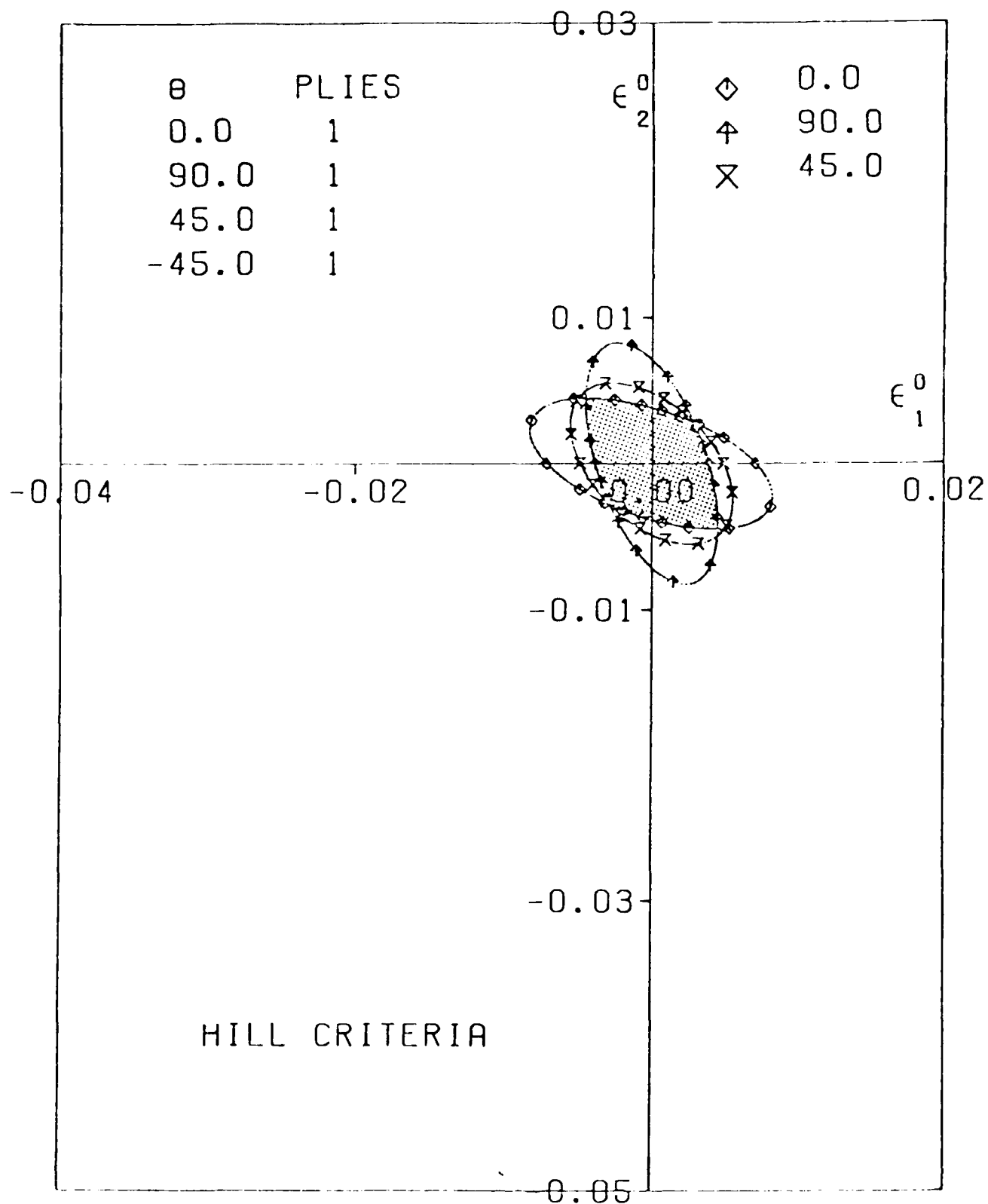


Figure 20. Failure Envelopes for $[0/90/+45]_s$ - Laminate on the Basis of Hill Failure Criteria.

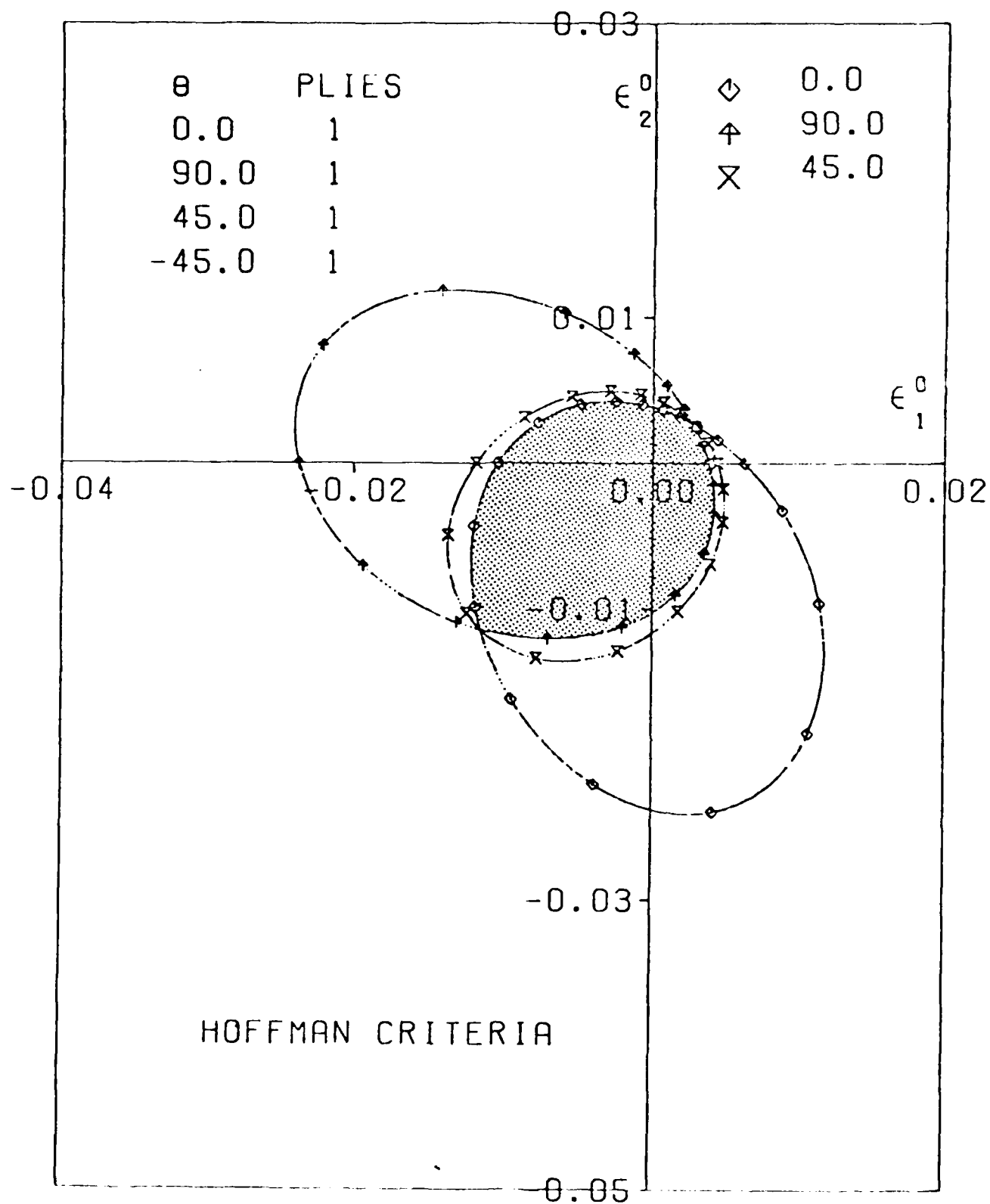


Figure 19. Failure Envelopes for $[0/90/+45]_s$ - Laminate on the Basis of Hoffman Failure Criteria.

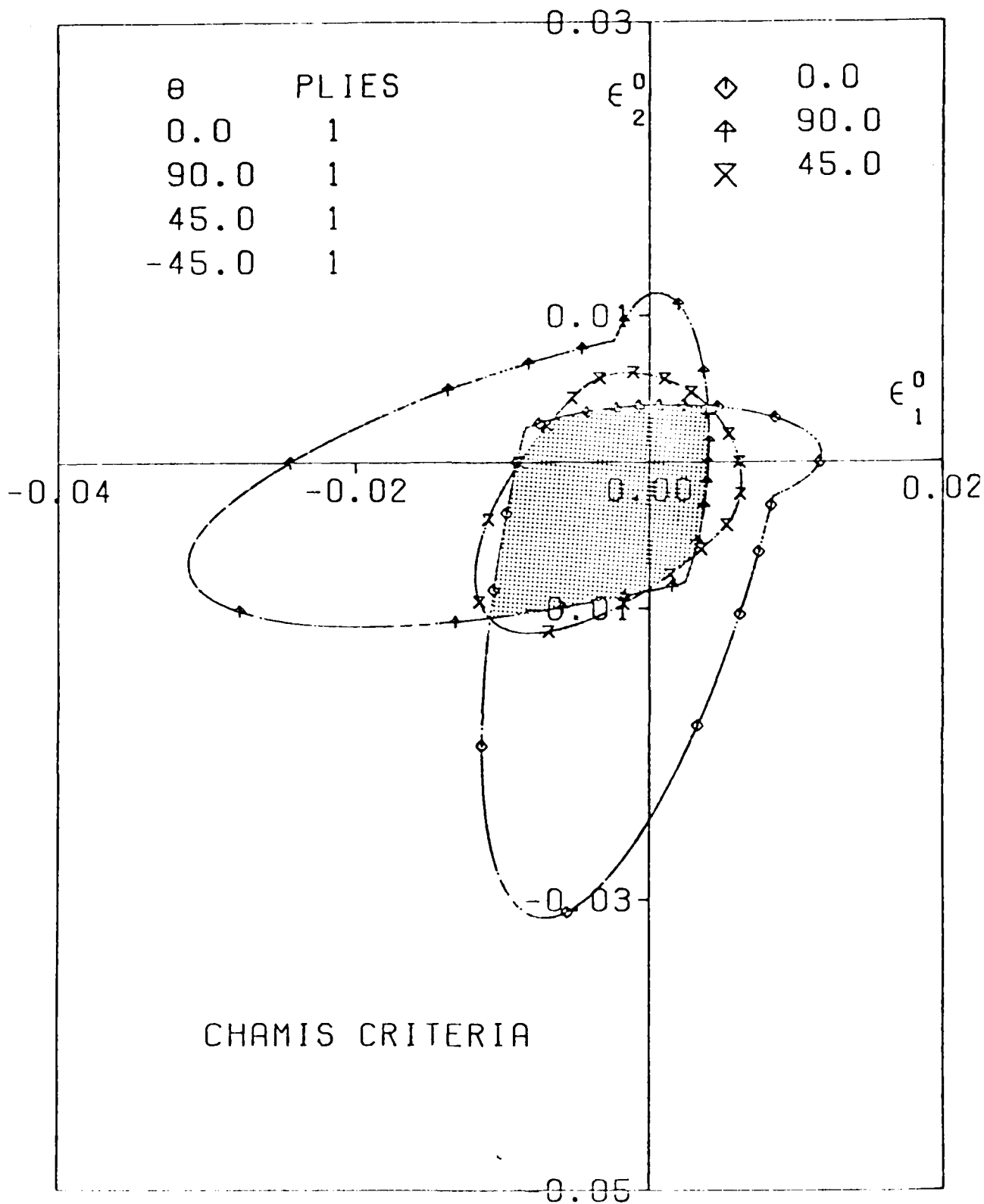


Figure 18. Failure Envelopes for $[0/90/+45]_s$ - Laminate on the Basis of Chamis Failure Criteria.

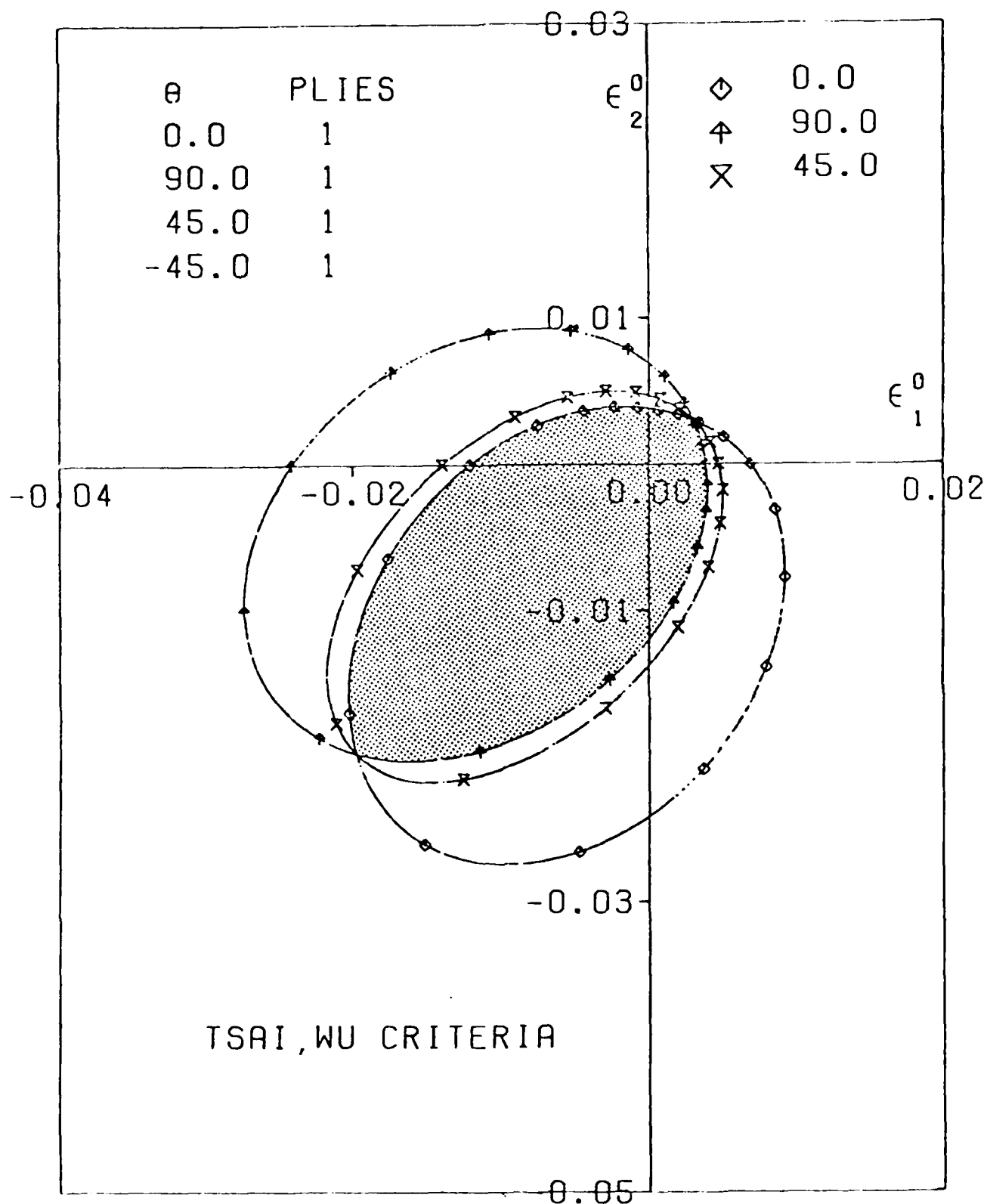


Figure 17. Failure Envelopes for $[0/90/+45]_s$ - Laminate on the Basis of Tsai, Wu Failure Criteria.

have been given in Figures 17 - 25. The failure surface corresponding to -45° ply is the same as that for 45° ply.

Figures 17 - 22 give the failure surface for laminates of T300/5208 graphite epoxy material. Figure 23 shows how the $\pm 45^\circ$ control of the first ply failure strength of the laminate will be affected for the higher shear strength S ($= 99$ MPa) of the material. Figures 24 - 25 show the further improvement of the ply strengths when the ply strength properties y , y' and s are given as: $y = 94$ MPa, $y' = 94$ MPa, $s = 82.8$ MPa (called idealized material).⁽¹⁰⁾ The most important feature of the idealized material is that in all the laminates, each ply fails at the same load. This prediction is based upon Tsai-Wu criteria. The other criteria also predict that the last ply strength of the laminate is very close to the first ply strength.

Table 24 gives the description of figures for failure envelopes pertaining to different failure criteria. In all the figures the surface bounded by the first ply strength for all combinations of σ_1 , σ_2 loadings ($\sigma_3 = 0$) are shaded. A quantitative comparison of first ply failure strength predictions on the basis of different failure criteria are given in Table 25. In each quadrant of loading condition, the criteria predicting approximately the same first ply strength are divided into different groups. The group with the highest magnitude is denoted as A and the one with the next lower magnitude is denoted as B, and so on. The percentage difference in predicted strengths between each group in different quadrants of loading conditions is given in Table 25. The computation of the percentage difference in strength predictions is done either for a uniaxial load or for a hydrostatic load. The maximum relative percentage difference in first ply failure strengths in the tension-tension loading condition is 20%, that for tension-compression and compression-tension is 54%, and that for compression-compression is 71%.

A comparison was made with experimental results for a large number of laminates under uniaxial loading. Since the loading condition is uniaxial, there exists a good agreement

X = Longitudinal tensile strength
 X' = Longitudinal compressive strength
 Y = Transverse tensile strength
 Y' = Transverse compressive strength
 S = Longitudinal shear strength

$$F = \begin{bmatrix} F_{xx} & F_{xy} & 0 \\ F_{xy} & F_{yy} & 0 \\ 0 & 0 & F_{xx} \end{bmatrix} \quad \bar{F} = \begin{bmatrix} \bar{F}_x \\ \bar{F}_y \\ 0 \end{bmatrix} \quad \sigma = \begin{bmatrix} \sigma_x \\ \sigma_y \\ \sigma_s \end{bmatrix}$$

A superscript T denotes transposition of the matrix and the subscripts x, y and s denote the longitudinal, transverse and shear directions, E denotes the Young's modulus. The quadratic polynomial failure criteria, through the use of stress strain relations, can be expressed in strain space as follows:

$$\epsilon^T G \epsilon + \bar{G}^T \epsilon = 1$$

where the elements of matrix G and vector \bar{G}^T are dependent upon the ply modulus matrix, Q_{ij} and quadratic polynomial coefficients F_{ij} and \bar{F}_i of Table 22.

d. Results and Discussion

For the computation of results for this report, the material properties of T300/5208 graphite epoxy material as given below have been considered:

$$\begin{array}{ll}
 E_x = 181 \text{ GPa} & E_y = 10.3 \text{ GPa} \\
 \nu_x = 0.28 & E_s = 7.17 \text{ GPa} \\
 X = 1500 \text{ MPa} & X' = 1500 \text{ MPa} \\
 Y = 40 \text{ MPa} & Y' = 246 \text{ MPa} \\
 S = 68 \text{ MPa} &
 \end{array}$$

The successive ply failure surfaces of all the four ply orientations, 0° , 90° , 45° and -45° of the $[0/90/+45]_s$ - laminate

b. Maximum Strain

Tensile Strain

$$\epsilon_x \leq \frac{X}{E_x}$$

$$\epsilon_y \leq \frac{Y}{E_y}$$

$$\epsilon_s \leq \frac{S}{E_s}$$

Compressive Strain

$$|\epsilon_x| \leq \frac{X'}{E_x}$$

$$|\epsilon_y| \leq \frac{Y'}{E_y}$$

$$|\epsilon_s| \leq \frac{S}{E_s}$$

Failure occurs when one of the equalities is met.

c. Quadratic Polynomial

Four quadratic polynomial failure criteria given in Table 23 have been considered.

TABLE 23
QUADRATIC POLYNOMIAL FAILURE CRITERIA

Criteria Parameter	Tsai-Wu (12)	Chamis (13)	Hoffman (14)	Wu (15)
Equation	$\sigma^T F_0 + \bar{\sigma}^T \bar{F}_0 = 1$	$\sigma^T F_0 = 1$	$\sigma^T F_0 + \bar{\sigma}^T \bar{F}_0 = 1$	$\sigma^T F_0 = 1$
F_{xx}	$\frac{1}{XX'}$	$\frac{1}{X^2} \left(\frac{1}{X'} \right)^\dagger$	$\frac{1}{XX'}$	$\frac{1}{X^2}$
F_{yy}	$\frac{1}{YY'}$	$\frac{1}{Y^2} \left(\frac{1}{Y'} \right)^\dagger$	$\frac{1}{YY'}$	$\frac{1}{Y^2}$
F_{xy}	$F_{xy}^* \sqrt{F_{xx} F_{yy}}$	$F_{xy}^* \sqrt{F_{xx} F_{yy}}$	$F_{xy}^* \sqrt{F_{xx} F_{yy}}$	$F_{xy}^* \sqrt{F_{xx} F_{yy}}$
F_{xy}^*	$-1 < F_{xy}^* < 1^\ddagger$	Material Property ‡	$-\frac{1}{2} \sqrt{\frac{YY'}{XX'}}$	$-\frac{1}{2} \frac{Y}{X}$
F_{ss}	$\frac{1}{S^2}$	$\frac{1}{S^2}$	$\frac{1}{S^2}$	$\frac{1}{S^2}$
\bar{F}_x	$\frac{1}{X} - \frac{1}{X'}$		$\frac{1}{X} - \frac{1}{X'}$	
\bar{F}_y	$\frac{1}{Y} - \frac{1}{Y'}$		$\frac{1}{Y} - \frac{1}{Y'}$	

† The values within the parenthesis are used when the corresponding stress component is compressive.

‡ In the Tsai-Wu criteria F_{xy}^* is taken to be $-1/2$.

‡ In Chamis criteria F_{xy}^* varies from material to material. For 1300/1208 $F_{xy}^* = -1/2$.

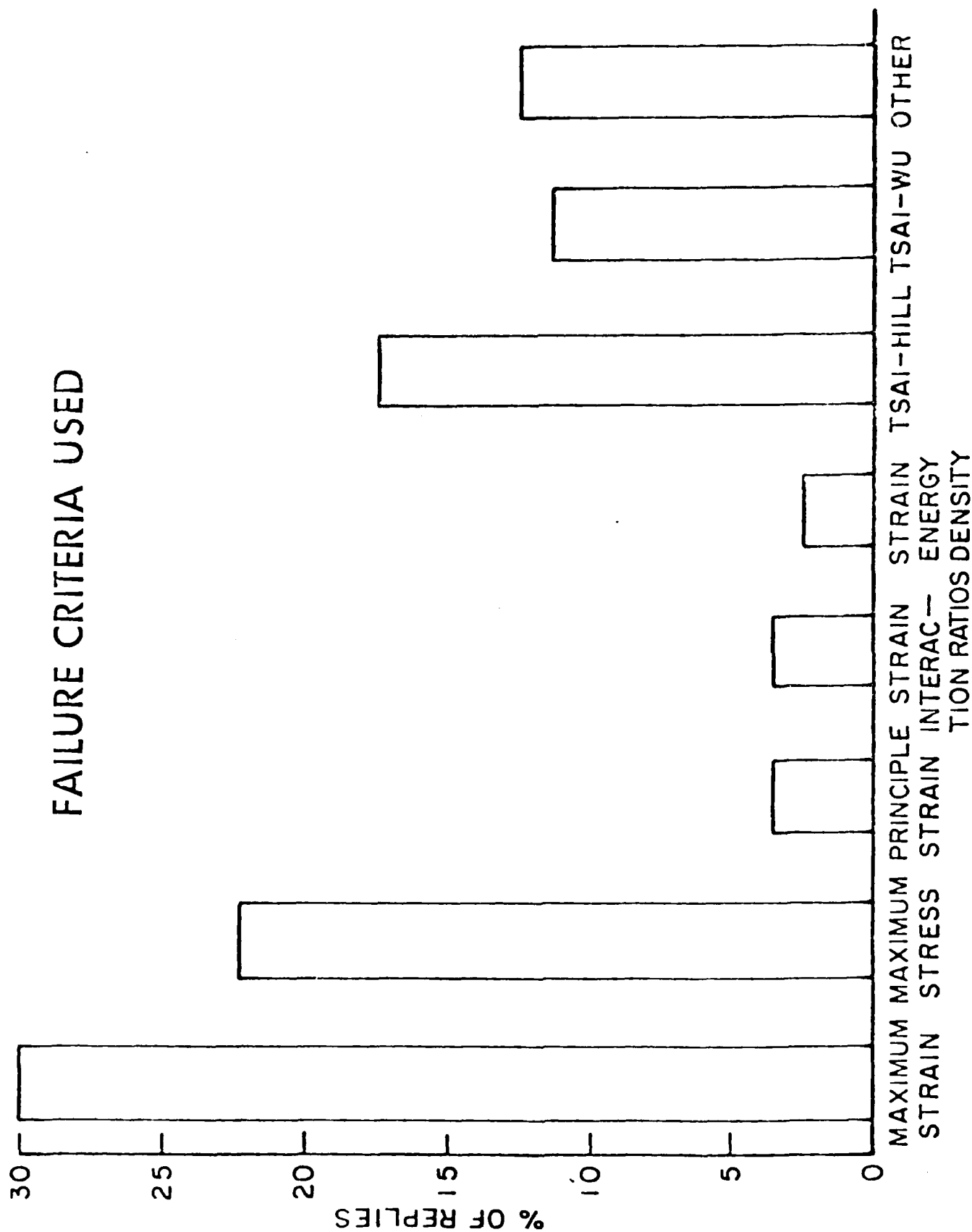


Figure 16. AIAA Failure Criteria Survey Response.

are presented. These calculations are made on the basis of lamination theory. It has been assumed that the strength of the lamina in the laminate is the same as that of the independent lamina. The failure analysis results are valid only up to the first ply failure strength of the laminate. The surviving lamina may or may not be able to carry the load exceeding the FPF load of the laminate. No curing stresses were considered in these calculations though they may have considerable influence on the first ply failure strengths. A quantitative comparison has been done among the first ply failure strength predictions from different theories. It has been observed that the first ply failure predictions by these theories differ up to 20% in the first quadrant of inplane loading, up to 54% in the second and the fourth quadrants of inplane loading and up to 71% in the third quadrant of inplane loading.

Figure 16 shows the failure criteria survey response obtained by the AIAA composite materials subcommittee. On the basis of this response we have chosen maximum stress, maximum strain and quadratic polynomial (Tsai Wu, Chamis, Hoffman, and Hill¹²⁻¹⁵) failure criteria for a comparative treatment in this work. Reference 11 gives an extensive survey of failure theories. The theories considered in this investigation are given below:

a. Maximum Stress

Tensile Stresses

$$\sigma_x \leq X$$

$$\sigma_y \leq Y$$

$$\sigma_s \leq S$$

Compressive Stresses

$$|\sigma_x| \leq X'$$

$$|\sigma_y| \leq Y'$$

$$|\sigma_s| \leq S$$

Failure occurs when one of the equalities is met.

SECTION IV
MECHANICS OF COMPOSITES AND ADHESIVE BONDED JOINTS

1. FAILURE STUDY

On the basis of a recent survey conducted by AIAA composite structures subcommittee,⁽⁸⁾ the failure criteria used by more than ninety percent design engineers was considered in Ref. 9. These failure criteria are maximum stress, maximum strain and quadratic polynomial (Tsai-Wu, Chamis, Hoffman and Hill) failure criteria. Failure envelopes for all these failure criteria were drawn for $[0/90/+45]_s$ laminate made of T300/5208 graphite epoxy material in stress space. For the first ply failure strength, a great deal of difference in the predictions made by these failure criteria was observed. Depending upon the failure criteria being compared, the maximum percentage difference ranged to 71%. Because of the criticality of failure criteria in structural design and for a better confidence in the predicted strength, it is necessary to have a unique failure criteria for the accurate prediction of composites. Computer aided optimum designs may not be optimum if the correct failure criteria is not considered. Also, it has been seen that in Chamis, maximum stress and maximum strain failure criteria, $+45$ plies control the first ply failure for a set of loading conditions in the second and the fourth quadrants. This is based upon the shear strength $S = 68$ MPa. For a higher value the shear strength $S (= 99$ MPa), it has been seen that the laminate strength is governed by 0° or 90° layers for all combinations of inplane loads.

The objective of the present paper is to conduct a comparative study of these commonly used failure theories in strain space on the lines of Ref. 9. To achieve this objective, these theories have been included in a computer code, A Digital Algorithm for Composite Laminate Analysis - Fortran,¹⁰ and the results obtained for a $[0/90/+45]_s$ - laminate made of T300/5208 graphite epoxy composite material have been given. Failure envelopes for quadratic polynomial, maximum stress and maximum strain failure criteria



Controlled Delivery
Thermograph



Typical Syringe
Background Noise

Figure 15. Microcalorimeter Recorder Traces.

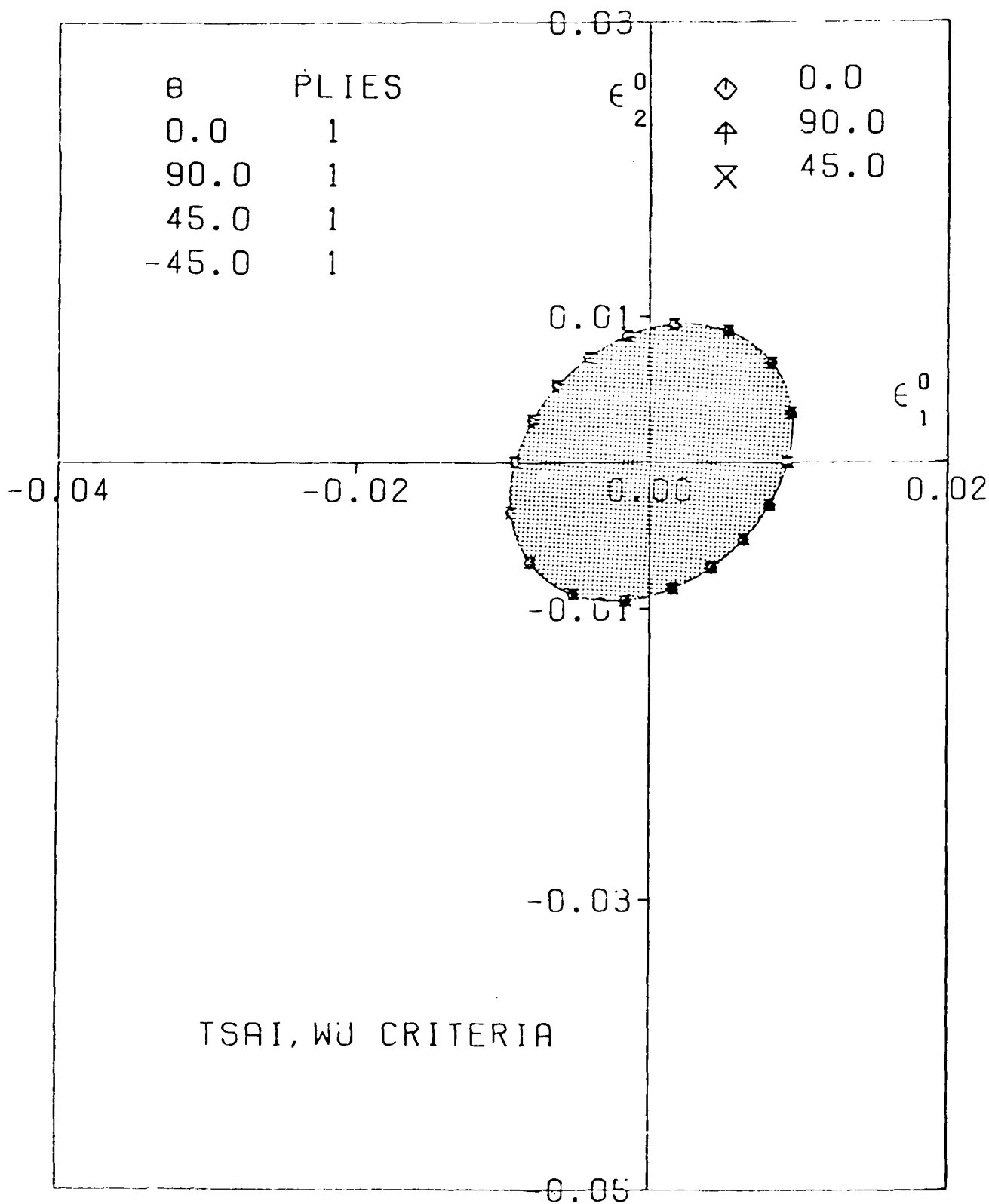


Figure 24. Failure Envelopes for [0/90/+45] - Laminate on the Basis of Tsai, Wu Criteria for Idealized Material.

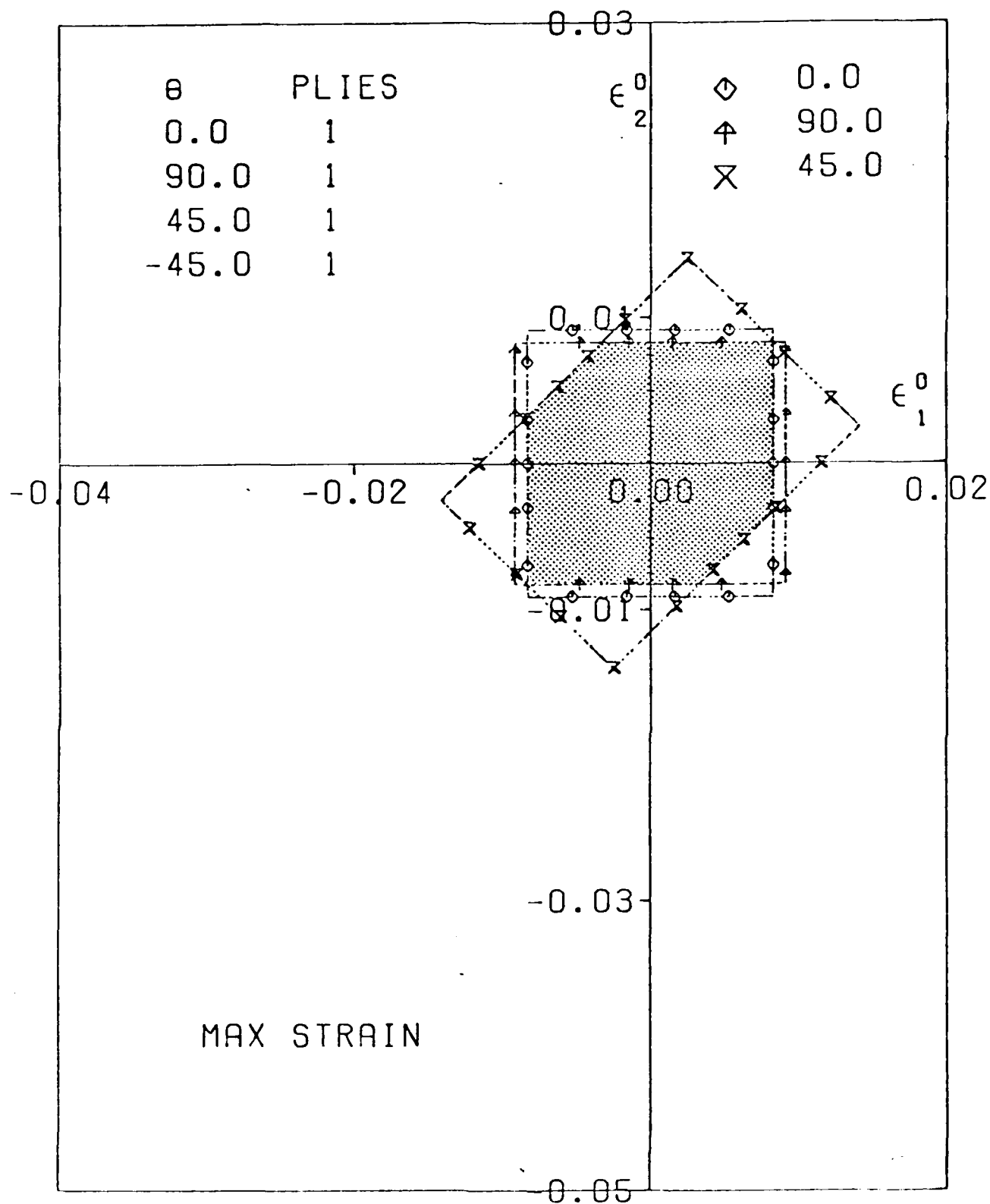


Figure 25. Failure Envelopes for [0/90/+45] - Laminate on the Basis of Maximum Strain Failure Criteria for Idealized Material.

TABLE 24
TABLE OF FAILURE ENVELOPES FOR $[0/90/\pm 45]_S$ LAMINATES

Criteria	Figure Number
Tsai, Wu [4]	2 (TW)
Chamis [5]	3 (CH)
Hoffman [6]	4 (HO)
Hill [7]	5 (HI)
Max. Stress	6 (MS)
Max. Strain	7 (MN)

The symbols within the parenthesis denote the abbreviated name of the failure criteria used in this study.

TABLE 25
COMPARISON OF FIRST PLY FAILURE PREDICTIONS
IN STRAIN SPACE

Quadrant	Group	Criteria	Max % Difference
1	A	CH, MN	
	B	TW, MS	16%
	C	HO, HI	20%
2 & 4	A	TW	10%
	B	HO	18 - 24%
	C	CH, MS, MN	
	D	HI	54%
3	A	TW	41%
	B	HO	16%
	C	CH	13%
	D	MS, MN	
	E	HI	71%

between the experimental and predicted strengths with one exception, $[15/0/-15]_s$ laminate. The exceptional case, in which the predicted strength is about 50% more than the experimental strength, has been explained by using three dimensional stress analysis results which show an interlaminar shear failure before the ply failure. For biaxial loadings, contingent upon the magnitude and direction of the strain component, the enormous difference among the predicted strengths by different failure theories cause concern about the reality of computer aided optimum designs. Therefore, it is necessary to establish a unique failure theory to predict the strength of composite materials.

For comparison, the predictions by Tsai-Wu, maximum strain and maximum stress failure criteria, along with the experimental results for $[\phi/90/-\phi]_s$ and $[\phi/0/-\phi]_s$ laminates $[\phi = 0(15)90]$ are shown in Figures 26 - 27. For the laminates tested for this study it has been observed that when the laminate is matrix dominated in the loading direction, the first ply failure strength represents the ultimate strength of the laminate. Also, in the case of fiber dominated laminates in the loading direction, the experimental values lie between the first and last ply strengths of the laminate, tending to the last ply failure strengths. For $[15/0/-15]_s$ laminate the failure has been investigated on the basis of a three dimensional stress analysis. The cause of failure of that laminate is attributed to the presence of a high interlaminar shear stress component τ_{xz} .

2. EFFECT OF CURING STRESSES ON LAMINATES

It has been observed that in certain laminates cracks develop at the free edge due to pure residual curing stresses. To better understand the causes of these cracks, we have conducted stress analysis of composite laminates studied in Reference 17. The theory developed by Pagano¹⁸ for the stress analysis of layered composites has been utilized. The material properties considered for these computations are as follows:

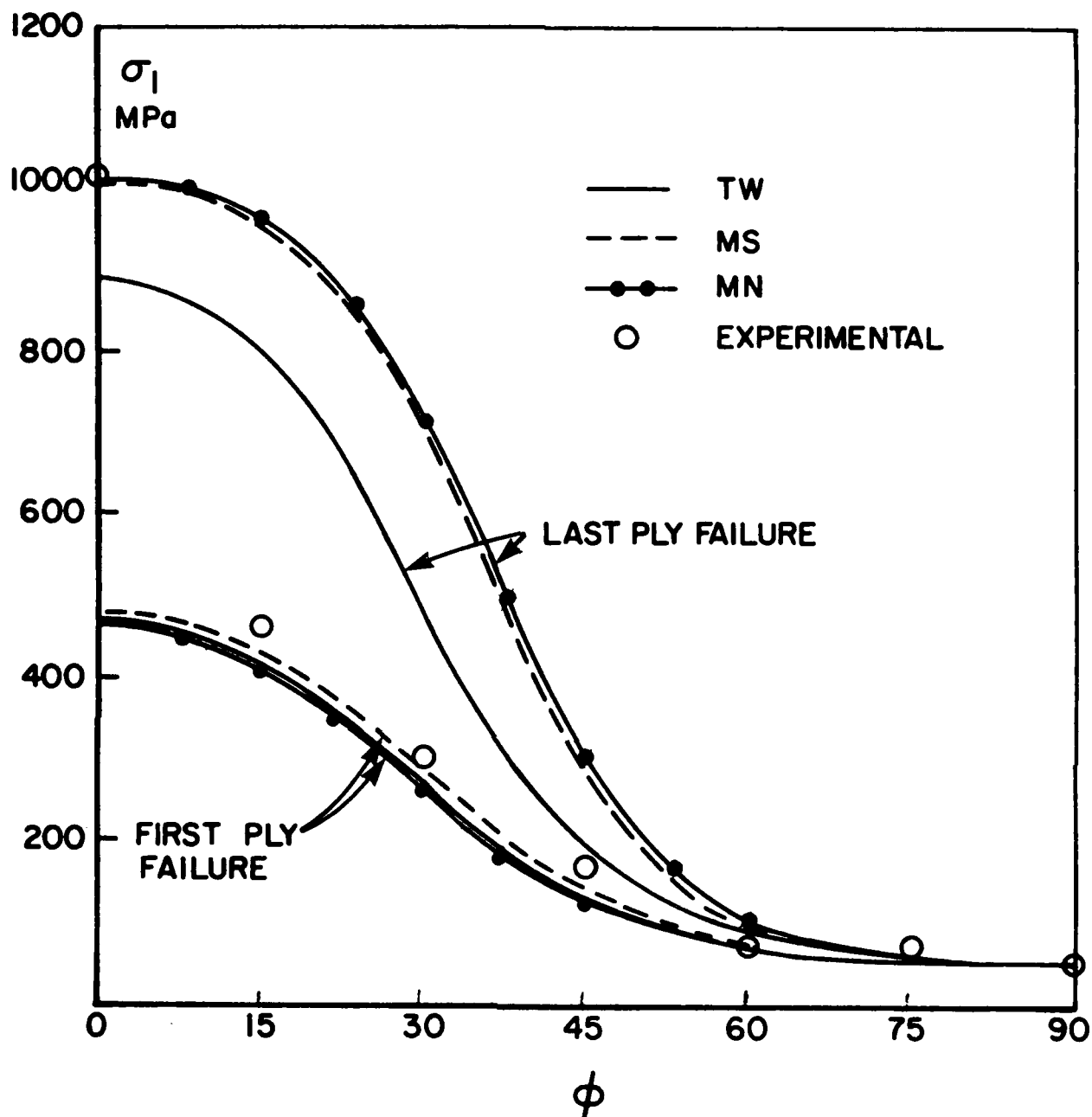


Figure 26. Comparison of Predicted and Experimental Strengths for $[\phi/90/-\phi]_s$ - Laminates.

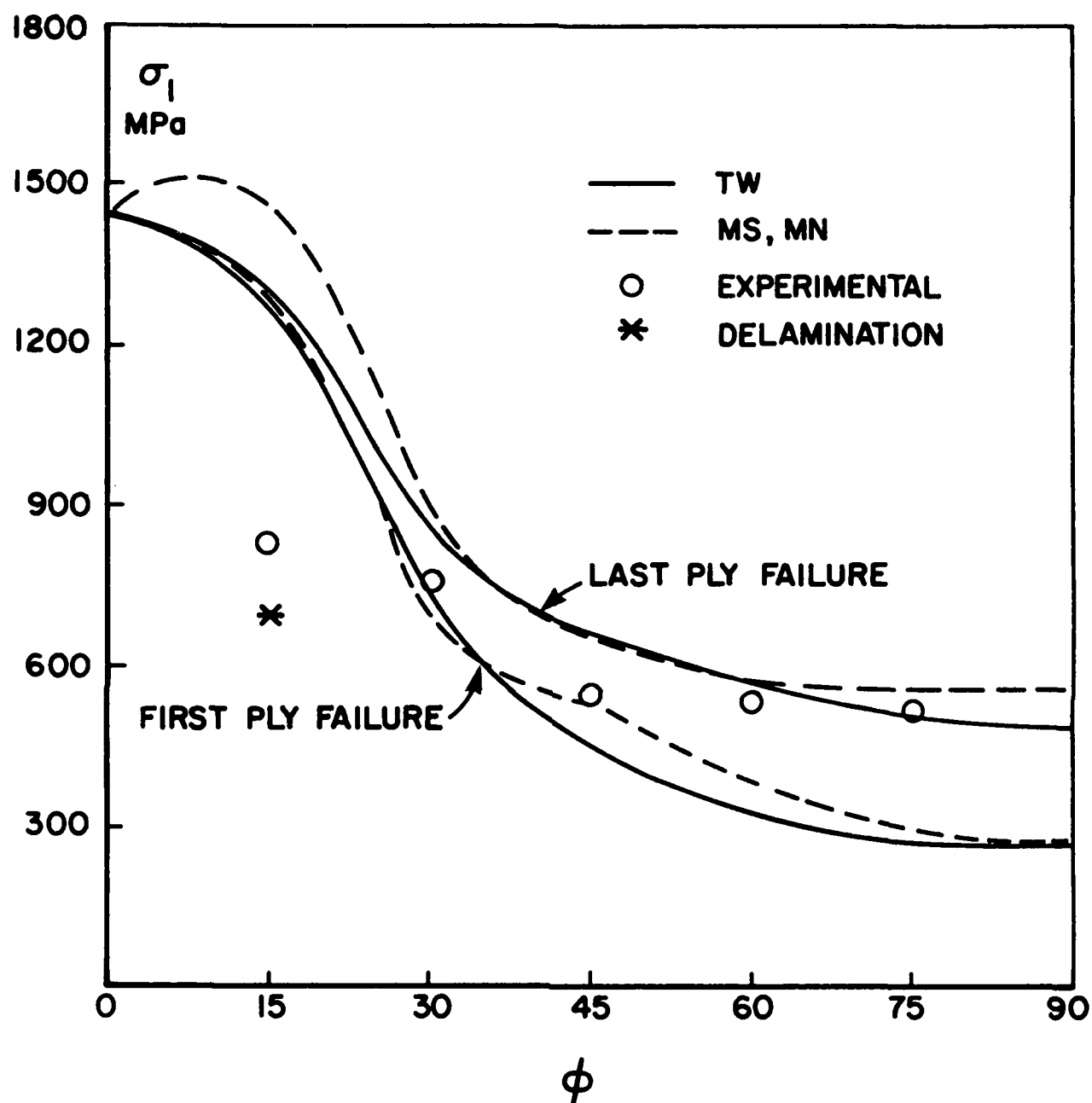


Figure 27. Comparison of Predicted and Experimental Strengths for $[\phi/0/-\phi]_s$ - Laminates.

$E_x = 20 \text{ MSI}$	$\nu_{xy} = .29$
$E_y = 1.7 \text{ MSI}$	$\nu_{xz} = .29$
$E_z = 1.7 \text{ MSI}$	$\nu_{yz} = .6$
$G_{xy} = .66 \text{ MSI}$	$\alpha_x = .05 \text{ } \mu\epsilon/^{\circ}\text{F}$
$G_{xz} = .66 \text{ MSI}$	$\alpha_y = 16.0 \text{ } \mu\epsilon/^{\circ}\text{F}$
$G_{yz} = .53 \text{ MSI}$	$\Delta T = -200^{\circ}\text{F}$

Figures 28- 31 show the stress component σ_x at the 0/90 interface of $[0_2/90_n]_s$ - laminates ($n = 1, 2, 4, 8$) along the width of the laminate, due to curing stresses only. At the free edge there is a great deal of difference in predicted stress component σ_x by the lamination theory and the Pagano theory. Further, we calculated the averaged stress components σ_x and σ_z over a distance h_0 (a ply thickness) along the width, on the basis of Ref. 19, to predict the crack development in the 90° plies of the laminate. Averaged stress components for pure curing stresses and pure mechanical inplane unidirectional loads, for a large number of laminates considered here are given in Table 25. For laminates $[0_4/90_4]_s$ and $[0/90]_{4s}$, which were studied by Kistner, Whitney and Browning,²⁰ the following material properties were considered:

$E_x = 21 \text{ MSI}$	$\nu_{xy} = 0.25$
$E_y = 1.6 \text{ MSI}$	$\nu_{xz} = 0.25$
$E_z = 1.6 \text{ MSI}$	$\nu_{yz} = 0.6$
$G_{xy} = 0.8 \text{ MSI}$	$\alpha_x = -.5 \text{ } \mu\epsilon/^{\circ}\text{F}$
$G_{xz} = 0.8 \text{ MSI}$	$\alpha_y = 12.38 \text{ } \mu\epsilon/^{\circ}\text{F}$
$G_{yz} = 0.6 \text{ MSI}$	$\Delta T = -200 \text{ } ^{\circ}\text{F.}$

The objective of this investigation was to predict the development of the first crack in the laminate. The information available at this point of time is not sufficient to derive any conclusions from the data provided in Table 26. Figures 28 - 31

TABLE 26

AVERAGE STRESS COMPONENTS $\bar{\sigma}_x$ AND $\bar{\sigma}_z$, NONMECHANICAL (SUP.N) AND MECHANICAL (SUP.M), OVER A DISTANCE h_0 (A PLY THICKNESS) FROM THE EDGE

Laminate	Stress \rightarrow n	$\bar{\sigma}_x^N$ (ksi)	$\bar{\sigma}_z^N$ (ksi)	$\frac{\bar{\sigma}_x^M}{\epsilon_1 10^6}$ (psi)	$\frac{\bar{\sigma}_z^M}{\epsilon_1 10^6}$ (psi)
(0 ₂ /90 ₂) _s	1	6.1	2.0	1.8	0.17
	2	5.9	1.8	1.8	0.16
	4	5.4	1.6	1.8	0.15
	8	4.9	1.5	1.8	0.13
(±30/90 _n) _s	1	5.6	.97	2.4	1.1
	2	4.9	.68	2.4	1.0
	4	4.2	.32	2.4	0.9
	8	3.2	-.06	2.4	0.8
(±60/90 _n) _s	1	1.2	-.72	2.0	0.42
	2	1.0	-.75	2.0	0.4
	4	0.63	-.72	2.0	0.34
	8	0.28	-.70	2.0	0.31
(0 ₄ /90 ₄) _s (0/90) _{4s}		5.1	2.0	1.8	0.2
		4.3	0.7	1.6	0.07

ϵ_1 is the applied unidirectional inplane strain.

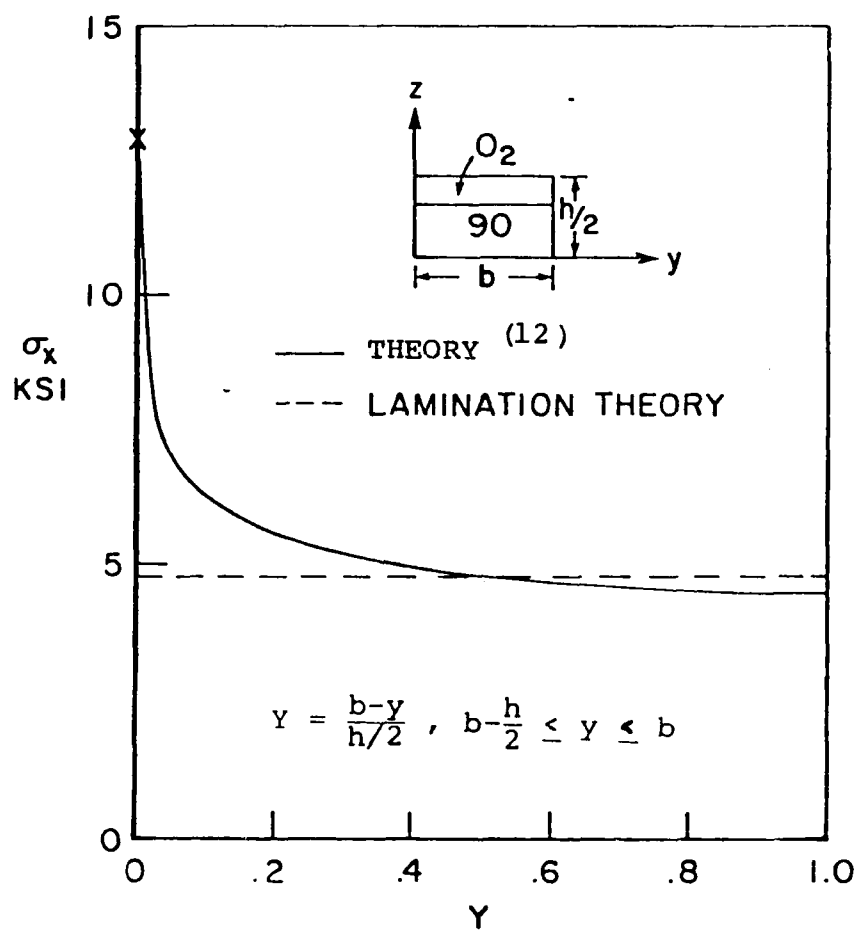


Figure 28. Stress Component σ_x Near the Free Edge of $[0_2/90]_s$ Laminate Along the Width at the 0/90 Interface, Due to Residual Strains.

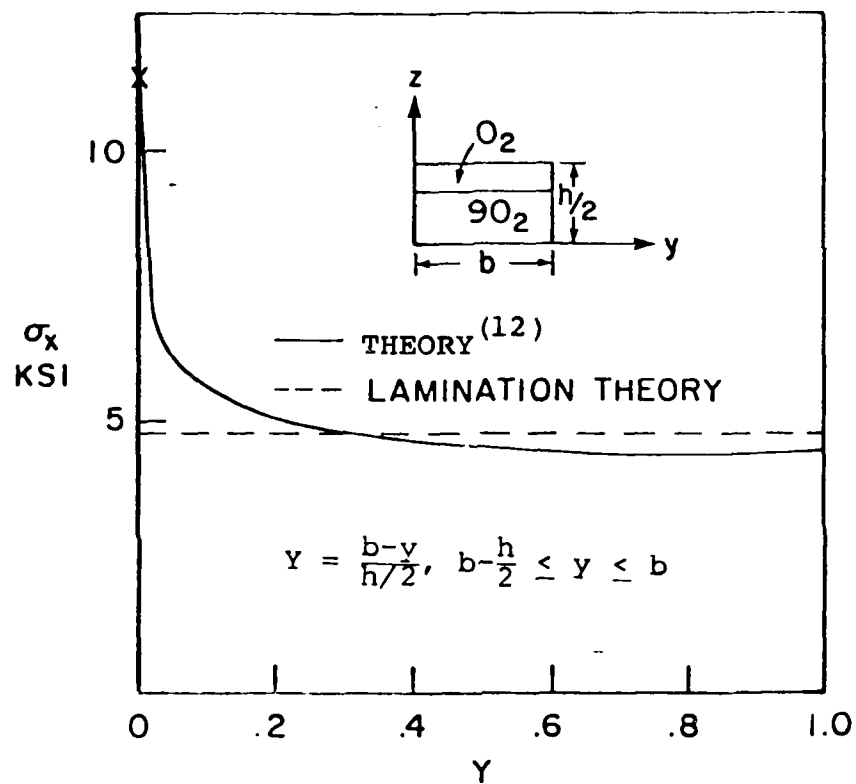


Figure 29. Stress Components σ_x Near the Free Edge of the $[0_2/90_2]_s$ Laminate Along the Width at the 0/90 Interface, Due to Residual Strains.

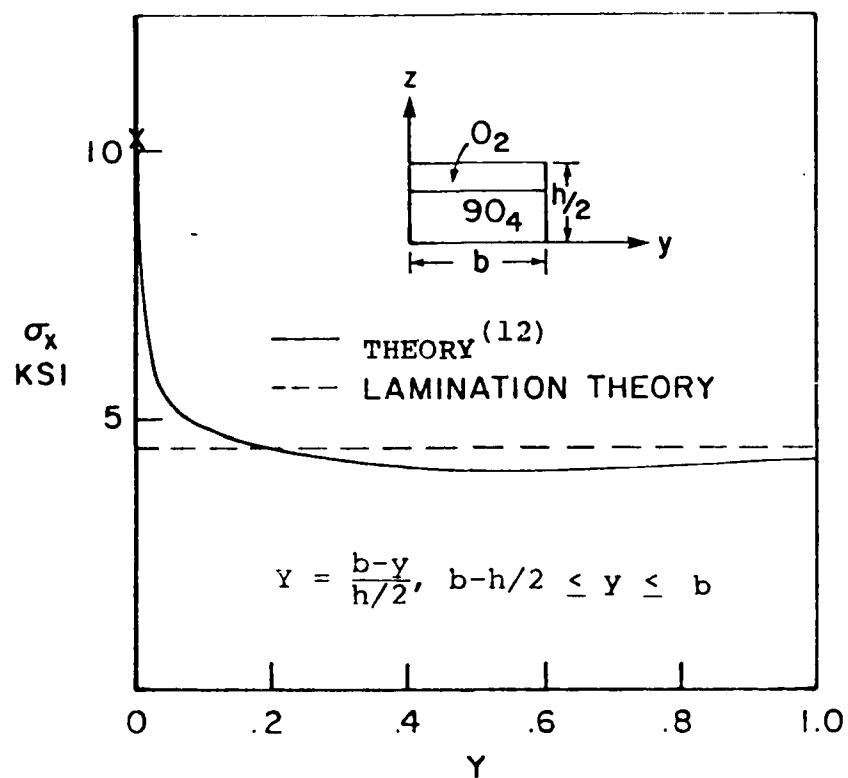


Figure 30. Stress Component σ_x Near the Free Edge of the $[0_2/90_4]_s$ Laminate Along the Width at the 0/90 Interface, Due to Residual Strains.

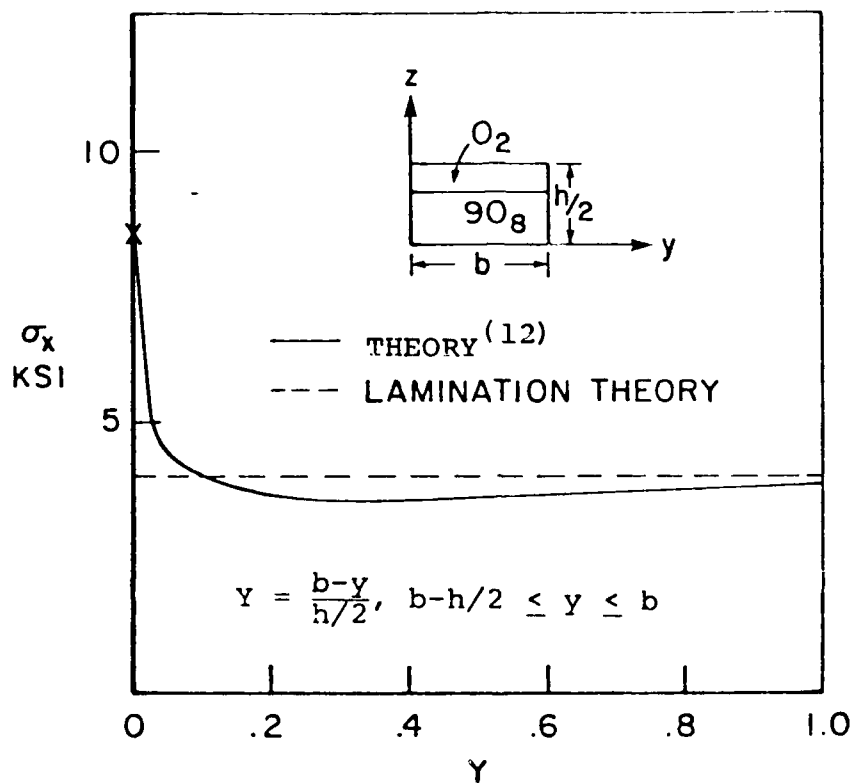


Figure 31. Stress Component σ_x Near the Free Edge of the $[0_2/90_8]_s$ Laminate Along the Width at the 0/90 Interface, Due to Residual Strains.

show that at the free edge region the residual stress component σ_x calculated by the lamination theory is considerably less than actual value. Further work is required to arrive at definite conclusions.

3. FATIGUE STUDY

a. Fatigue Behavior of Graphite/Epoxy

The fatigue failure of composites is known to be very complicated because of the anisotropy of a particular laminate as well as of the constituents properties, loading condition, and other variables. Fatigue failure of composite laminates is preceded by subcritical failures such as multiple cracking of plies and delamination. The influence of tensile loading on the initiation and growth of the subcritical failure significantly differ from that of compressive loading because of the difference in tensile strength and compressive strength of the most resin matrix. Furthermore, the criticality of the ply cracking and delamination to the ultimate fatigue failure appears to be different from tension to compression.

It is one of the main goals of this study to understand the fatigue behavior of composite laminates under different loading conditions. To achieve this objective, a series of fatigues are conducted under tension-tension, tension-compression, and compression-compression loading for a variety of values of mean stress levels. Based on the fatigue data obtained so far, the fatigue life is presented in the form of S-N and constant-life curves and the subcritical failure is presented in terms of loss of modulus, crack density, and delamination as function of fatigue cycle.

The material system investigated in this program was T300/1034C graphite/epoxy supplied in prepreg form by Fiberite Corporation. The panels of the $[0/45/90/-45]_{2s}$ laminate were fabricated in an autoclave according to the manufacturer's recommended cure cycle. Straight-sided coupon specimens were cut

from the panels using a diamond-impregnated saw. All specimens were 2.5" long in gage section and 0.75" wide. The free-edges of some specimens were ground with sand paper and then polished with 0.5 micron polishing powder in order to facilitate microscopic examination.

The various loading conditions were considered employing ten mean stress levels (S_m) of 0, 10, 20, 30, 42.5, 50, -10, -20, -30, and -42.5 ksi, and four different stress amplitudes, S_r . A side support device was used to prevent specimen buckling in the case of which the minimum excursion fatigue stress is compression. All fatigue tests were conducted using MTS testing machines with load control mode at frequency of 10 Hz. The fatigue test was terminated at either fatigue failure or 5×10^6 cycles for those specimens to generate fatigue life data. The damages in the form of loss of modulus, transverse cracks, and delamination incurred during fatiguing were periodically assessed at various fractions of fatigue life by interrupting fatigue testing. An extensometer with 1" gage length was used to measure the modulus change. The applied static load in this test was limited to less than the maximum or minimum fatigue stress. The transverse cracks in each off-axis ply and the location of free-edge delamination were documented by scanning the specimen lengthwise under a microscope. The specimen then was subjected to x-ray radiography to delineate the delamination growth toward the middle of the specimen. TBE is used to enhance the x-ray image.

Table 27 presents the result of static strength test with Weibull parameters estimated by maximum likelihood method. The tensile strength appears to be slightly greater than the compressive strength. The transverse cracks developed under static test were also documented on both free-edges by incremental step loading. The average value of cracks in both free edges were divided by specimen gage length to obtain crack density. Figure 32 shows the typical results of crack density vs. applied tensile stress. The first crack occurred in the 90 deg. ply around 60 ksi of applied stress. The cracks in the 90 deg. plies monotonically

IMPROVED MATERIALS FOR COMPOSITE AND ADHESIVE JOINTS
(U) DAYTON UNIV OH RESEARCH INST R KIM ET AL JUL 84
UDR-TR-83-117 AFWAL-TR-84-4074 F33615-81-C-5056

272

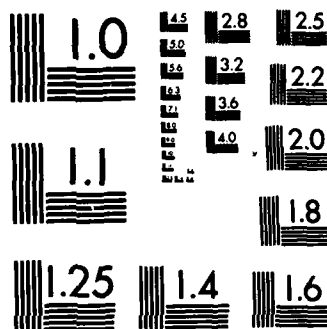
F/G 11/4

ML

END

FILMED

0.740



MICROCOPY RESOLUTION TEST CHART
NATIONAL BUREAU OF STANDARDS-1963-A

TABLE 27
RESULT OF STATIC STRENGTH

	Strength, Ksi				Mean ksi	Weibull Parameter $\hat{\alpha}_g$ $\hat{\beta}_g$	
Tension	81.34	73.38	78.13	79.09	76.55	17.8	78.98
	84.02	72.64	81.61	71.08			
Compression	70.54	70.55	71.32	72.07	74.29	21.6	76.01
	77.73	75.93	71.40	77.94			

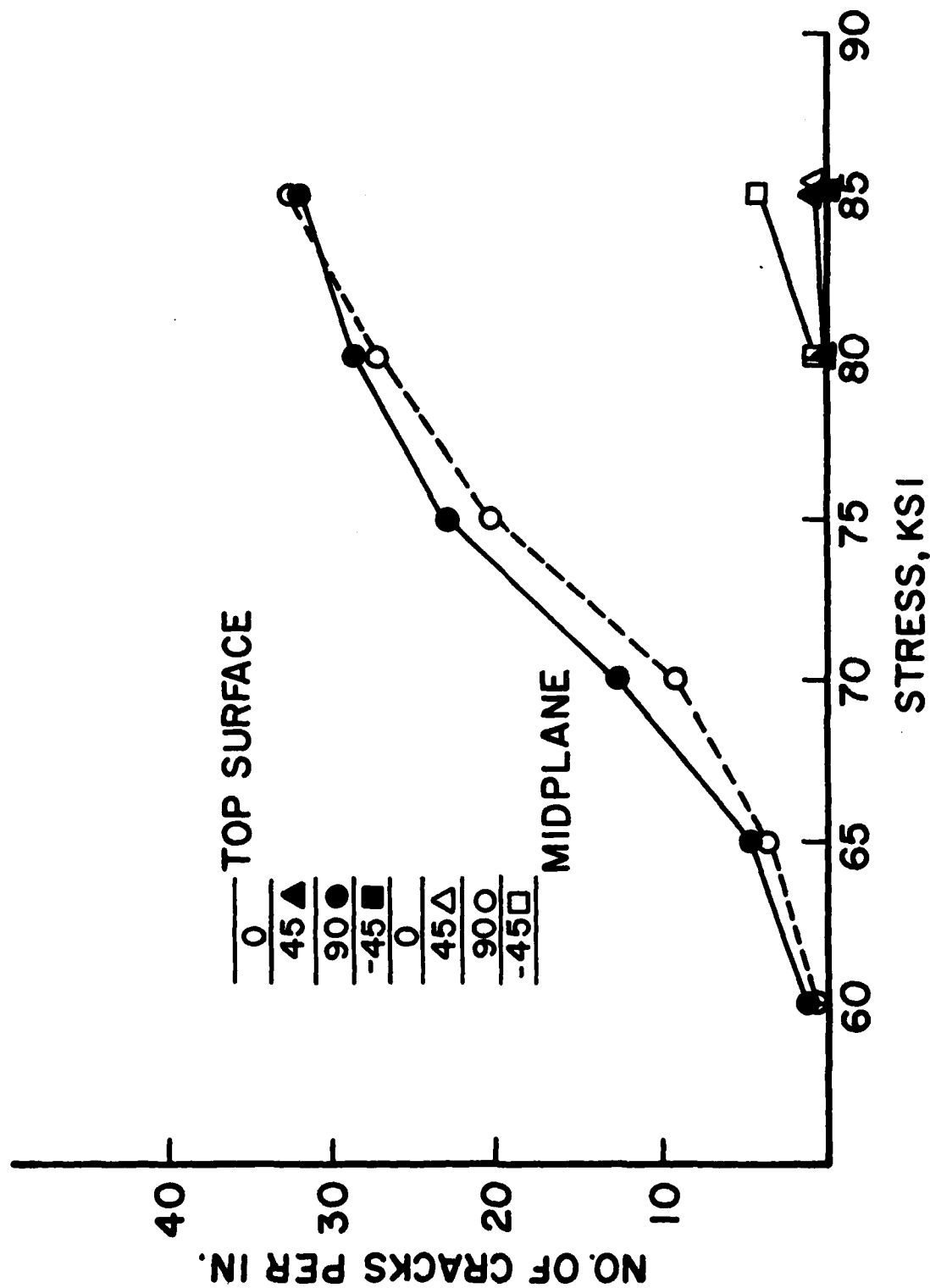


Figure 32. Crack Density vs. Applied Uniaxial Tensile Stress for Gr/Ep T300/1034C with [0/45/90/-45]_{2s}.

increases as increasing applied stress. The first crack in the 45 and -45 deg. occurred around 80 ksi as shown in Figure 32. Most of the transverse cracks were arrested at the interface and extended along the interface as shown in Figure 33. In compression, no transverse crack was found up to the last incremental step ranging from 90 to 97% of the compressive strength.

Table 28 presents the summary of fatigue life data obtained in this program. The Weibull shape parameter $\hat{\alpha}_p$ is obtained by pooling all data for each mean stress level and scale parameter $\hat{\beta}$ is the characteristic fatigue life corresponding to $\hat{\alpha}_p$. The stress magnitude S_r and its characteristic life $\hat{\beta}$ were fitted to the power law of S-N relation by the least square method. The S-N curves are presented in Figures 34 and 35 for positive and negative mean stress, respectively. All the regression lines in Figures 34 and 35 gave a reasonable fit to the series of characteristic life data from which it was computed.

The correlation coefficients range from 0.93 to 0.99. This least square fit is used to estimate the value of stress amplitude, S_r which corresponds to a particular value of fatigue life to construct the constant fatigue life curves as shown in Figure 36. The open and solid circles indicate the fatigue strength obtained from Figures 34 and 35 for each fixed value of fatigue life. The solid line represents another least square lines defining relation between S_r and S_m . These regression lines were forced to pass through the static tensile and compressive strength on the mean stress axis since stress amplitude is zero for these points. The peaks of constant life curves appear in the tension-dominated quadrant. This is possibly due to the fact that the static tensile strength is slightly greater than the compressive strength for this laminate. It is also noted that the peak moves further into the right as decreasing fatigue life.

Figures 37 - 44 present the crack density vs. fatigue cycle for one specimen of each stress level of tension-compression and tension-tension fatigue. The plotted crack density is the

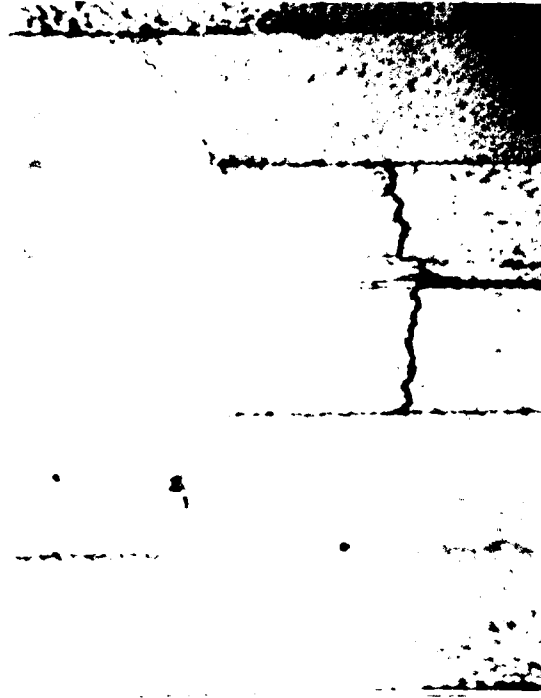


Figure 33. Microphotograph Showing Cracks of $[0/45/90/-45]_{2s}$ Laminate at 80 ksi of Static Tension.

TABLE 28
FATIGUE DATA
T300/1034C [0/45/90/-45]_{2s}

Mean, S_m ksi	S_r ksi	S_{max}/S_{min} ksi	Cycle to Failure					Weibull Parameters	
			5×10^6 *	5×10^6 *	5×10^6 *	5×10^6 *	5×10^6 *	$\hat{\sigma}_p$	$\hat{\delta}$
0	25	25/-25	426,940	1,459,260	565,060	525,750	1,542,400	2.33	1,064,410
	30	30/-30	66,260	72,240	191,520	254,860	226,890		
	35	35/-35	26,440	14,690	26,470	22,570	44,980		
	40	40/-40							
10	30	40/-20	2,357,620	1,974,590	912,000	670,790		2.22	1,668,820
	35	45/-25	167,440	435,490	190,540	251,780			
	42.5	52.5/-32.5	68,170	18,500	41,860	26,590			
	50	60/-40	3,180	6,130	810	3,240			
20	25	45/-5	839,100	2,403,910	2,837,440	82,190		1.11	1,594,830
	30	50/-10	142,790	193,440	462,970	251,450			
	35	55/-15	58,580	92,750	30,420	100,490			
	40	60/-20	16,860	410	250	10,890			
30	25	55/5	40,130	53,400	102,250	38,490		1.30	60,160
	30	60/0	11,350	14,990	11,370	5,480			
	35	65/-5	130	3,170	380	870			
	40	70/-10	270	230	2,640	1,220			
42.5	17.5	60/25	578,150	361,210	819,100	3,510,170		1.65	1,662,110
	22.5	65/20	53,350	37,430	46,190	25,560			
	25.0	67.5/17.5	9,590	12,920	3,480	7,180			
	27.5	70/15	2,640	3,080	4,270	4,360			
50	15	65/35	1,022,650	2,391,910	502,100	2,309,000		1.80	1,722,580
	17.5	67.5/32.5	162,100	7,130	241,700	188,880			
	20	70/30	10,300	16,400	3,250	17,510			
	22	72/28	6,950	16,960	4,150	8,510			

* Run Out

TABLE 28 (CONTINUED)
FATIGUE DATA
T300/1034C [0/45/90/-45] 2s

Mean, S_m ksi	S_r Ksi	S_{max}/S_{min} Ksi	Cycle to Failure			Weibull Parameters		
						a_p	β	
-10	30	20/-40	595,510	865,930	285,640	366,600	1.93	571,450
	35	25/-45	46,550	205,080	70,910	29,800		110,380
	42.5	32.5/-52.5	6,080	7,040	13,780	9,050		9,430
	50	40/-60	3,700	1,150	4,930	1,400		3,190
-20	25	5/-45	175,620	32,700	3,941,300	5×10^6 *	0.98	3,030,850
	30	10/-50	53,580	156,870	11,310	21,550		60,330
	35	15/-55	10,550	660	2,140	9,090		5,570
	40	20/-60	670	620	1,220	230		680
-30	25	-5/-55	37,860	459,400	46,190	28,110	1.10	152,640
	30	0/-60	32,300	57,520	48,010	6,640		36,740
	35	5/-65	2,570	440	470	700		1,080
	40	10/-70	430	1,390	780	360		750
-42.5	17.5	-25/-60	3,075,770	1,121,810	5.8×10^6 *	403,230	1.17	3,509,330
	22.5	-20/-65	57,940	1,110	7,750	11,140		21,440
	27.5	-15/-70	910	1,770	2,350	2,010		1,780

* Run Out

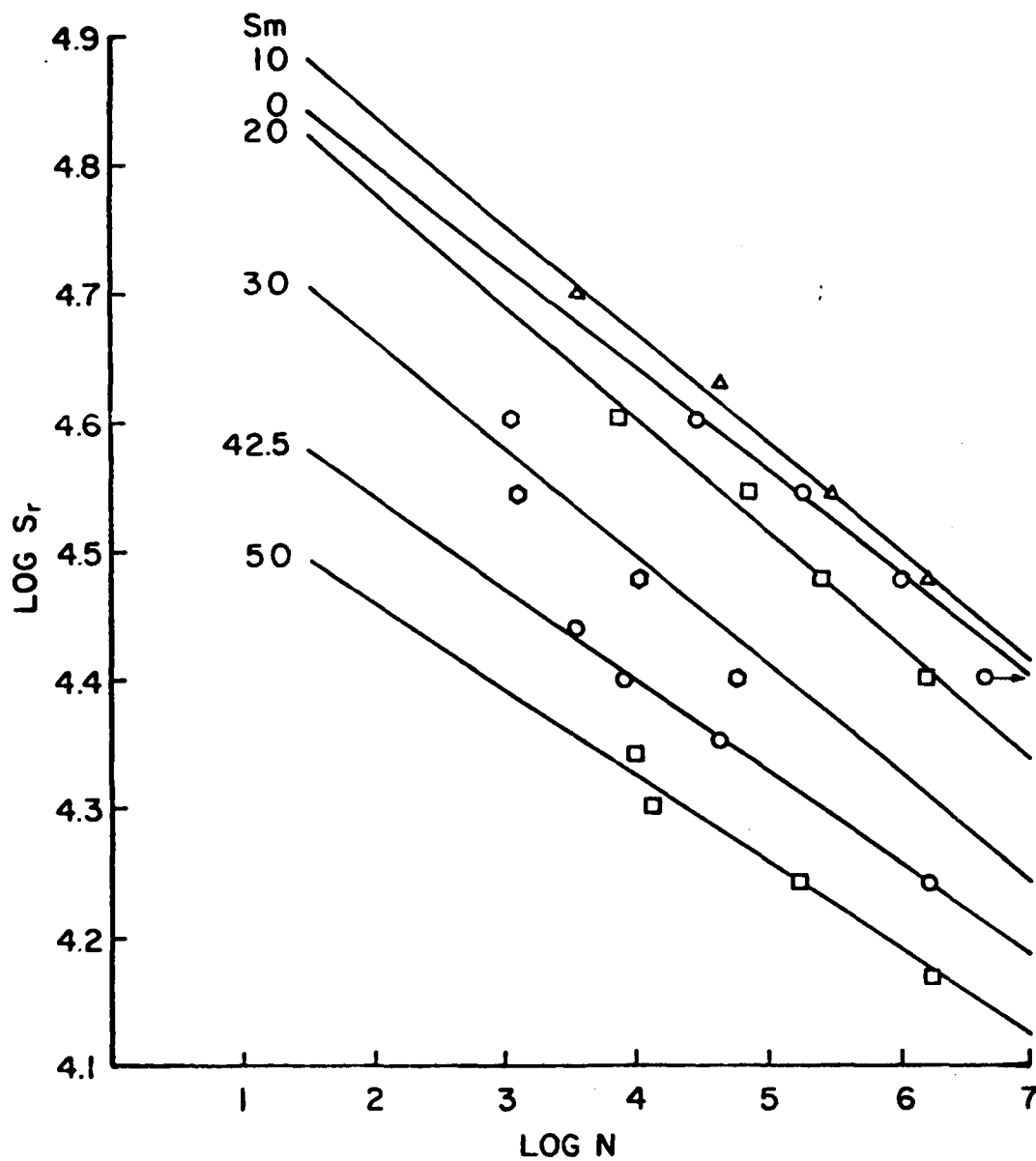


Figure 34. S_r - N Curves for Positive Mean Stress, S_m ($S_r = S_{\max} - S_m$).

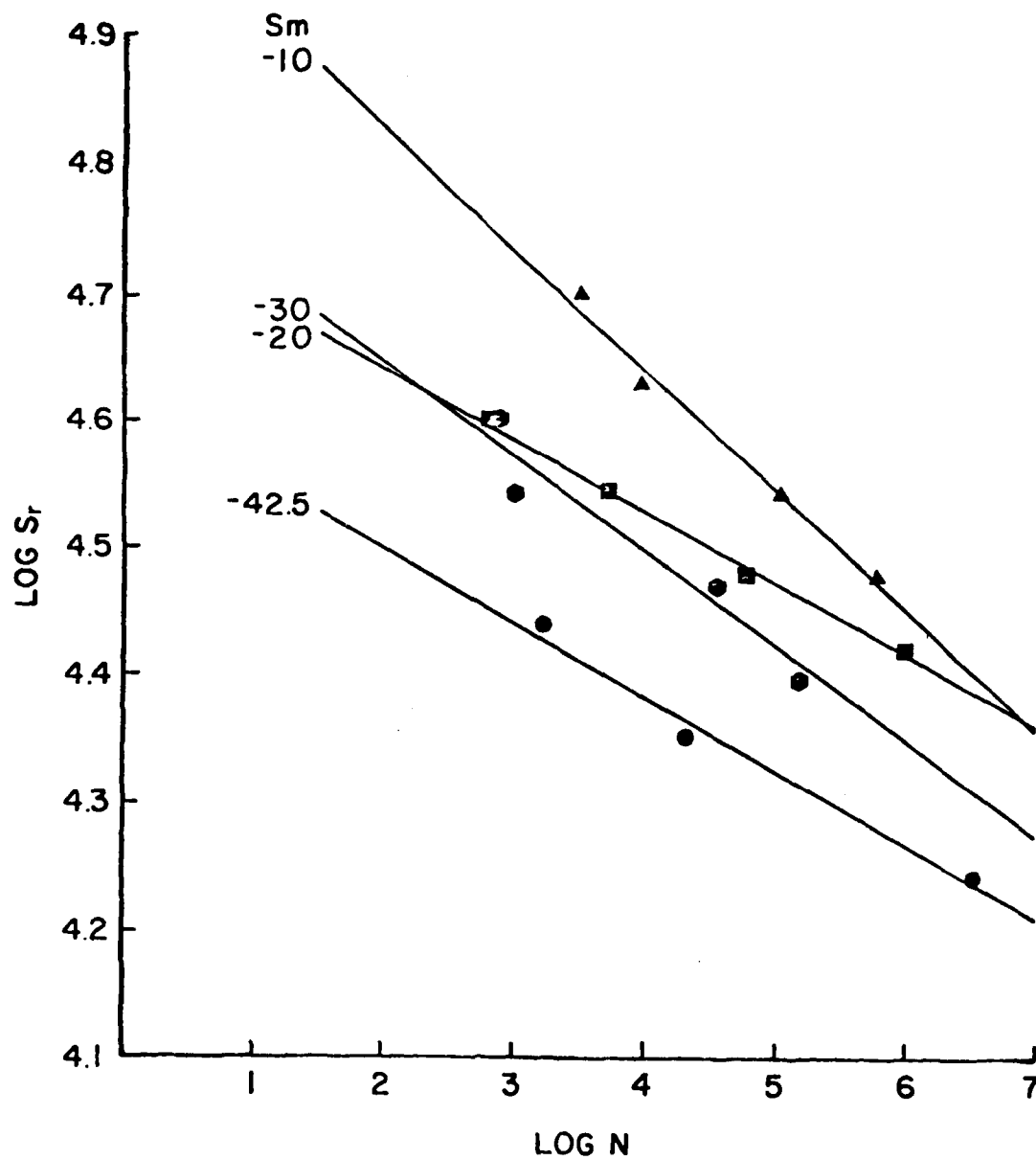


Figure 35. S-N Curves for Negative Mean Stress, S_m ($S_r = S_{\max} - S_m$).

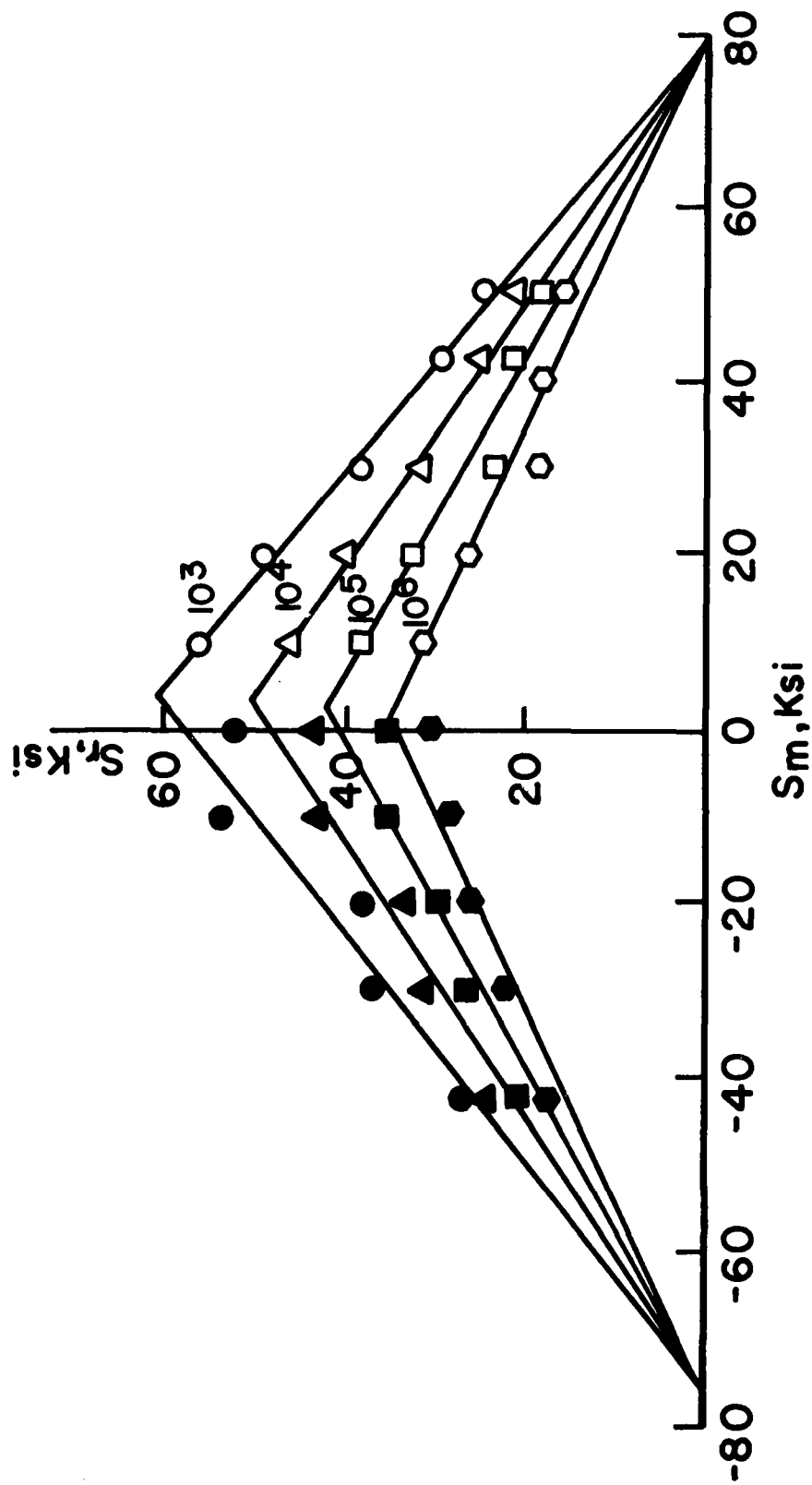


Figure 36. Constant Life Curve for Gr/Ep T300/1034C with $[0/45/90/-45]_{2s}$ Orientation.

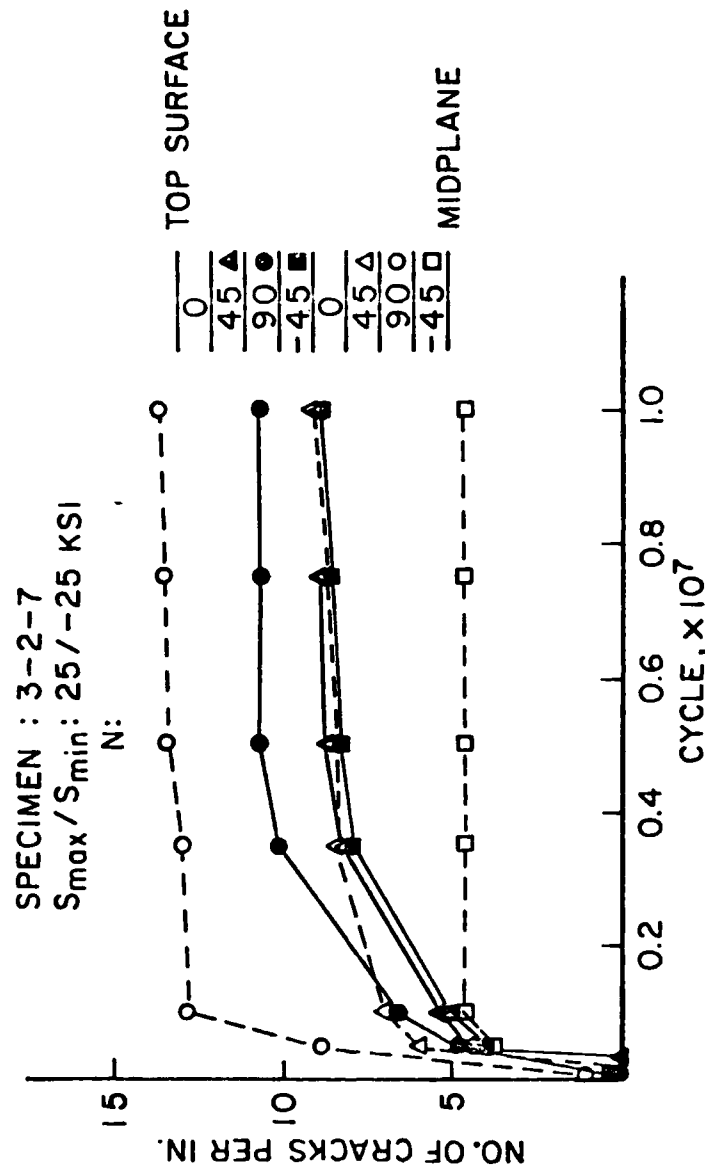


Figure 37. Crack Density vs. Number of Cycle for Gr/Ep T300/1034C with [0/45/90/-45]_{2s}.

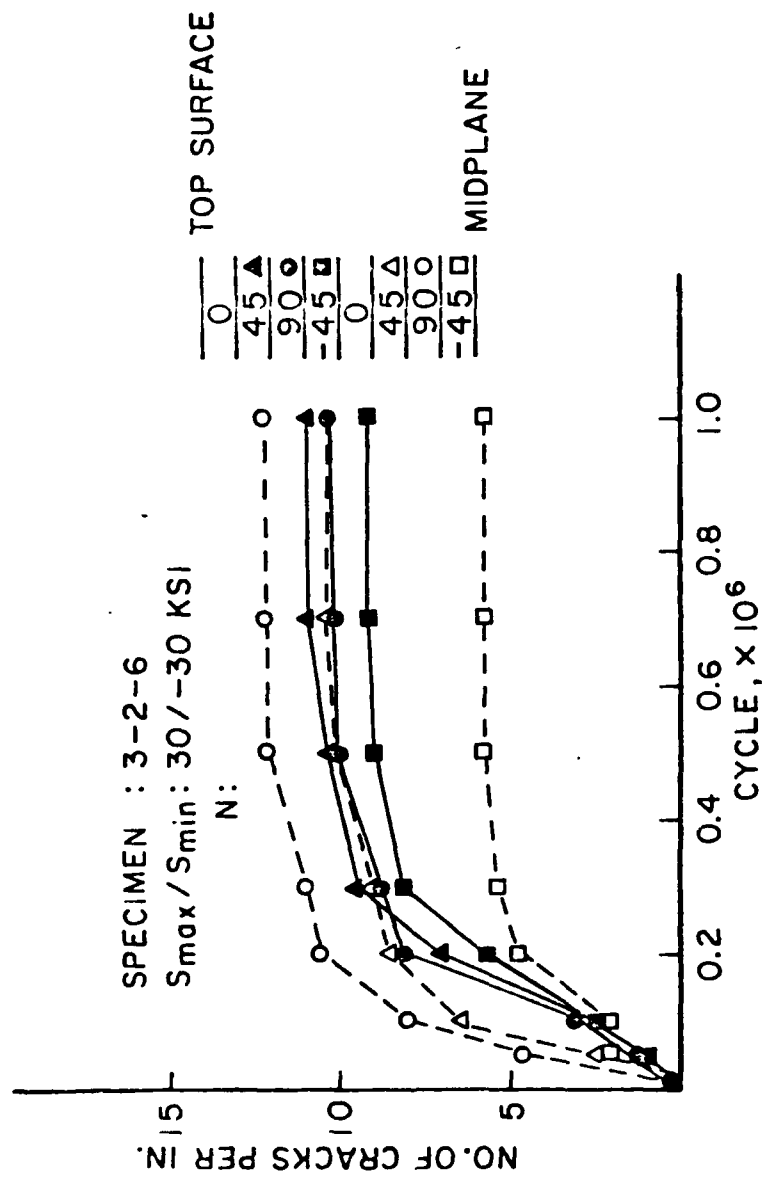


Figure 38. Crack Density vs. Number of Cycle for Gr/Ep T300/1034C with $[0/45/90/-45]_{2s}$.

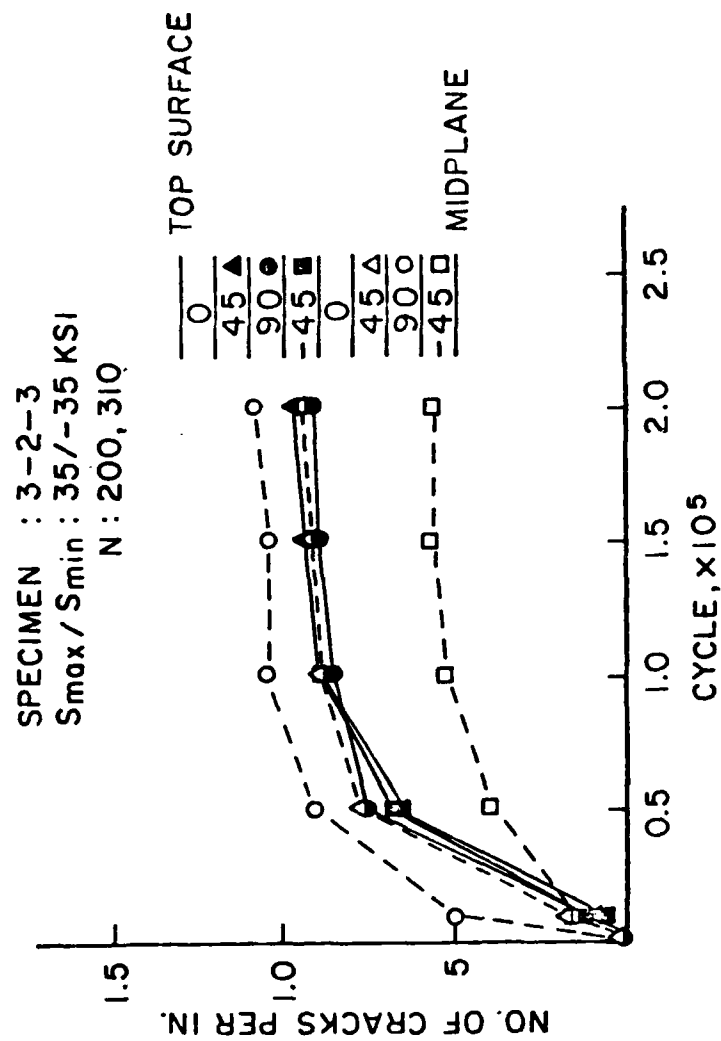


Figure 39. Crack Density vs. Number of Cycle for Gr/Ep T300/1034C with $[0/45/90/-45]_{2s}$.

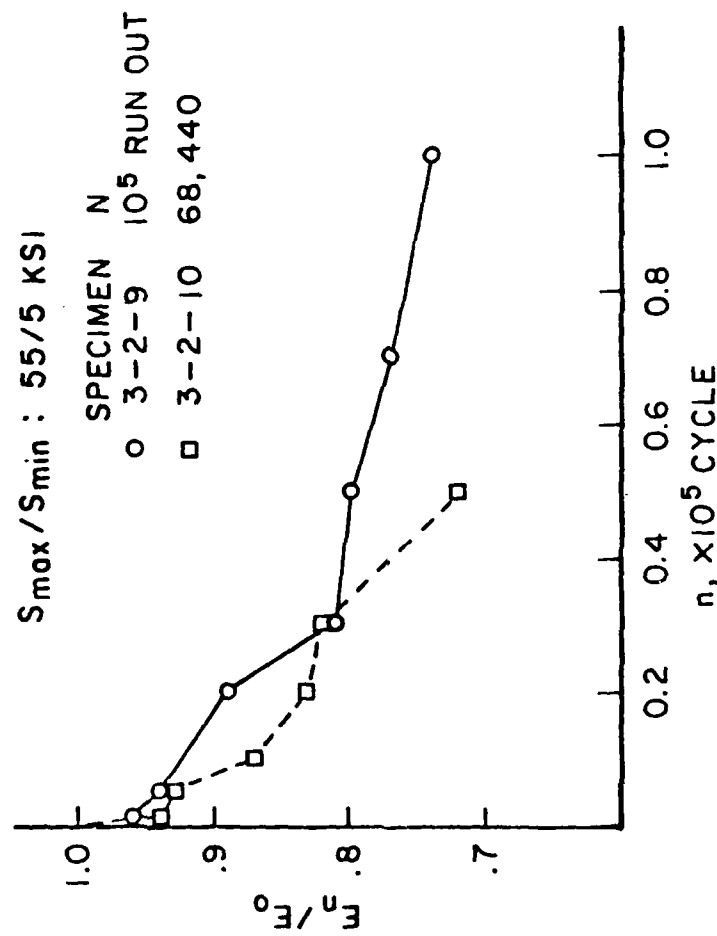


Figure 51. Change of Longitudinal Modulus as Function of Number of Cycle for Gr/Ep T300/1034C with $[0/45/90/-45]_{2s}$.

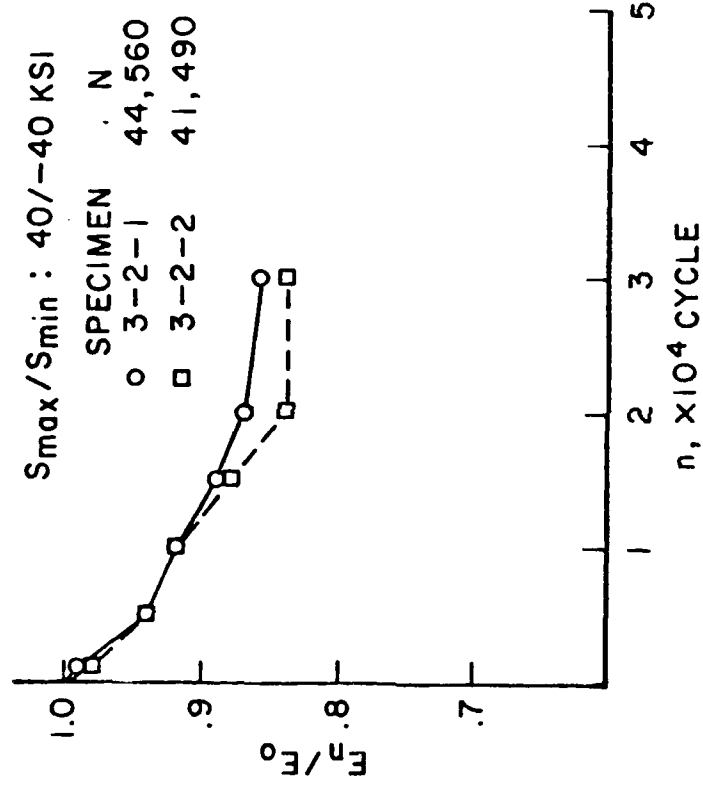


Figure 50. Change of Longitudinal Modulus as Function of Number of Cycle for Gr/Ep T300/1034C with $[0/45/90/-45]_{2s}$.

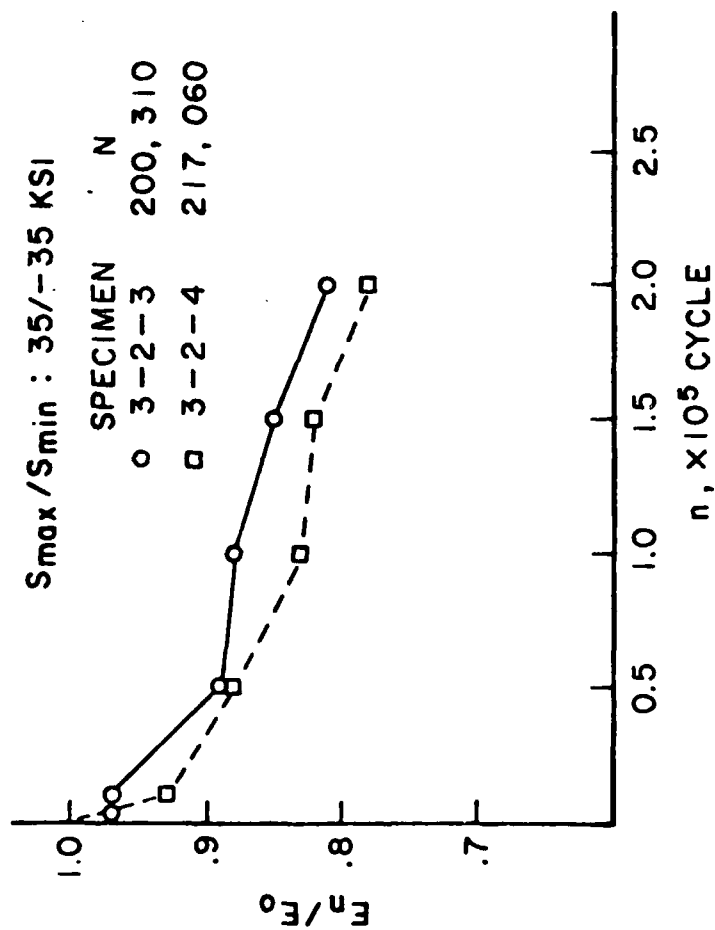


Figure 49. Change of Longitudinal Modulus as Function of Number of Cycle for Gr/Ep T300/1034C with $[0/45/90/-45]_{2s}$.

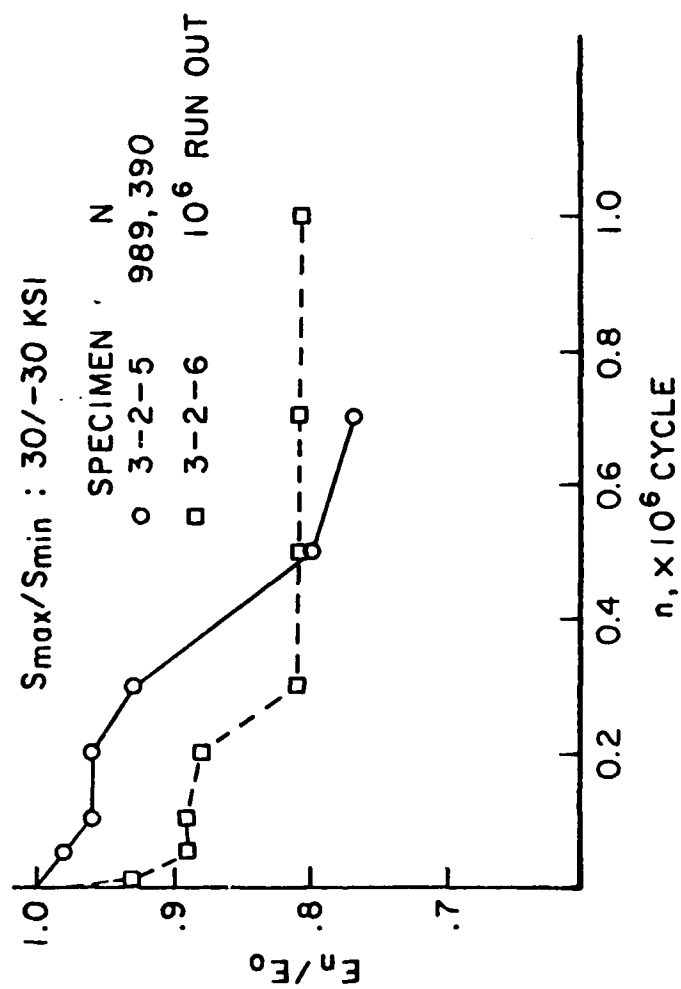


Figure 48. Change of Longitudinal Modulus as Function of Number of Cycle for Gr/Ep T300/1034C with $[0/45/90/-45]_{2s}$.

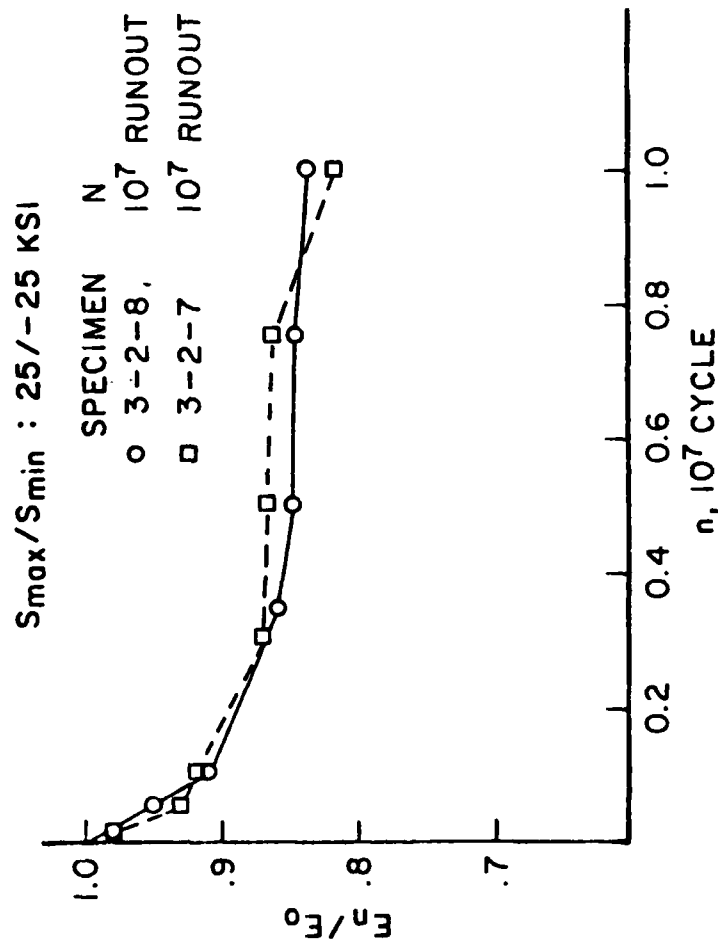


Figure 47. Change of Longitudinal Modulus as Function of Number of Cycle for Gr/Ep T300/1034C with $[0/45/90/-45]_{2s}$.

47 to 54 present the E_n/E_o vs. number of fatigue cycle, where E_n and E_o are the longitudinal modulus at number of cycles and prior to fatigue, respectively. In most cases, the modulus decreases rapidly in the early stage of fatigue life and thereafter decreases rather moderately as a function of fatigue cycle. The degree of change in modulus is different from specimen to specimen as well as the fatigue stress level. In compression-compression fatigue, the modulus practically remains unchanged until the last measurement which is equivalent to more than 80% of the fatigue life. The delamination was also observed by examining free-edges and the x-ray. The microphotographs of two typical specimens are presented in Figures 55 and 56. The major delamination occurred at the interface between the 90/-45 and 45/90 plies. The same characteristics of delamination was observed in all other specimens. This laminate does not show any delamination under static loading. Figures 57 to 64 show the progress of the delamination toward the middle of the specimen as increasing fatigue cycle. Delamination in all specimens was found at the first inspection period which indicated the cycle in Table 29. Thus, the delamination occurred earlier than at the indicated cycle. The amount of the delamination growth near the fatigue failure varies from specimen to specimen as well as the nature of the fatigue stress.

During the examination of free edge, a number of fiber break was observed in some specimens. A typical fiber break in fatigue is shown in Figure 65.

b. Fatigue Behavior of Graphite/Thermoplastic Composites

A series of fatigue tests conducted on graphite cloth reinforced polyetheretherketone and epoxy matrix composite to evaluate their fatigue performance. A technical report on this work was completed during this reporting period and is attached to F33615-81-C-5056 for the period Dec. 82 - Feb. 83 as Appendix II. Thus, a brief description only is given. Different fatigue failure modes were investigated using three types of laminates,



Figure 46. Microphotograph Showing the Damage Developed at the Region Between the End Tab and the Side Support Device Under Compression Fatigue. $S_{max}/S_{min} = 0/-60$ ksi, $n = 10,000$ cycles, and fatigue life, $N = 24,950$. T300/1034C [0/45/90/-45]_{2s}.

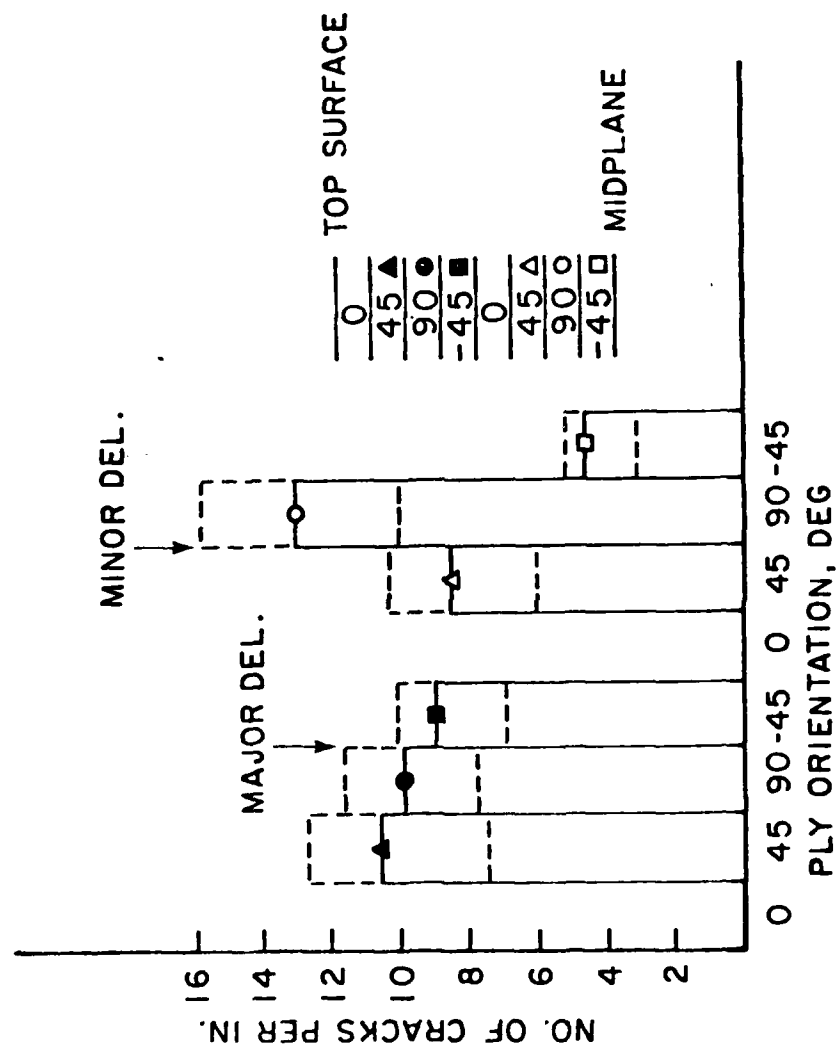


Figure 45. Crack Density for Each Angle Ply for Gr/Ep T300/1034C with $[0/45/90/-45]_2$.

average of two symmetrical plies with respect to the midplane of the laminate. The stacking sequence shown in Figures 37 to 44 is one half of the laminate thickness. The open circle and solid circle for the 90 degree ply represents the average value of the two inner ply and the two outer ply from the midplane, respectively. The crack density increases rapidly in the early stage of fatigue life and remains unchanged for the rest of fatigue life for all specimens. The saturated crack density tends to be independent upon the fatigue stress levels for the laminates considered in this test. However, Figures 37 to 44 indicate that the saturated crack density appears to be somewhat dependent upon the position of the ply within the laminate. To clarify this, the average crack density of the respective angle ply for all the specimens are presented in Figure 45. The dotted line indicates the range of crack density. The smaller crack density in the -45 ply at the midplane is due to the thickness of the ply where two plies are stacked together. There is a considerable difference between two 90 degree plies which are surrounded with the same angle plies but in different positions relative to the midplane. Fatigue loading causes more cracks in the 45 and -45 deg plies but less cracks in the 90 deg plies in these laminates. The reason for this difference is unknown at present. In compression-compression ($S_{max}/S_{min} = -5/-55$ and $0/-60$ ksi) no transverse crack in all angle plies and no delamination were observed except for the unsupported small area. Thus, the specimens apparently failed without any indication of damage related to matrix. All four specimens tested (two specimens at each stress level) indicated some damage at the unsupported area as shown in Figure 46. However, this damage was confined to the end tab area without growing as an increasing cycle. Two specimens were broken at the end tab area and the other two specimens were broken far away from the damage area. Thus, the influence of this type of damage on fatigue life remains in question at present.

The change of modulus as function of fatigue cycle was measured by an extensometer with one inch gage length. Figures

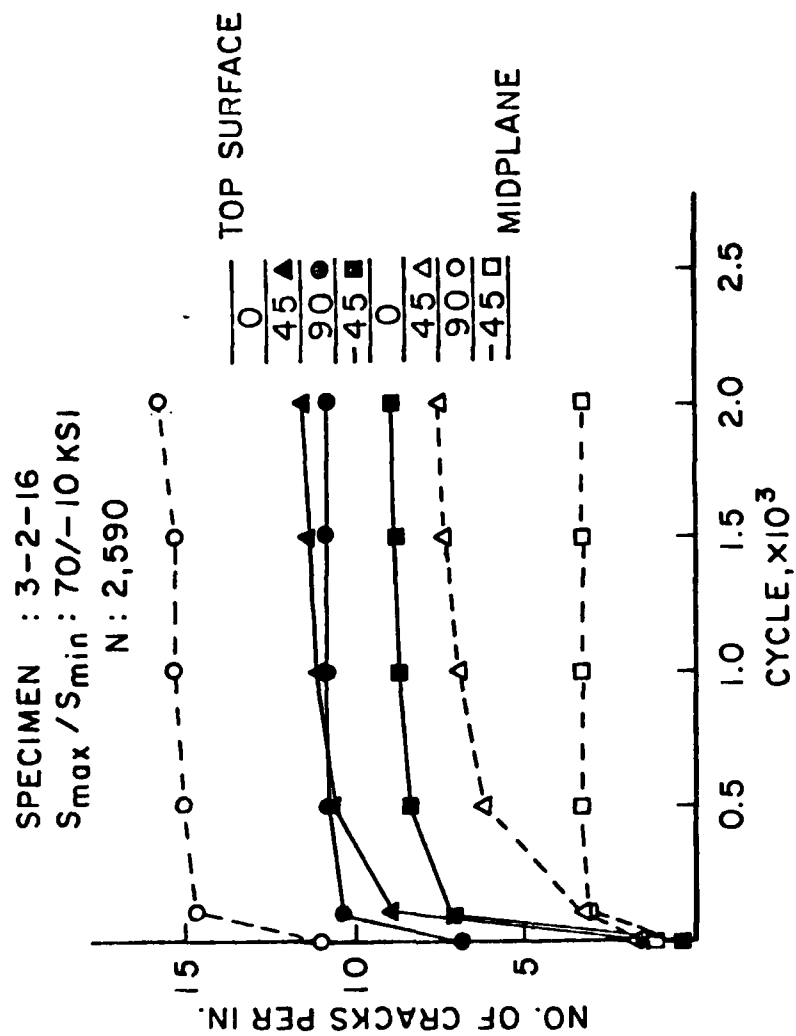


Figure 44. Crack Density vs. Number of Cycle for Gr/Ep T300/1034C with $[0/45/90/-45]_{2s}$.

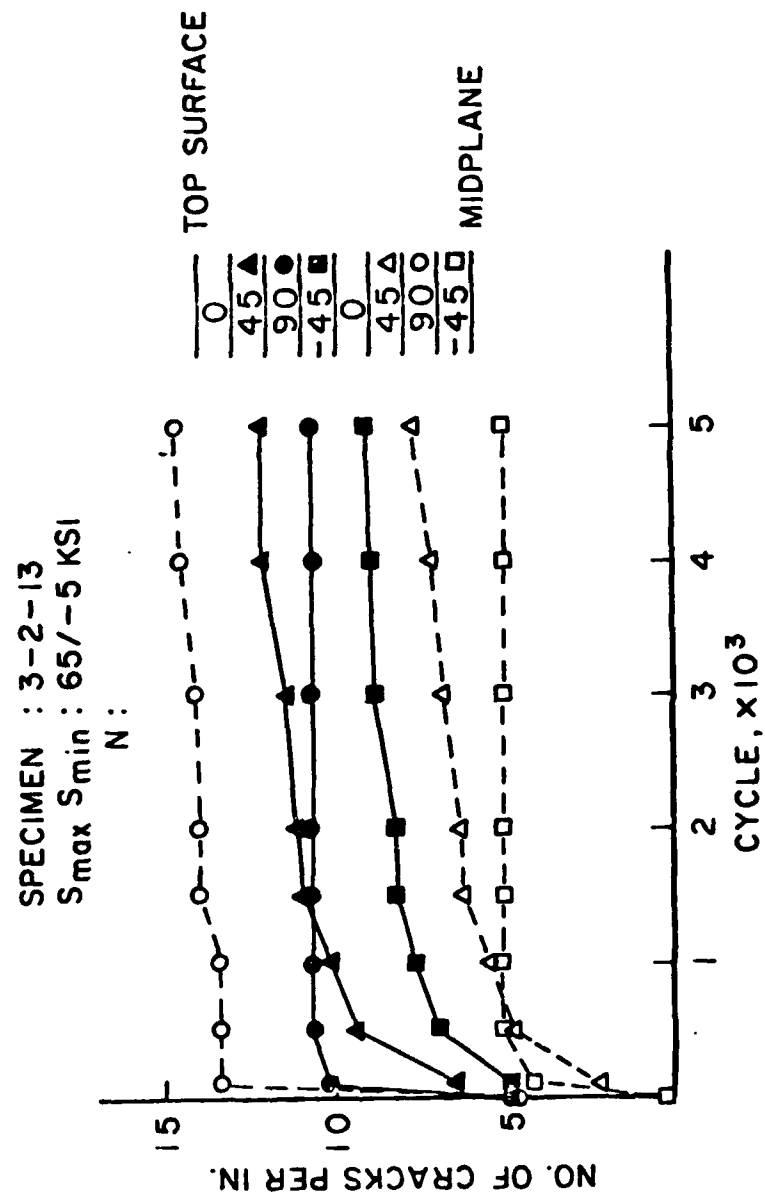


Figure 43. Crack Density vs. Number of Cycle for Gr/Ep T300/1034C with [0/45/90/-45]_{2s}.

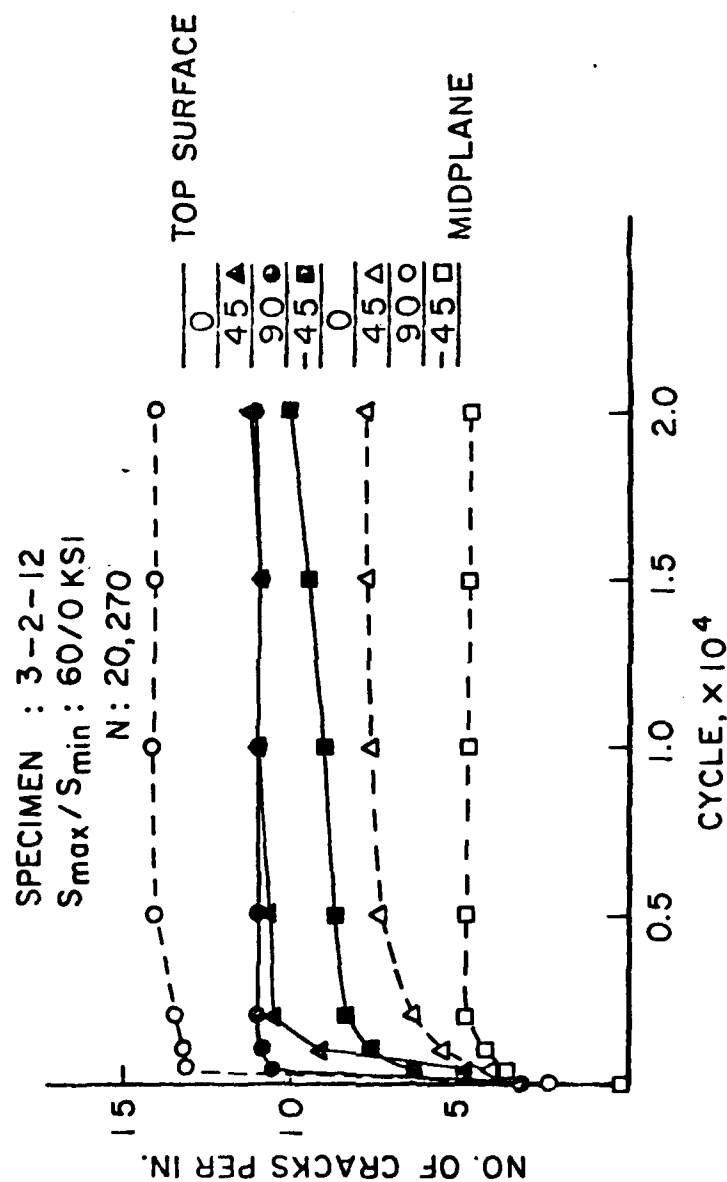


Figure 42. Crack Density vs. Number of Cycle for Gr/Ep T300/1034C with [0/45/90/-45]_{2s}.

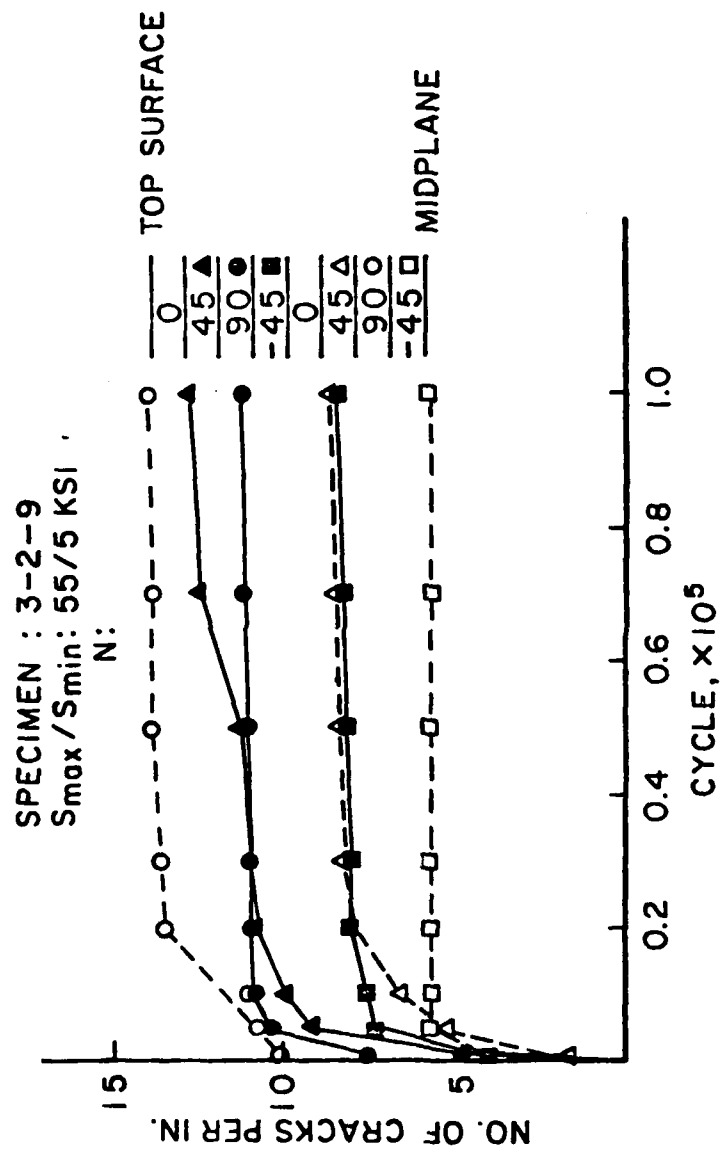


Figure 41. Crack Density vs. Number of Cycle for Gr/Ep T300/1034C with $[0/45/90/-45]_{2s}$.

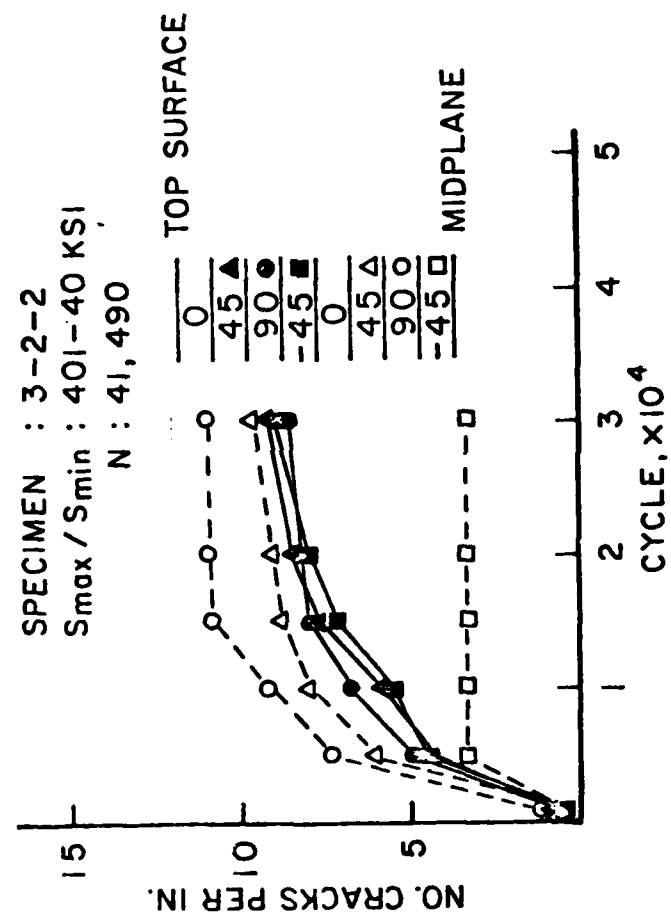


Figure 40. Crack Density vs. Number of Cycle for Gr/Ep T300/1034C with $[0/45/90/-45]_{2s}$.

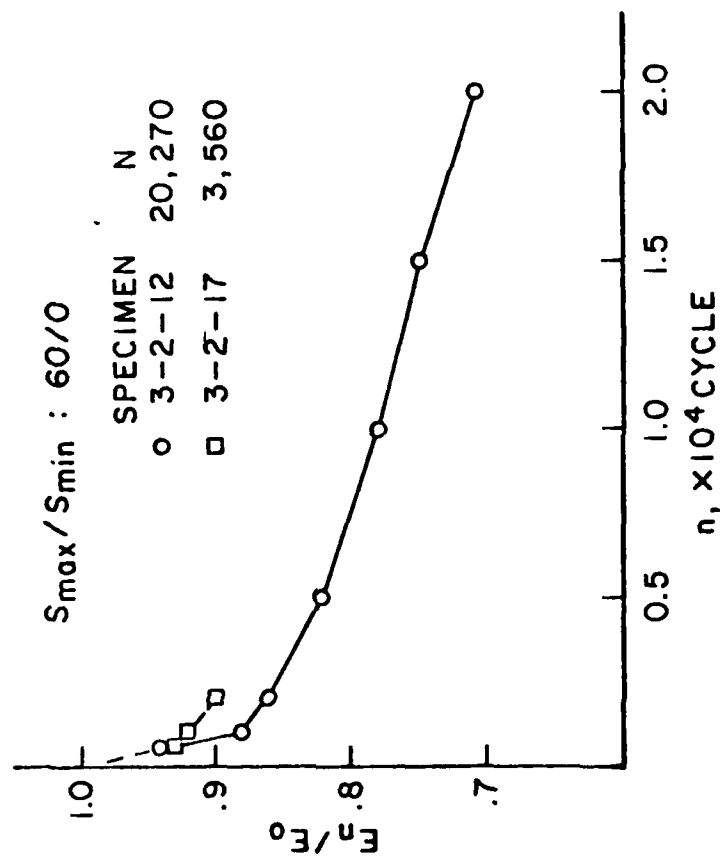


Figure 52. Change of Longitudinal Modulus as Function of Number of Cycle for Gr/Ep T300/1034C with $[0/45/90/-45]_{2s}$.

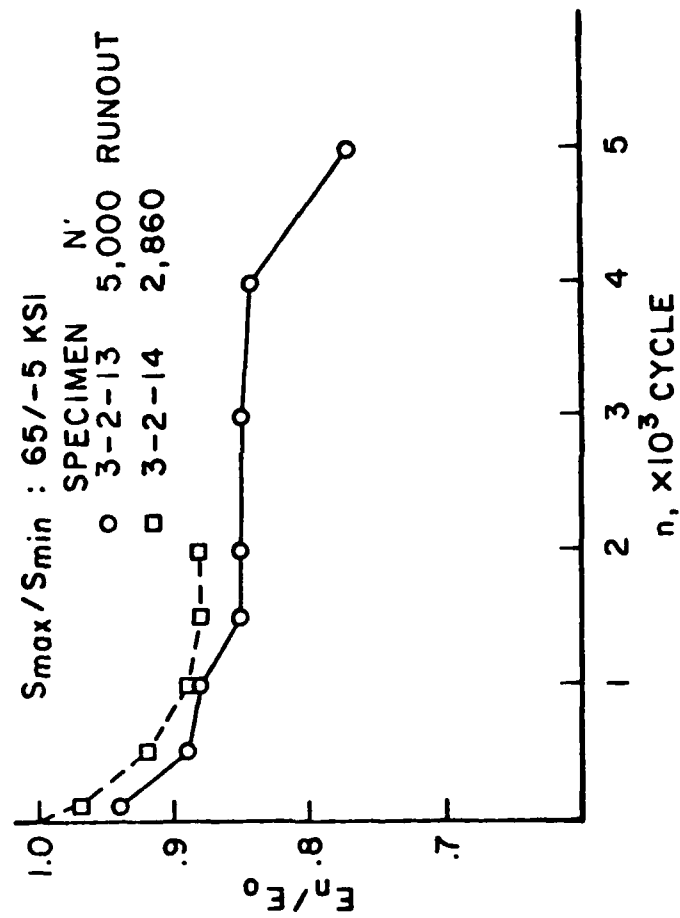


Figure 53. Change of Longitudinal Modulus as Function of Number of Cycle for Gr/Ep T300/1034C with $[0/45/90/-45]_{2s}$.

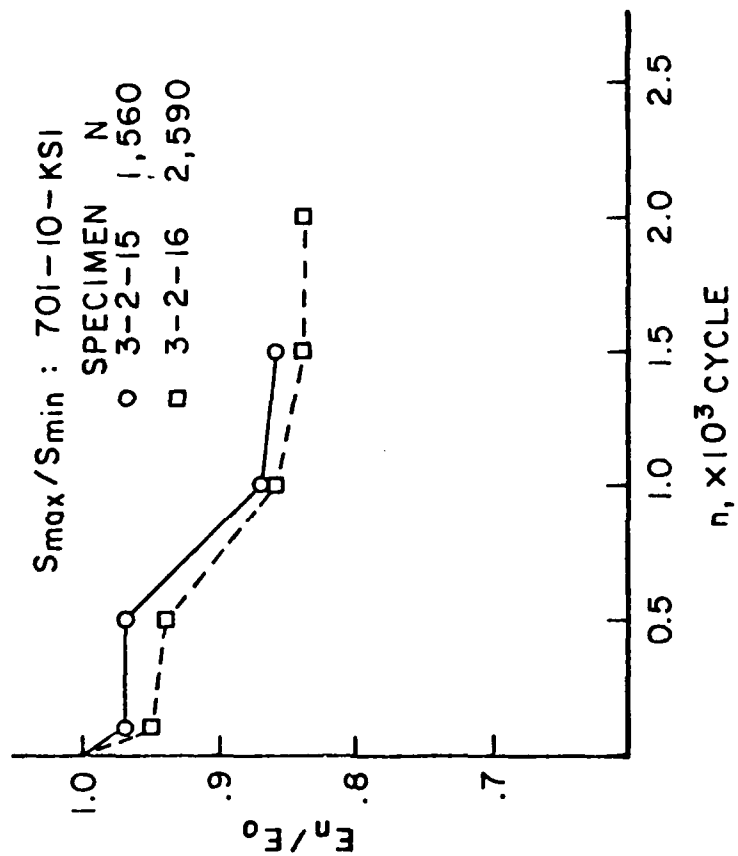


Figure 54. Change of Longitudinal Modulus as Function of Number of Cycle for Gr/Ep T300/1034C with $[0/45/90/-45]_{2s}$.



Specimen 3-2-1, $S_{\max} S_{\min} = 45/-45$ ksi, $n = 30,000$ cycle

Figure 55. Microphotograph Showing the Damage Through the Thickness for Gr/Ep T300/1034C with $[0/45/90/-45]_{2s}$.



Figure 56. Microphotograph Showing the Damage Through the Thickness for
Gr/Ep T300/1034C with $[0/45/90/-45]_{2s}$.

SPECIMEN 3-2-7

SPECIMEN 3-2-8

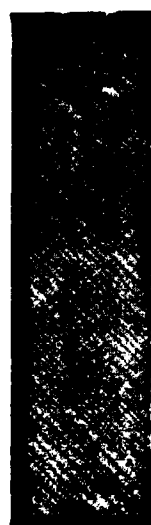
n, cycle



1×10^4



5×10^5



3×10^6



7.5×10^6

Figure 57. X-ray Pictures Showing Delamination Growth as Function of Fatigue Cycle, n for T300/1034C Gr/Ep. $S_{\max}/S_{\min} = 25/-25$ ksi.

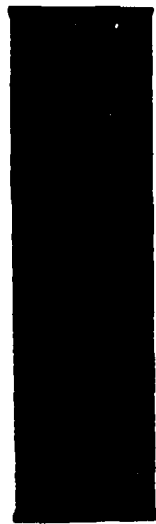
SPECIMEN 3-2-5

SPECIMEN 3-2-6

n, cycle



1×10^4



1×10^5



3×10^5



7×10^5

Figure 58. X-ray Picture Showing Delamination Growth as a Function of Fatigue Cycle, n for T300/1034C Gr/Ep. $S_{\max}/S_{\min} = 30/-30$ ksi.

SPECIMEN 3-2-3

SPECIMEN 3-2-4

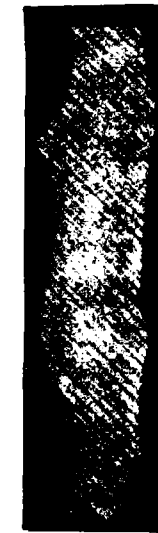
n, cycle



1×10^3



5×10^4



1.5×10^5

Figure 59. X-ray Pictures Showing Delamination Growth as Function of Fatigue Cycle, n for T300/1034C Gr/Ep. $S_{\max}/S_{\min} = 35/-35$ ksi.

SPECIMEN 3-2-1

SPECIMEN 3-2-2

n, cycle



1×10^3



1×10^4



2×10^4



Figure 60. X-ray Pictures Showing Delamination Growth as Function of Fatigue Cycle, n for T300/l034C Gr/Ep. $S_{\max}/S_{\min} = 40/-40$ ksi.

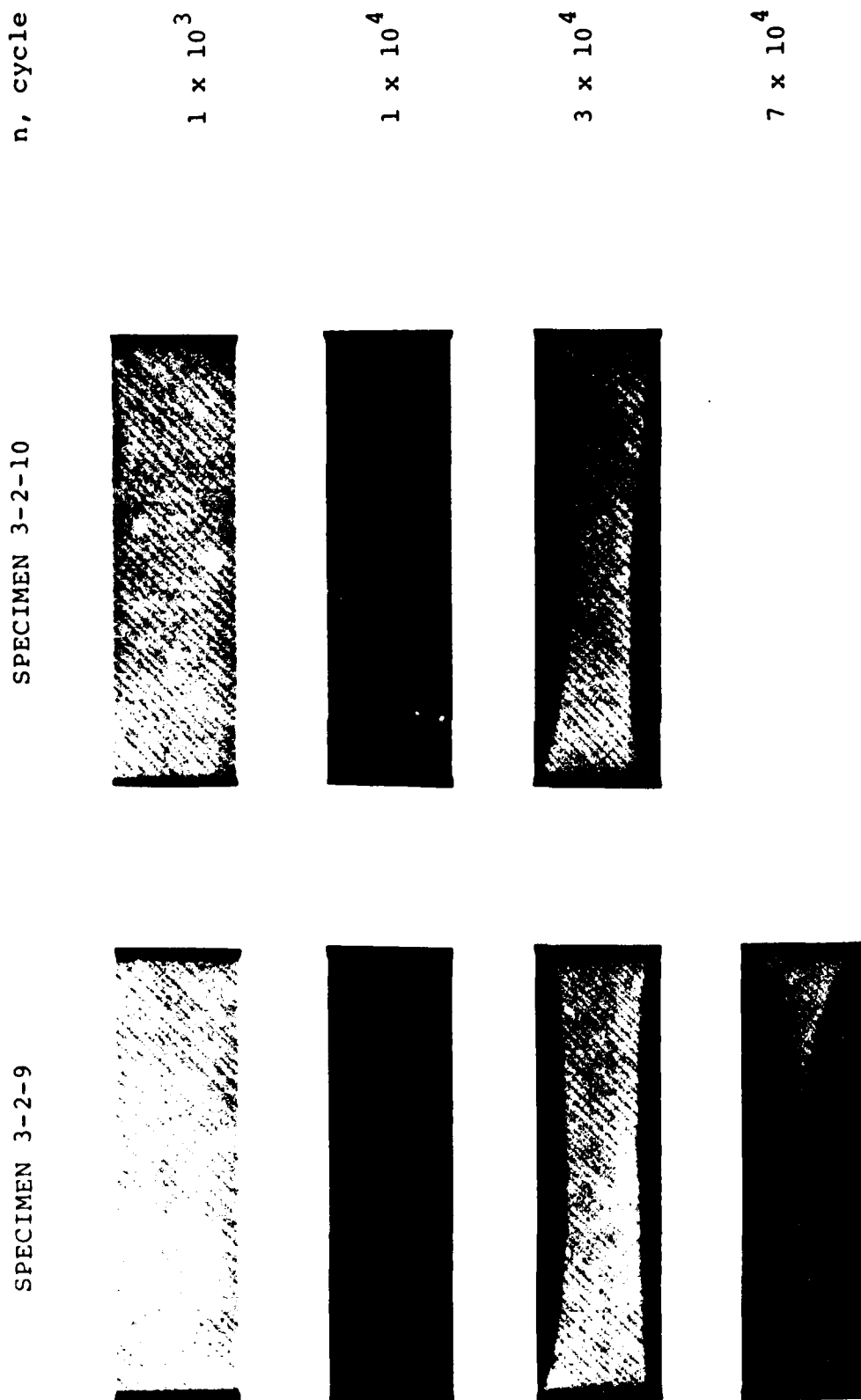


Figure 61. X-ray Pictures Showing Delamination Growth as Function of Fatigue Cycle, n for T300/1034C Gr/Ep. $S_{\max}/S_{\min} = 55/5$ ksi.

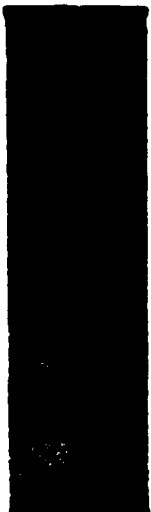
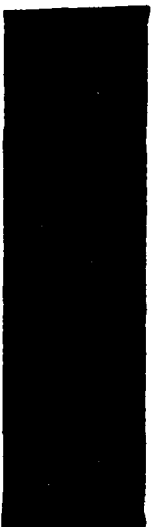
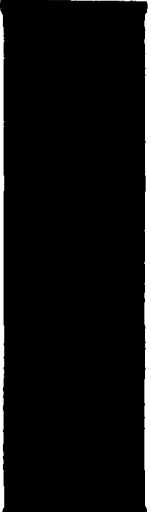





SPECIMEN 3-2-11	SPECIMEN 3-2-12	n, cycle
		5×10^2
		2×10^3
		1×10^4
		2×10^4

Figure 62. X-ray Pictures Showing Delamination Growth as Function of Fatigue Cycle, n for T300/1034C Gr/Ep. $S_{\max}/S_{\min} = 60/0$ ksi.

SPECIMEN 3-2-13

SPECIMEN 3-2-14

n, cycle



1×10^2



1×10^3



2×10^3



4×10^3

Figure 63. X-ray Pictures Showing Delamination Growth as Function of Fatigue Cycle, n for T300/1034C Gr/Ep. $S_{max}/S_{min} = 65/-5$ ksi.

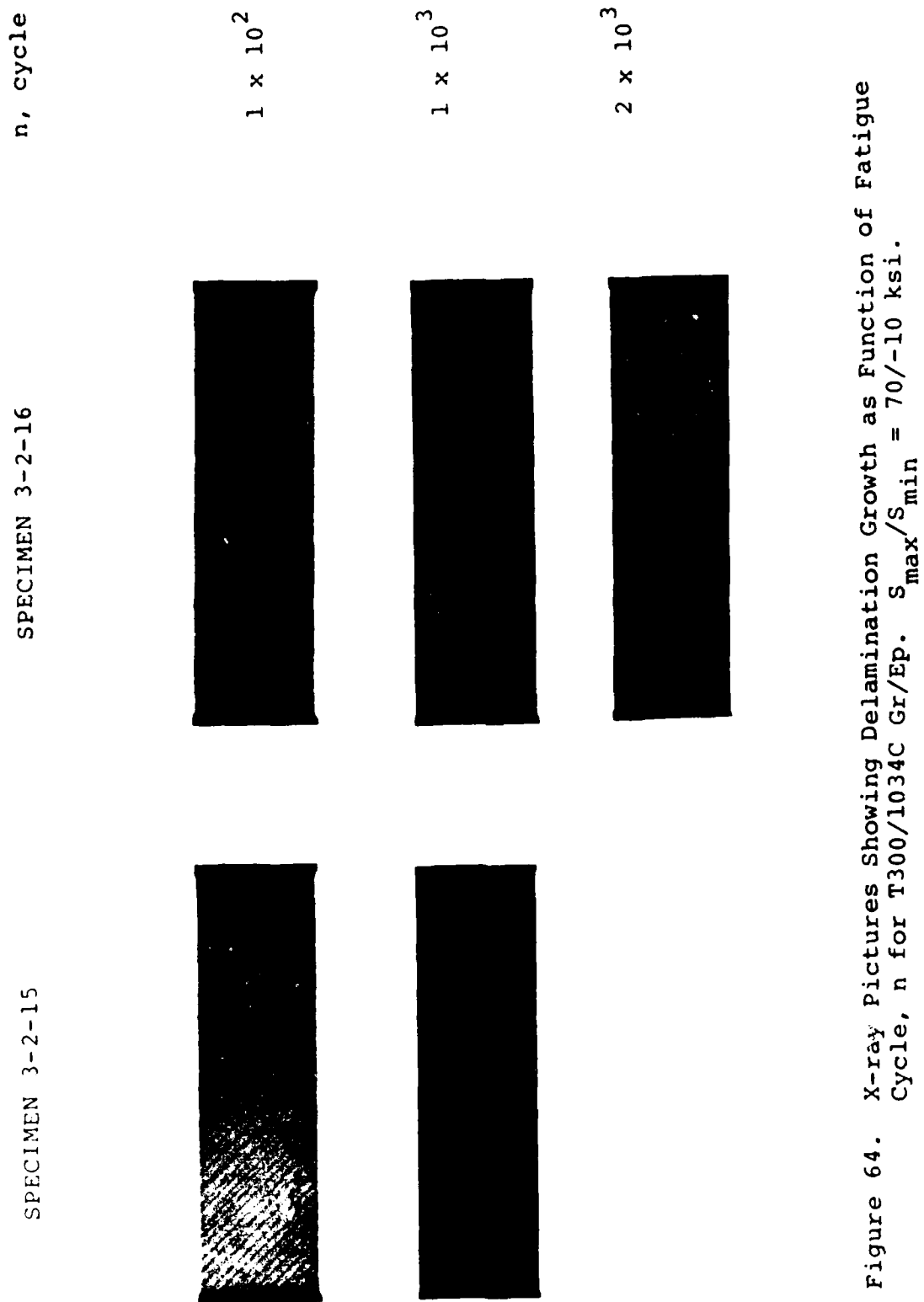


Figure 64. X-ray Pictures Showing Delamination Growth as Function of Fatigue Cycle, n for T300/1034C Gr/Ep. $S_{\max}/S_{\min} = 70/-10$ ksi.

TABLE 29

ONSET OF DELAMINATION UNDER FATIGUE
(DELAMINATION OCCURRED PRIOR TO THE INDICATED CYCLE)

Stress Range, ksi	25/-25	30/-30	35/-35	40/-40	55/5	60/0	65/-5	70/-10
Cycle	10,000	10,000	1,000	1,000	1,000	500	100	100

PATENTS

1. C. Fowler, Patent disclosure applied for in 1983 on a "Iso Dynamic Extensometer" used in the stress analysis of brittle NEAT resins.

PRESENTATIONS

1. S. R. Soni, "Stress and Strength Analysis of Composite Laminates at Delamination," Fourth International Conference on Composite Materials, Tokyo, Japan, October 24-26, 1982.
2. S. R. Soni, "Design Analysis of Thick Composites," 28th National Society for Advancement of Material and Process Engineering Symposium, Disneyland Hotel, Anaheim, California, April 12-14, 1983.
3. S. R. Soni, "A New Look at Commonly Used Failure Theories in Composite Laminates," 24th AIAA/SDM Conference, Lake Tahoe, Nevada, May 2-4, 1983.
4. John T. Hartness and R. Y. Kim, "A Comparative Study on Fatigue Behavior of Polyetheretherketone and Epoxy with Reinforced Graphite Cloth," 28th National SAMPE Symposium and Exhibition, April 1983.
5. John T. Hartness, "Polyetheretherketone Matrix Composites," 14th National SAMPE Technical Conference, October 1982.
6. John T. Hartness, "Thermoplastic Matrix Composites," N.A.T.E.-SPE, October 1982.
7. M. F. Koenig, and J. T. Grant, "Deconvolution as an Aid to Quantification in Electron Spectroscopy Studies of Surfaces and Thin Films," IX International Vacuum Congress, V International Conference on Solid Surfaces, Madrid, Spain, Sept. 26-Oct. 1, 1983.
8. M. F. Koenig and J. T. Grant, "Direct Comparison of Deconvoluted XPS Data with that Obtained Using a Monochromatized Source," 34th Pittsburgh Conference and Exposition on Analytical Chemistry and Applied Spectroscopy, Atlantic City, NJ, March 7-12, 1983.

PUBLICATIONS (CONT'D)

11. R. Y. Kim and W. J. Park, "Statistical Analysis of Composite Fatigue Life," Progress in Science and Engineering of Composites, ed. T. Hayashi, et. al., Tokyo, Japan, October, 1982.
12. M. F. Koenig and J. T. Grant, "Deconvolution in X-ray Photoelectron Spectroscopy," Journal of Elec. Spec. and Rel. Phen. to be published in 1983.

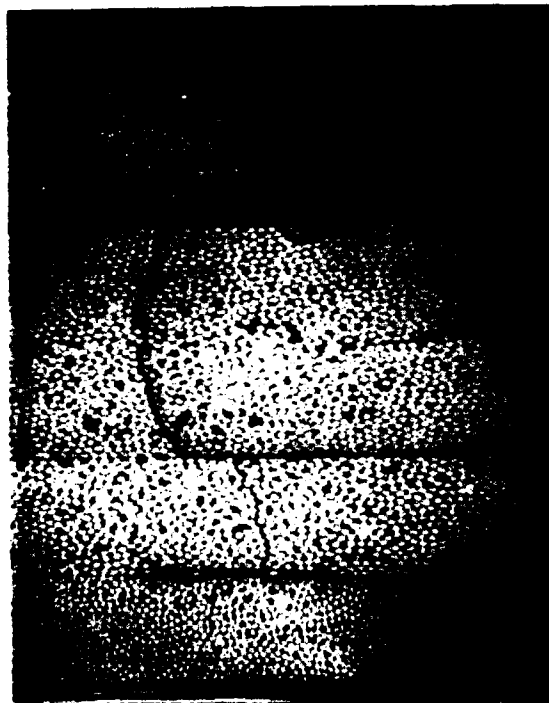
SECTION V
PUBLICATIONS AND PRESENTATIONS

The following presentations and publications cover work carried out under this contract. They were either prepared or appeared publicly during this reporting period.

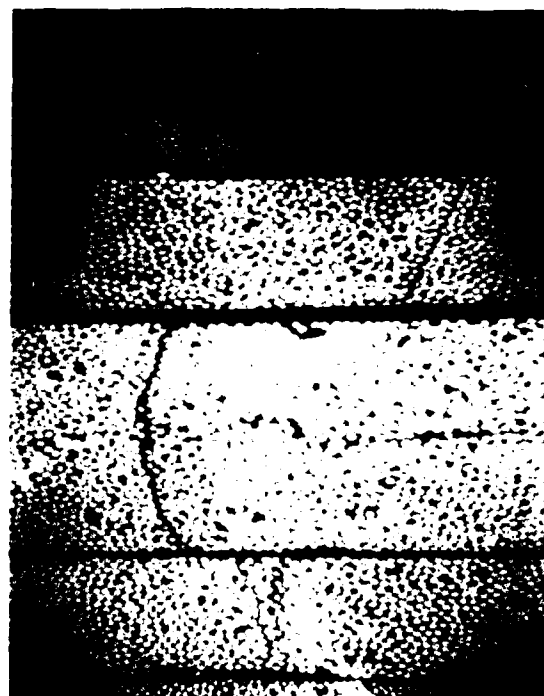
PUBLICATIONS

1. S. R. Soni and N. J. Pagano, "Global-Local Laminate Variational Model," International Journal of Solids and Structures, 19, 3, 207-228, 1983.
2. S. R. Soni, "A Digital Algorithm for Composite Laminate Analysis - Fortran," U.S. Air Force Materials Laboratory, Report No. AFWAL-TR-81-4073 (Revised), July 1983.
3. M. J. Rich, L. T. Drzal, and P. F. Lloyd, "Adhesion of Graphite Fibers to Epoxy Matrices: I. The Role of Fiber Surface Treatment," J. Adhesion, 1183, Vol. 16, pp. 1-30.
4. M. J. Rich, L. T. Drzal, M. F. Koenig, and P. F. Lloyd, "Adhesion of Graphite Fibers to Epoxy Matrices: II. The Effect of Fiber Finish," J. Adhesion, 1983, Vol. 16, pp. 133-152.
5. M. J. Rich, V. B. Gupta, L. T. Drzal, C. Y-C. Lee, "The Effect of Moisture on α - Relaxation in Cured Epoxy Resin," Poly. Preprints, Vol. 24, N. 2, 1983.
6. M. J. Rich, L. T. Drzal, and M. F. Koenig, "Moisture Induced Interfacial Effects on Graphite Fiber - Epoxy Matrix Interfacial Shear Strength," 38th Annual Reinforced Plastics/Composites Conference, 1983, paper 4-F.
7. R. Y. Kim, and J. T. Hartness, "A Comparative Study on Fatigue Behavior of Polyetheretherketone and Epoxy with Reinforced Graphite Cloth," Materials and Processes-Continuing Innovations, 28th National Sampe Symposium and Exhibition, Vol. 28, April 1983.
8. R. Y. Kim, "Prevention of Free-Edge Delamination," Materials and Processes - Continuing Innovations, 28th National Sampe Symposium and Exhibition, Vol. 28, April 1983.
9. R. Y. Kim, and R. M. Aoki, "Transverse Crack and Delamination in Composite Materials," Fibre Science and Technology, Vol. 18, 1983.
10. R. Y. Kim, "In-Plane Tensile Strength of Multidirectional Composite Laminates," Progress in Science and Engineering of Composites, ed. T. Hayashi, et. al., Tokyo, Japan, October, 1982.

95,000 cycle



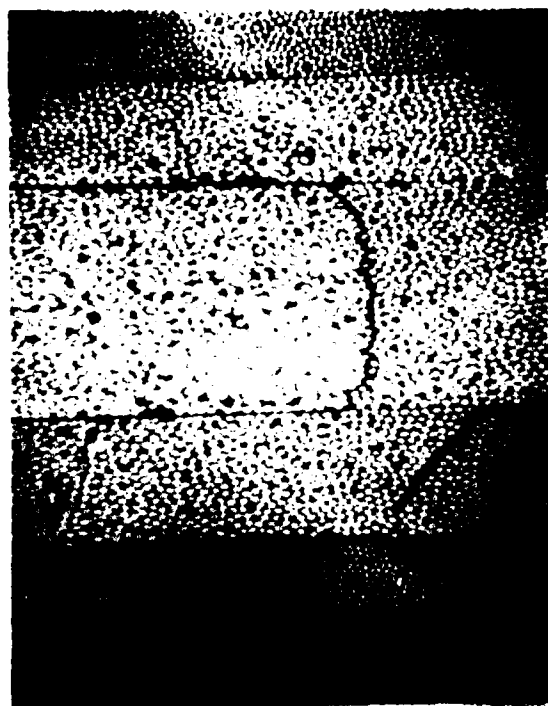
245,000 cycle



90/45

+45/-45

Enlarged view of the 95,000
cycle



245,000 cy

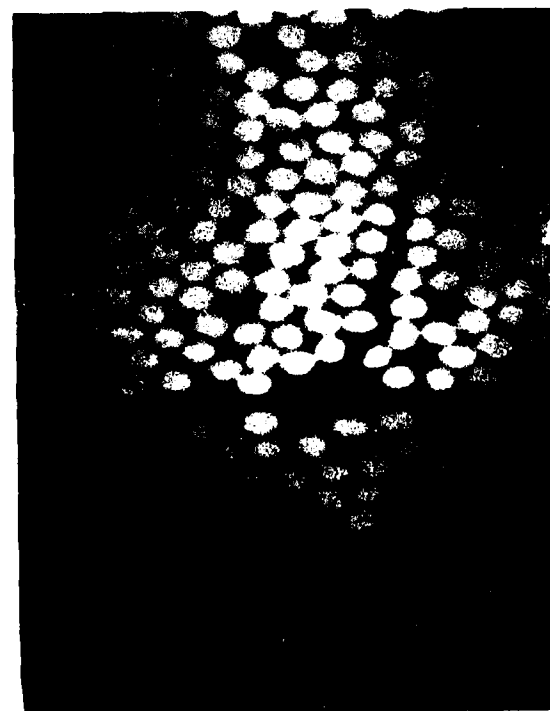
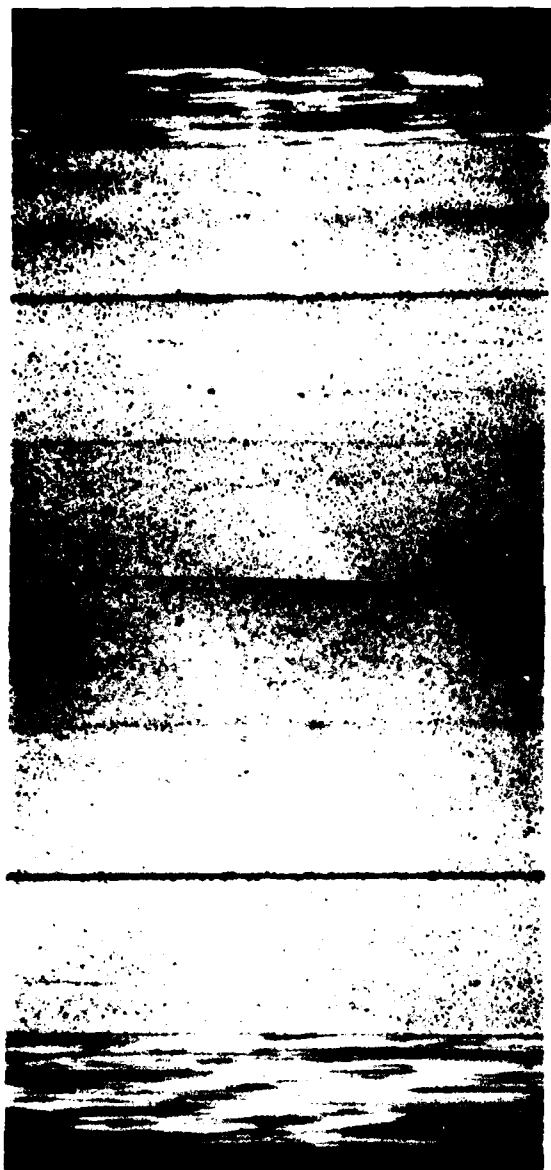


Figure 69. T300/5208 [0/90/+45] T-T Fatigue, $S_{max} = 50$ ksi
#54-5.

+45/-45



+45/-45



4000 cycle

No evidence of Delamination at the Other Interfaces.

Figure 68. T300/1034C $[0_3/45_3/-45_3/90_3]$ C-C Fatigue $S_{max} = 45$ ksi #3-10-2.

the last loading step prior to failure. The last incremental stress level applied ranges from 93% to 97% of the ultimate compressive strength. The failure surface reveals some degree of delamination. We conducted fatigue test under compression - compression with minimum fatigue stress -45 ksi, $R = 10$, and $f = 10$ Hz. The specimen shows clear delamination after 4,000 cycles. Figure 68 shows the microphotograph of the free-edge delamination at both interfaces of the 45/-45 plies. These delaminations were extended over the entire specimen length. It is also noted that no transverse cracks were found on the entire free-edges. For the $[0/90/+45]_s$ laminate, the specimens were tested under tension-tension fatigue to induce delamination by shear since the σ_z is compression under applied tension. This specimen shows extensive delamination due to tensile σ_z under applied compression. Figure 69 shows the delamination under tension-tension fatigue with maximum fatigue stress 50 ksi and $R = 0.1$. The delamination occurs mostly at the interfaces of +45/-45 plies where the maximum τ_{xz} is presented and was limited to a short distance unlike the $[0_3/+45_3/90_3]_s$ laminate. This delamination is also followed by a number of transverse cracks as shown in Figure 69.

This study is being continued to improve our understanding of the delamination mechanisms and prediction capability of onset of delamination in composite laminates.

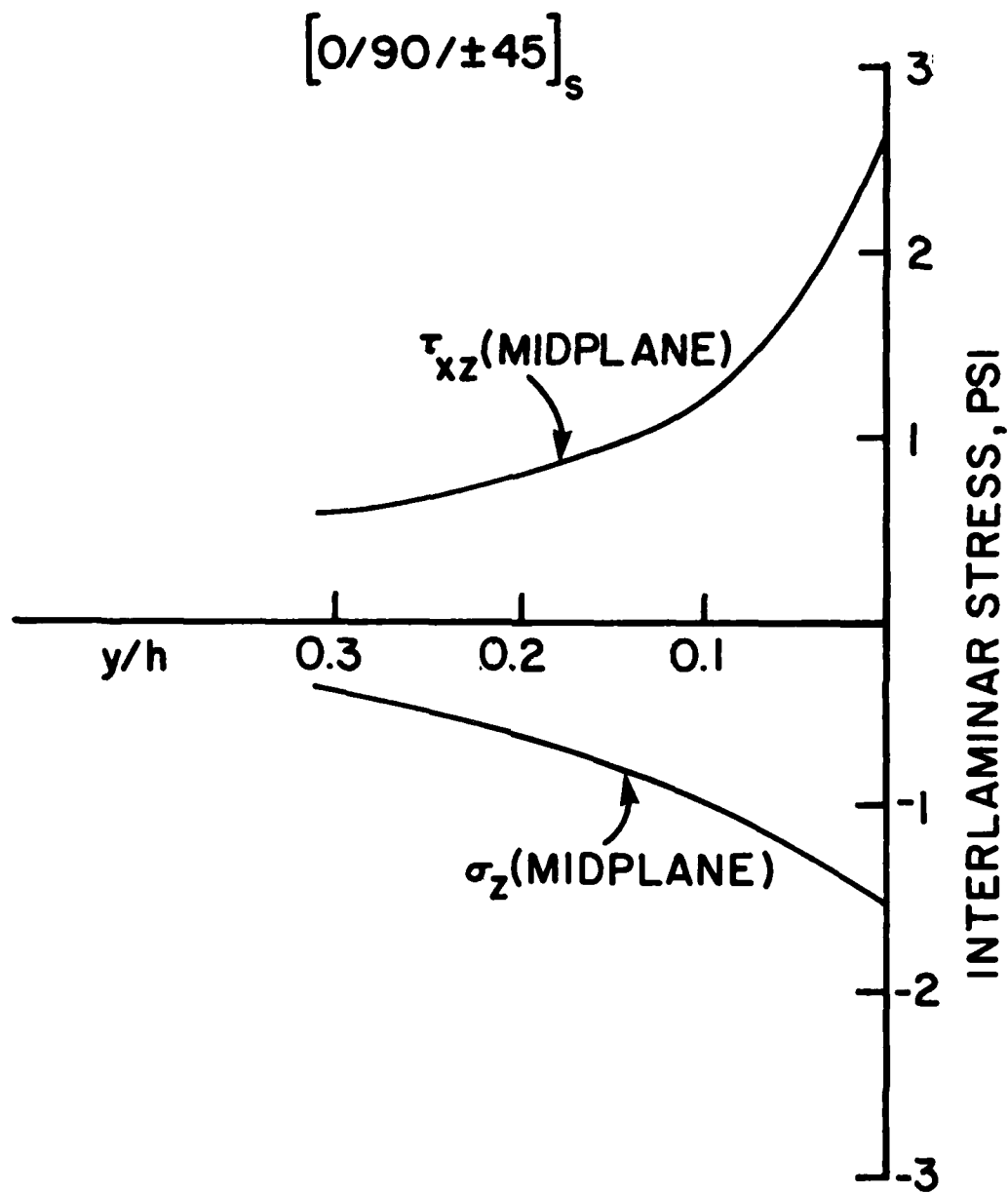


Figure 67. Interlaminar Stress Distribution Along Specimen Width for $[0/90/\pm 45]_s$.
 h is one half of specimen thickness.

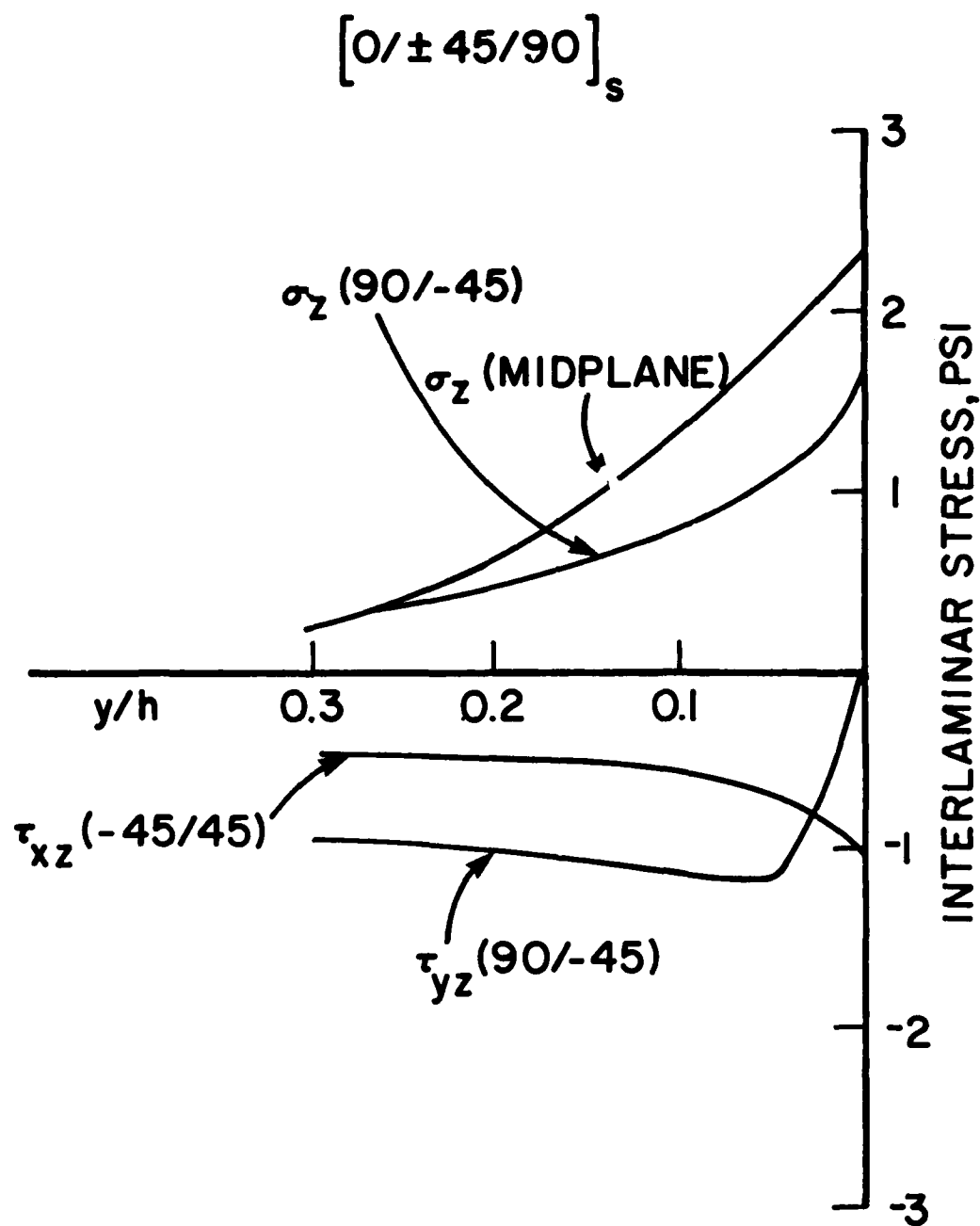


Figure 66. Interlaminar Stress Distribution Along Specimen Width for $[0/+45/90]_s$.
h is one half of specimen thickness.

we have conducted the stress analysis of a number of composite laminates made of T300/1034C Fiberite. Based on the stress analysis result, two stacking sequences of quasi-isotropic laminate, $[0/+45/90]_s$ and $[0/90/+45]_s$ were chosen for preliminary study. The interlaminar stress components were calculated at various points along the thickness as well as the width corresponding to a half of laminate thickness from the free-edge. Figures 66 to 67 show the distribution of each stress component along specimen width at the interfaces indicated. The peaks of the stress curves indicate the maximum value of the respective stress component around the free-edge region. The τ_{yz} component is not shown in the $[0/90/+45]_s$ laminates since its magnitude was found to be very small compared with τ_{xz} . In the $[0/+45/90]_s$ laminate, the maximum stress failure theory assumes that delamination would occur when the value of anyone of stress components first reaches its respective strength prior to the ultimate failure of specimen. Under applied tension, delamination will occur at the midplane due to tensile σ_z . When the applied load sign is reversed, that is, compression, the sign of all the stress components become opposite. Thus, we would expect delamination by shear at either the interface of $-45/45$ or $90/-45$ in considering $X'_T/\sigma_z < S_s/\tau_{xz}$ where X'_T and S_s are the transverse compressive strength and the interlaminar shear strength, respectively. The initial calculation indicates that this laminate will fail before the τ_{xz} reaches the interlaminar shear strength of the material system. In order to stimulate delamination in this laminate, we increased the number of the constituent ply threefold; that is $[0_3/+45_3/90_3]_s$ for experiment. This is based on the result of previous work that the thicker the laminate, the smaller the stress requires for onset of delamination, although the stress magnitudes remains unchanged. Straight sided coupon specimen with $3/4$ " wide and $2\ 5/8$ " long was tested under compression with the aid of a side supported device. The specimen was tested by a number of incremental loading and unloading. After each incremental loading, the specimen was examined under a microscope to locate delamination area. No delamination was found until

properties were also determined from four replicas. The test data is available upon request.

A series of tests was also conducted to develop a methodology to determine the strain energy release rate utilizing onset of delamination and its growth as part of the program of AFWAL/MLBM. The material system used in this study was AS1/3502 Hercules. The laminate was $[+30/+30/90_2]_s$ containing various sizes of starter cracks in the form of fail strips (Teflon tape and prepreg backing paper). These starter cracks were embedded along the free-edge at the laminate mid-plane during the layup. Four different sizes of starter cracks, 1/16, 1/8, 3/16, 1/4 inches were investigated. All specimens with 1" wide and 8" long were instrumented with axial and transverse strain gage. Each specimen was tested in four successive incremental loadings until final failure using the MTS testing machine. The strains and opening of the free-edge delamination were measured during each test and after each loading the specimen was subjected to x-ray radiograph to delineate the extent of delamination front toward the middle of the specimen. A total of 50 specimens were tested in this program and the test data is available upon request.

5. DELAMINATION STUDY

An extensive theoretical and experimental work on free-edge delamination has been conducted over the last two years. The analysis of free-edge delamination in composite laminates was conducted by employing the global-local model and introducing a failure theory. The analytical results were favorably compared with the results of an extensive experimental program. In this work, however, only the interlaminar normal stress σ_z is treated as a significant factor. This work is included in the technical report AFWAL-TR-82-4182.

Recently, it was decided to induce the interlaminar shear stress components in the analysis of delamination. A preliminary result obtained so far will be presented in this report. For this,

TABLE 30
TEST MATRIX OF MIXED MODE FRACTURE FOR
T300/1034C GRAPHITE/EPOXY

Orientation, Deg.	Notch Type	No. of Specimen	Type of Loading
0	CN	3	Tension
7	"	"	"
10	"	"	"
15	"	"	"
15	EN	"	Compression
15	CN	"	Tension
30	"	"	"
45	"	"	"
45	EN	"	Compression
45	CN	"	Tension
60	"	"	"
75	"	"	Compression
90	"	"	Tension
90	"	"	Compression

$[+45]_{2s}$, $[0/90/+45]_s$, and $[0, 90]_{2s}$. Tensile coupons of each laminate were fatigued until final failure or to the prescribed cycle under several fatigue stress levels at laboratory environment. The major parameters studied in this paper were S-N relationship and stiffness change. The damage incurred during fatigue tests was also examined at several intervals of fatigue life by interrupting the fatigue test. The fatigue data indicated that the polyetheretherketone system shows excellent fatigue properties and appears to be superior to the epoxy system in overall fatigue performance. Because of the excellent fatigue properties of graphite cloth/polyetheretherketone composite as described previously, an extensive test program has been initiated to evaluate the static and fatigue properties of this material system fabricated with unidirectional tape instead of cloth. The details of the material system and its processing is given in Section I. The static characterization has been completed and the results are presented in Section I. Tension-tension fatigue tests are being conducted on the 90, $+45$, and quasi-isotropic laminates to generate the fatigue life data. All specimens were fatigued until final failure for various values of maximum fatigue stress with $R = 0.1$ and 10 Hz of frequency.

4. FRACTURE TEST

A fracture test was conducted to examine the applicability of the off-axis tensile test to determine the mixed mode fracture characteristics of a unidirectional composite. The material system used in this test was T300/1034C graphite/epoxy. A variety of off-axis specimens were cut from unidirectional panels to produce data from pure Mode I to a number of ratios of K_I/K_{II} . The ratio of crack to specimen width was 0.2 for all specimens. Two types of notches, center notch (CN) and edge notch (EN), were made using a diamond wire saw and the tip of the notch was then sharpened with a razor blade. Table 30 presents the test matrix. In addition, three rail shear tests with a notch was conducted to produce pure K_{II} Mode. The longitudinal, transverse, and shear



Specimen 3-2-13, $S_{\max}/S_{\min} = 65/-5$ ksi, $n = 5,000$ cycles

Figure 65. Microphotograph Showing Fiber Breaks in the 0 Degree Ply for Gr/Ep T300/1034C with $[0/45/-45/90]_{2s}$.

REFERENCES

1. "Improved Materials for Composites and Adhesives," Final Report, AFWAL-TR-81-4154.
2. "Improved Materials for Composites and Adhesive Joints," Annual Progress Report, AFWAL-TR-82-4182.
3. D. T. Clark, W. J. Feast, ed. Polymer Surfaces, New York: John Wiley and Sons, 1978, Chapt. 16, p. 324.
4. P. H. van Cittert, Z. Physik 69 (1931) 298. For a recent review see: A. F. Carley and R. W. Joyner, J. Electron Spec. and Rel. Phen. 16 (1979) 1.
5. H. H. Madden and J. E. Houston, J. Appl. Phys. 47 (1976) 3071.
6. L. T. Drzal, M. J. Rich, J. D. Camping, and W. J. Park, "Interfacial Shear Strength and Failure Mechanisms in Graphite Fiber Composites," 35th Reinforced Plastics/Composites Conference, 1980, Paper 20C.
7. L. T. Drzal, M. J. Rich, and D. L. Hall, "Structure-Property Relationships at the Composite Interphase," 15th Biennial Conference on Carbon, 1981, Paper FC-14.
8. R. C. Burk, "Standard Failure Criteria Needed for Advanced Composites," Astronautics and Aeronautics, June 1983, pp. 58-62.
9. S. R. Soni, "A Comparative Study of Failure Envelopes in Composite Laminates," communicated for publication in J1. Reinforced Plastics and Composites.
10. S. R. Soni, "A Digital Algorithm for Composite Laminate Analysis - Fortran," AFWAL-TR-81-4073, (Revised) July 1983.
11. R. S. Sandhu, "A Survey of Failure Theories of Isotropic and Anisotropic Material," AFFDL-TR-72-71, Wright Patterson Air Force Base, Dayton, Ohio, 1972.
12. S. W. Tsai, and E. M. Wu, "A General Theory of Strength for Anisotropic Materials," J1. Composite Materials, Vol. 5, 1971, p. 58.
13. C. C. Chamis, "Failure Criteria for Filamentary Composites," Composite Materials: Testing and Design, ASTM STP 460, ASTM, 1970, p. 336.

REFERENCES (CONCLUDED)

14. O. Hoffman, "The Brittle Strength of Orthotropic Materials," J. Composite Materials, Vol. 1, 1967, p. 200.
15. R. Hill, "A Theory of the Yielding and Plastic Flow of Anisotropic Metals," Proceedings of the Royal Society, Series A, Vol. 193, 1948, p. 281.
16. S. W. Tsai, and M. Knight, "Optimizing Ply Properties," 28th National SAMPE Symposium, April 12-14, 1983, Anaheim, CA.
17. D. L. Flaggs and M. H. Kural, "Experimental Determination of the In Situ Transverse Lamina Strength in Graphite/Epoxy Laminates," J1. Composite Materials, Vol. 16, March 1982, p. 103.
18. N. J. Pagano, "Stress Fields in Composite Laminates," Int. J1. Solids and Structures, Vol. 14, 1978, p. 385.
19. R. Y. Kim and S. R. Soni, "Experimental and Analytical Studies on the Onset of Delamination in Laminated Composites," University of Dayton Research Report UDR-TR-83-40.
20. M. D. Kistner, J. M. Whitney, C. E. Browning, "First Ply Failure of Graphite/Epoxy Laminates," Second US-Japan Symposium on Composite Materials, June 6-8, 1983, held at NASA-Langley Research Center, Hampton, Virginia under the auspices of ASTM.

APPENDIX A

POLYETHERETHERKETONE (PEEK)/GRAPHITE LAMINATE
MECHANICAL AND THERMOPHYSICAL
PROPERTY CHARACTERIZATION

A total of 16 types of mechanical property tests are proposed on the composite laminates. Where it is most convenient laminates will be supplied per our instruction as to specific lay-up geometry and ply number. When a complex or special laminate is needed such as Mode I, prepreg material will be fabricated into the desired laminate on site at AFWAL. Processing information will be supplied by ICI.

The following tables show the laminate lay-up geometry, number of plies, as well as the required number of laminates assuming a 24" x 24" composite.

STATIC MECHANICAL PROPERTY
TEST MATRIX

Test Type	Test Temperature			
	-67°F	72°F	250°F	350°F
0° Tension	10	10	10	10
90° Tension	5	5	5	5
+45° Tension	5	5	5	5
Quasiisotropic Tension	5	5	5	5
+30, 90	-	5	-	-
+45, 90 [1st ply failure] ¹	-	5	-	-
0° Compression	-	5	5	-
0° Flexure	5	5	5	5
90° Flexure	5	5	5	5
4-pt Interlaminar Shear	5	5	5	5
In plane Shear ²	-	2-3	-	-
Mode I	-	5	-	-

¹Composite lay-up geometry may change as data reduction and analysis precedes

²Except for 2-3 rail shear tests, all of the inplane shear data will be obtained from the +45° tension data.

DYNAMIC AND TIME DEPENDENT MECHANICAL
PROPERTY TEST MATRIX

Test Type	Test Temperature			
	-67°F	72°F	250°F	350°F
+45° Tensile Creep	-	12	12	-
<u>Fatigue</u> <u>+45</u> Tension-Tension Tension-Compression Compression-Compression				
	10	10	10	-
	10	10	10	-
Quasiisotropic Tension-Tension Tension-Compression Compression-Compression				
	10	10	10	-
	10	10	10	-
Notched Quasiisotropic Tension-Tension Tension-Compression Compression-Compression				
	10	10	10	-
	10	10	10	-

Note: All fatigue specimens
will be loaded to four
stress levels.

THERMOPHYSICAL PROPERTY TEST MATRIX

Test Type	Comments
C-Scan	All as received panels and all on site fabricated panels
Specific gravity	All as received panels and all on site fabricated panels
Photomicrographs	" "
Per ply thickness	" "
Rheometrics	-65°F to 660°F selected panels
0° x 90° Thermal Expansion (TMA)	Selected Panels
DSC	Selected Panels
TGA	Selected Panels

TEST MATRIX FOR STATIC MECHANICAL PROPERTY TESTS
AFTER ELEVATED TEMPERATURE, HIGH HUMIDITY AGING

Test Type	Aging Condition					
	500 & 1000 Hr 300°F Air			Saturation 160°F Under Water		
	Test Temp			Test Temp		
	72°F	250°F	350°F	72°F	250°F	350°F
0° Flexure	5	5	5	5	5	5
90° Flexure	5	5	5	5	5	5

Static	
Laminate	No. of Plies (n)
0° - Tension	12
90° - Tension	12
<u>+45°</u> - Tension	16
Quasiisotropic-Tension	16
<u>+30</u> , 90 (To be supplied as tape)	-
<u>+45</u> , 90 (To be supplied as tape)	-
0° - Compression	12
0° - Flexure	12
90° - Flexure	12
0° - 4 pt Interlaminar Shear	12
<u>+45</u> Rail Shear	8
Mode I (To be supplied as tape)	-

Note: Per ply thickness is assumed to be approx. 5 mil.

Dynamic

Laminate	No. of Plies (n)
$\pm 45^\circ$ - Tensile Creep	16
$\pm 45^\circ$ - Fatigue	8
Quasiisotropic - Fatigue	16

Laminate Needs

Laminate Type	Plies	Size	No.
0°	12	24" x 24"	3
±45°	16	24" x 24"	1
Quasiisotropic*	16	24" x 24"	13
±45°	8	24" x 24"	7

*[0,±45,90]_{2s} actual lay-up

[0,+45,-45,90,0,+45,-45,90,90,-45,+45,0,90,-45,+45,0]

END

FILMED

7-85

DTIC